FLUID FLOW AND HEAT MODELING IN THE WELLBORE AND ITS APPLICATIONS

A Dissertation

by

GIBRAN MUSHTAQ HASHMI

Submitted to the Office of Graduate and Professional Studies of
Texas A&M University
in partial fulfillment of the requirements for the degree of

DOCTOR OF PHILOSOPHY

Chair of Committee,	Abu Rashid Hasan
Committee Members,	Ding Zhu
	Hadi Nasrabadi
	Faruque Hasan
Head of Department,	Jeff Spath

May 2019

Major Subject: Petroleum Engineering

ABSTRACT

Heat and fluid transport govern many problems in the field of petroleum engineering. Their applications are widespread in almost all aspects of the petroleum production system. This study focuses on one aspect of this system: the wellbore conduit and the fluid and thermal flow inside the wellbore. In this work, multiple fluid and heat flow models are developed to aid in different applications such as transient testing, production rate estimation, and artificial lift. All the models developed are validated using field data or data from literature.

The first category of models is developed for *short-term testing*. Given that short-duration tests (closed-chamber tests (CCT) and slug) can last only a few minutes, particularly in high-conductivity reservoirs, the challenge was approached with a two-fold strategy. First, a forward model was developed to design the chamber length to ensure that interpretable test data was collected. Second, the CCT and slug tests were combined so that the total test duration could be controlled, particularly in high-conductivity reservoirs. The approach presented here allowed individual treatment of slug, CCT, and reverse-slug or injection test for underpressured reservoirs. Overall, the models present a simple, yet complete approach to design and analysis of these short-term tests.

The next category of models helps to determine production rate by analyzing thermal flow from the wellbore into the formation. The objective of this part of the study is two-fold: to estimate rate from measured temperature data available for downhole

telemetry with a rigorous *transient analytical model*, and to show the possible use of the computed rates to perform pressure transient analysis for both the pre- and post-cleanup periods. Comparing and contrasting permeability estimates from the two periods provides guidance on the suitability of this approach. Another application presented here explores determining zonal contributions similarly using transient analytical model and temperature logging data gathered during a production logging job.

Lastly, a simplified modeling approach is presented for the *design of plunger lift* for wells in gas reservoirs with significant water production. The proposed model allows for an efficient design of plunger lift by incorporating energy balance in the wellbore.

To my wife, daughter, parents and siblings.

ACKNOWLEDGEMENTS

My special thanks go to my advisor, Dr. A. R. Hasan, who not only financially supported but also encouraged and helped me throughout this project. His insightful implementations of the ideas often led to important improvements. Without his guidance and patience, this work would never be fulfilled. He was a constant support in times of stress, not only in the matters of academics but also provided healthy advice in financial matters.

I also wish to thank the Department of Petroleum Engineering at Texas A&M University for the role they played in the financial support given to me and all my teachers whose valuable lessons led me to attain better understanding of the petroleum engineering concepts in order to successfully complete this task.

Well-deserved thanks extend to Mr. Shah Kabir of Hess Corporation who provided us with excellent technical assistance and field data that enabled us to test our models. His constant encouragement and comments helped improve this work considerably. Credit also goes to my colleagues at Halliburton who provided great support while I struggled to finish this dissertation with a full-time job and family.

I especially wish to thank Dr. Hadi Nasrabadi, Dr. Faruque Hasan, Dr. Ding Zhu and Dr. Jerome Schubert for agreeing to serve on my committee.

I also want to thank my research group members and friends for their support and suggestions. They were often the people to provide initial feedback or suggest improvements whenever I got stuck.

Finally I wish to express my gratitude to my family. First and foremost to my parents who encouraged me at each step and helped me throughout my entire course of study. Their emotional support meant the world at times. My siblings also provided deep moral support and encouragement. Last but not the least, I also wish to thank my wife and baby daughter for their unconditional support. Their love, patience and understanding knew no bounds, and always drove me to my best.

CONTRIBUTORS AND FUNDING SOURCES

This research study was supervised by a dissertation committee consisting of Dr. Rashid Hasan (advisor), Dr. Ding Zhu, and Dr. Hadi Nasrabadi of the Department of Petroleum Engineering, and Dr. Faruque Hasan of the Department of Chemical Engineering. Dr. Jerome Schubert graciously accepted to substitute in place of Dr. Ding Zhu during the preliminary and final thesis defense.

Part of the data analyzed for Chapter 4 was provided by Shah Kabir from Hess Corporation. His insights during most of the projects really propelled this thesis forward.

All the work conducted for the dissertation was completed by the student independently. The project was financially supported, in part, by the Crisman Institute for Petroleum Research at Texas A&M University.

NOMENCLATURE

a	lumped parameter defined by Eq. 3.5, 1/sec, 1/t
A	parameter defined by Eq. A.12, dimensionless
B	formation volume factor, RB/STB
C	friction pressure loss as a fraction of gas potential energy change, dimensionless
c_f	formation compressibility, psi^{-1}, Lt^2/m
c_p	specific heat capacity of fluid, Btu/lbm-°F, L^2/t^2T
C_J	J-T coefficient, (°F)/(lb_f/ft^2), TLt^2/m
c_t	total system compressibility, psi^{-1}, Lt^2/m
C_T	thermal storage parameter, dimensionless
c_w	water compressibility, psi^{-1}, Lt^2/m
d	tubing diameter, ft, L
D	depth of well, ft, L
f	friction factor, dimensionless
F	frictional loss, ft-lbf, mL^2/t^2
g	gravitational acceleration, ft/sec^2, L/t^2
g_c	conversion factor, 32.17 lbm-ft/lbf-sec^2
g_G	geothermal gradient, °F/ft, T/L
h	reservoir thickness, ft, L
h_i	initial aquifer hydraulic head, ft, L

h_o initial hydraulic head at the well, ft, L

h_w changing hydraulic head at the well, ft, L

h_L height of liquid column present in the wellbore before reservoir inflow, ft, L

J conversion factor, 778 ft-lbf/Btu

k permeability, md, L^2

k_a thermal conductivity of the annular fluid, Btu/hr-ft-°F, mL/t^3T

k_c thermal conductivity of cement, Btu/hr-ft-°F, mL/t^3T

k_e thermal conductivity of formation, Btu/hr-ft-°F, mL/t^3T

k_r relative permeability, md, L^2

$k_{rg,max}$ maximum relative permeability of gas, md, L^2

$k_{rw,max}$ maximum relative permeability of water, md, L^2

L total wellbore measured depth, ft, L

L_j measured (from wellhead) depth of section 'j' of wellbore, ft, L

L_R relaxation parameter defined by Eq. 3.2, ft^{-1}, 1/L

m mass of fluid per unit depth, lbm/ft, m/L

M gas molecular weight, lb_m/lb-mol

m' parameter defined by Eq. A.11, psi-D/STB

m_g mass of gas on top of plunger, m, lb_m

m_L mass of fluid on top of plunger, m, lb_m

m_p mass of plunger, m, lb_m

p pressure, psia, m/Lt^2

p_1 pressure at top of gas column, psia, m/Lt^2

p_2	pressure at bottom of gas column, psia, m/Lt^2
p_3	pressure at bottom of initial fluid in the wellbore, psia, m/Lt^2
p_{bh}	pressure at bottom of gas column, psia, m/Lt^2
p_c	pressure at casinghead, psia, m/Lt^2
p_i	initial reservoir pressure, psia, m/Lt^2
p_{rf}	pressure exerted by the fluid column developed through reservoir inflow, psig, m/Lt^2
p_t	pressure at tubinghead, psia, m/Lt^2
p_{tb}	gas pressure at tubing bottom, psia, m/Lt^2
p_{wf}	bottomhole pressure, psia, m/Lt^2
p_{wh}	pressure at top of gas column, psia, m/Lt^2
$\bar{p}$	average reservoir pressure, psia, m/Lt^2
q	volumetric production rate, STB/D, L^3/t
Q	heat transfer rate per unit length of wellbore, Btu/hr-ft, ML/t^3
r_e	reservoir radius, ft, L
r_{inv}	radius of mud-filtrate invasion, ft, L
r_t	tubing radius, ft, L
r_w	wellbore radius, ft, L
s	skin, dimensionless
S	saturation, dimensionless
t	time, hr, t
T or T_f	fluid temperature, °F, T

T_{calc}	calculated fluid temperature, °F, T
t_D	$\alpha t/r_{wb}^2$, dimensionless time
T_D	dimensionless temperature defined by Eq. B.2.
T_{ei}	undisturbed earth or formation temperature, °F, T
t_s	time to shut-in, hr, t
t_{sp}	soak period, hr, t
U_t	overall-heat-transfer coefficient, Btu/hr-ft^2-°F, m/t^{3}T
v	fluid velocity, ft/hr, L/t
$\bar{v}$	fluid average velocity, ft/hr, L/t
V_c	volume of tubing/casing annulus, ft^3, L^3
v_{gc}	critical gas velocity needed for annular two-phase flow, ft/sec, L/t
v_{sg}	superficial gas velocity, ft/s, L/t
V_t	volume of tubing, ft^3, L^3
w	mass rate, lbm/hr, m/t
z	variable wellbore measured depth from surface, ft, L
Z	gas compressibilty factor, dimensionless
α	thermal diffusivity of the formation, ft^2/hr, L^2/t
γ	specific gravity, dimensionless
Δp_g	difference between gas chamber top and bottom pressure, psig, m/Lt^2
Δp_{if}	pressure exerted by column of initial fluid, psig, m/Lt^2
Δz	distance moved up by fluid in the wellbore, ft, L
Δz_g	height of gas column, ft, L

Δz_{if}	column depth of initial fluid in the wellbore, ft, L
Δz_{rf}	depth of reservoir fluid column in the wellbore, ft, L
ε	pipe roughness, ft, L
θ	well inclination (to horizontal) angle, degree
μ	fluid viscosity, cp, m/Lt
ρ	fluid density, lbm/ft^3, m/L^3
φ	formation porosity, dimensionless
ϕ	lumped parameter defined by Eq. B.13, °F/ft, T/L
Ψ	lumped parameter, Eq. B.17, °F/ft, T/L
$\left(\frac{dp}{dz}\right)_A$	accelerational pressure gradient, psi/ft, m/L^{2}t^2
$\left(\frac{dp}{dz}\right)_F$	frictional pressure gradient, psi/ft, m/L^{2}t^2
$\left(\frac{dp}{dz}\right)_H$	hydrostatic pressure gradient, psi/ft, m/L^{2}t^2

Subscripts

av	average
est	estimate
f	fluid
g	gas
j	time coordinate
n	final time coordinate
w	water

TABLE OF CONTENTS

Page

LIST OF FIGURES

Page

LIST OF TABLES

Page

CHAPTER I

INTRODUCTION

Oil and gas exploration and production is a complex but vital endeavor. The energy and products created from crude oil are endless and essential to our way of life. Without it most of modern everyday commodities would not exist in the same way. Not only that, many other fields benefit from the production of crude oil and the products obtained from it. This creates a tremendous demand of crude oil in the world and the on-going battle between the depleting energy resources and the initiatives to find new ones has given birth to a need of a greater workforce striving towards this important undertaking of satisfying this demand.

With rise in technology and data management, newer ways have arisen to characterize reservoir and produce wells more effectively and with it a crucial need to properly understand fluid and heat flow in the wellbore under different conditions. Effective and economic ways of reservoir characterization and production management are essential for the success during any well's lifecycle. Fluid and heat flow play an important part in both of these aspects. Oil and gas bearing pay zones are porous rock media that are found thousands of feet below the earth's surface. At such depth the fluids possess energy in the form of high pressure and temperature. Wells are drilled to produce these fluids from these pay zones. In producing these fluids, the engineers have to contend with two major types of fluid and energy flows. Fluid flows from the porous medium to the wellbore bringing energy along with it and then moves from the well

bottom, henceforth called bottomhole, to the wellhead dissipating some of that energy to the surrounding formation on its way to the top.

Modeling of fluid flow and heat distribution remains the cornerstone of many discoveries and inventions in the field of engineering. In petroleum engineering, the area has provided numerous applications. Yet newer applications or techniques keep springing up to this day. The field has the potential to shed light on some major issues in the realm of reservoir and production engineering. It provides uses in pressure transient testing, determining wellbore integrity, rate estimation, intelligent completions and even in artificial lift where modeling the flow accurately may allow optimization of the lift method.

In the past most of the modeling techniques have either focused on fluid flow and distribution of heat in the wellbore or in the reservoir. There have been fewer studies that have studied the problems by coupling the mechanics in both the reservoir and the wellbore. The aforementioned characteristic forms the backbone of this work. The synergy provided by this coupling of conduits involving different heat and fluid flow mechanisms can lend major utility to the models that are developed in this study.

The study of the distribution of heat and fluid flow is useful in any stage of petroleum production. From mud circulation while drilling to initial flow during reservoir evaluation to assisted flow during the last stages of production, proper modeling of heat and fluid flow can help provide information more efficiently about the reservoir and even optimize production operations.

The goal of this dissertation is to demonstrate the variety of applications of fluid and heat flow models in the wellbore in the petroleum industry. New models are to be developed for different phases in the life of the well which help ascertain evaluation and production efficiency. These studies include design of short-term fluid flow models to assist in reservoir evaluation; modeling heat and fluid flow to inversely conduct flow estimation; and finally modeling and optimization of flow during the employment of one of the lift methods i.e. plunger lift. The different models and their validations would provide for the main content of this thesis and serve as a reminder of the application of the underlying principles to all flow problems in the lifecycle of a producing or injecting well.

In the early stages after drilling a well, the reservoir(s) contributing to the well need to be understood. Models have been established in this work for such reservoir characterization. These models pertain to short-term tests which are increasingly used in industry to evaluate reservoir characteristics. Employing such models lead to significant cost and time savings. During the early days of the well, a well is often tested to establish reservoir parameters. A slug test can be carried out for an underpressured system where no fluid is produced on the surface since the reservoir pressure cannot sustain it. Similarly, in a closed chamber test (CCT), no fluid is produced at the surface either; however production happens in a closed chamber unlike a slug test where it takes place under open head. The system need not be underpressured for a CCT. In this dissertation we develop a model for slug test and closed chamber test. Design model for

these tests have not existed in literature or commercial software and this study aimed to provide those.

The next application for flow in the wellbore is during production where once again fluid and heat flow modeling can be shown to be of great use. This study develops a model to account for the variable heat flux between the wellbore and formation. During production most wells are lined with gauges that measure pressure and temperature. With proper forward modeling of heat transfer, temperature measurements can serve some really useful purposes. Coupling multiple temperature measurements to help with interpretation can provide further usefulness. These are more commonly known as distributed temperature measurements where the fluid temperature measurement is made at several depths along the wellbore. We use transient temperature models for the inverse modeling of temperature to estimate flow rates. The utility for the said model is shown with respect to both production data and logging data.

Lastly, we demonstrate the usefulness of flow modeling inside the wellbore during the last stage of a well's life. Often times when a well is nearing the end of its productive capability, it is put on artificial lift. There are several kinds of artificial lift that are available in the market for large and small scale operators. One such artificial lift technique that is often employed by small scale operators is plunger lift. Plunger lift works on the principle of reducing the static pressure in the wellbore causing the well flow to increase. In this study, we have used flow modeling to optimize the functioning of a plunger lift system, whereby the model predicts the casing pressure needed for optimized plunger performance. Together with a reservoir inflow model, it can also be

used to determine the time the plunger needs to sit in the wellbore and increase in well productivity. Thus this dissertation develops different models for fluid and heat flow in the wellbore and provides applications of those models during the different stages of a well's life.

In the next chapter, we discuss the available literature on the various studies and models presented in this study. The chapter is divided into three sections each for the three different modeling techniques pertaining to wellbore fluid and heat flow. Various applications of all the models presented are also mentioned.

In Chapter III, we demonstrate the theoretical development for all the models presented in this work. Chapter IV presents case studies where the estimations and the predictions are compared against field data and data from literature. A discussion of the applications and simulated examples that probe the possibility of extracting meaningful information and value from the presented work is highlighted in Chapter V. Chapter VI finally presents conclusions and some recommendations. The applications of such modeling presented in this work are far from exhaustive, but the models developed can be expanded to other uses and scenarios.

CHAPTER II

LITERATURE REVIEW

The subject of fluid flow and heat flow distribution has been covered by many researchers in different fields of study. Narrowing down to petroleum engineering and related disciplines, there has also been a vast amount of literature with regards to different applications in industry. For the sake of clarity, separate literature review has been done for the different models to be developed as the applications span different branches of the oil and gas industry.

Short-term Fluid Flow Models for Reservoir Evaluation

Short-term fluid flow models can provide more efficient means of reservoir evaluation. Short-term tests are increasingly used to assess formation characteristics, particularly in costly offshore environments. In addition to traditional closed-chamber tests (CCT) and slug tests, mini-DSTs with dual-packer assembly, surge or impulse tests, and short-term injectivity and falloff tests all fit this category. In all these tests, a small volume of fluid production or injection occurs within a short time frame; Soliman et al. (2004) discussed most of these tests in detail. Advantages of these tests include environment-friendly methods, reduced risk because of shorter tests that avoid burning reservoir fluids at the surface, and significant cost savings. Furthermore, with changes in the Security Exchange Commission's (SEC) reserves rules, a conventional DST is no longer necessary to book reserves. In this thesis, we focus on some of these short-term

tests and develop models that will aid in the design and analysis of these tests in the field.

Literature emphasized the merits of conventional tests that span over 50 years; the latest SPE monograph (2009) presents many aspects of conventional test data gathering and analysis. In addition to the traditional reservoir parameters of permeability, skin, and deliverability potential, long-duration testing may reveal reservoir geometry reflecting depositional environment and heterogeneity. Typically, such insights are gained after field development and production initiation; the advent of permanent downhole pressure sensors has led to information deferral.

Wireline-conveyed formation testers form the backbone of the conduct of mini-DSTs; Chapter 21 of Kamal (2009) presents interpretation methods for formation testers. They reduce operational risk, permit downhole fluid sampling, and allow estimation of reservoir permeability. However, the derived skin from a mini-DST is not a true reflection of formation impairment because of incomplete cleanup. Many successful case studies of mini-DSTs are documented by Frimann et al. (1998), Coelho et al. (2005), Gok et al. (2006), Daungkaew et al. (2007), Bertolini et al. (2009), Ramaswami et al. (2012), and Harmawan et al. (2012).

A slug test entails production of reservoir fluid into tubing or drillpipe with an open valve at surface. The flow rate, initiated by perforating, continues to decline with increasing backpressure as hydrocarbon flows into the drill pipe. As a result, both pressure and rate change continuously. The test terminates once the reservoir fluid reaches surface or when the backpressure from the rising fluid level kills the well in an

under-pressured formation. In contrast to slug test, the flow occurs against a closed surface valve in CCT. Consequently, air compression causes the surface/downhole pressure to build more rapidly in CCT than in slug tests, thereby minimizing the storage effect significantly.

Although Ferris and Knowles (1954) introduced the slug test in groundwater hydrology, Ramey et al. (1975) provided the methodology for its practical applications in the petroleum literature. Subsequently, Shinohara and Ramey (1979), Saldana and Ramey (1986), Grader and Ramey (1988), and Peres et al. (1993), among others, offered various improvements of the original premise of the interpretive tools intended for fully penetrating well in a homogeneous, infinite-acting reservoir. In underpressured reservoirs, the slug test principle works in reverse mode; that is, by way of fluid injection: Sufi and Thompson (1988) demonstrated this point in heavy-oil reservoirs. As shown by Kabir (1991), the slug test can also be used in sucker-rod pumping wells.

Alexander (1977) introduced closed-chamber testing in practice. In CCT the surface valve remains closed during the flow periods. Because of fluid containment within the wellbore, this test offers greater security and safety than a standard DST. Changes in surface pressure with time allow for estimation of the flow rate of single-phase reservoir fluid. Methods are available for rate estimation during two-phase flow situation, as shown by Kabir et al. (1991). Many studies have appeared for interpreting CCT data involving the convolution approach by handling pressure and computed rate; the studies of Simmons and Grader (1988) and Simmons (1990) are two such cases. Hegeman and Abbaszadeh (1988) devised another approach to interpret these tests based

on analytical solutions of the diffusivity equation. However, their method considered the reservoir without the wellbore and was strictly for analysis that required measured pressure and sandface rate. Over the years, the rate estimation approach has matured in terms of wellbore flow modeling. For instance, Mfonfu and Grader (1992) presented a complex wellbore modeling approach. In contrast, Petak et al. (1991) presented a simplified approach in that the wellbore-storage coefficient represents variable wellbore conditions at each time step.

Despite the abundance of publications in the area of CCT and slug testing over decades, convenient forward models are too few to allow test design calculations. Therefore, the objective of developing these particular fluid flow models is three-fold: first, to develop a coupled wellbore/reservoir model so that test design and analysis can be performed for both CCT and slug tests; second, to combine the two tests to prolong the test duration in high-conductive formations; third, to validate the tool's performance with published field data.

Heat and Fluid Flow to Inversely Predict Rate

Prediction of flow rate using heat flow modeling can be applied to various applications in a wellbore. This work shows two such applications where the rate estimated serves different purposes. Analytical transient heat flow modeling has been carried out to generate flow rate to be used during transient testing and to predict zonal contributions during production logging, thereby offering opportunities for permanent downhole surveillance.

Fluid flow and heat transfer modeling in transient testing has been studied by many since the 1990's. Forward and inverse modeling has both become possible with the analytical tools developed since. Some of the more notable works involve Kabir et al. (1996), Fan et al. (2000), Hasan et al. (2005), Izgec et al. (2007), and Bahonar et al. (2011 a, b). In forward modeling these tools help determine the bottomhole pressure (BHP), wellhead pressure (WHP) and the wellhead temperature (WHT) using the reservoir and wellbore completion parameters. Inverse modeling on the other hand, is more complicated. Kabir and Hasan (1998) and Izgec et al. (2010) explored the different issues with inverse modeling in terms of the placement of gauges.

Most often for drillstem testing, pressure and temperature measurements are made at the wellhead and bottomhole. Distributed temperature measurements in this context are rarely reported, although they are quite prevalent in permanent completions. Numerous studies have been done on Distributed Temperature Sensing (DTS) and various applications are discussed in literature. Some of these applications include matrix treatment diagnosis (Glasbergen et al. 2009, 2010, Tan et al. 2012), zonal contribution assessment (Tardy et al. 2012, Parta et al. 2010), fracture-stimulation diagnosis (Tabatabaei et al. 2012), and injection profiling (Gao et al. 2008, Hoang et al. 2012), among others. Wang et al. (2008) presented an inverse model based on steady-state energy balance using DTS technology. Duru and Horne (2010) made use of DTS data for estimating formation parameters, such as permeability and porosity, among others, during transient testing.

Applicability of fluid temperature data in transient testing can also be extended to the near wellbore region. Since the near-wellbore properties are altered by the drilling operation itself, and the invasion of mud during over-balanced drilling, near-wellbore formation damage has been studied by investigators from various perspective over the years. From the standpoint of transient-pressure testing, analysis of cleanup data was investigated by Larsen and Kviljo (1990) and Larsen et al. (1990). In these studies, the authors explored the variable-skin concept *en route* to establishing the attainment of cleanup. They showed with field data that the derived skin declines in a hyperbolic fashion in conventional tests. Stated differently, production of the invaded mud filtrate declines hyperbolically. This finding has considerable merit in that diminishing influence of the unwanted phase with time was learned.

Systematic studies have also evolved in understanding variable skin in wireline-formation testing, wherin similar tests are run, but at a much reduced scale of producing rate and time. Studies of Goode and Thambynagyam (1996), Alpak et al. (2008), Ramaswami et al. (2012), among others, are cases in point. As expected, declining skin turned out to be the norm. Skin evolution has also been observed by Clarkson et al. (2013) in coal-bed methane wells. They coined the term dynamic-skin ratio, which was included in the dimensionless type-curve variables and flowing-material-balance formulation to include the effect of changing skin. More recently, Theuveny et al. (2013) explored various nuances of near-wellbore and wellbore cleanup operation with a transient multiphase wellbore simulator coupled with a reservoir-flow simulator.

The objective of this part of the study is two-fold: to estimate rate from distributed temperature measurements, available for downhole telemetry, with transient analytical model, and to use the computed rates to perform transient analysis for both the pre- and post-cleanup periods. Comparing and contrasting permeability estimates from the two periods would provide guidance on the suitability of such a practice.

Another application of the proposed model is derived from production logs. The field of production logging (PL) dates far back to the 1930s when the first temperature surveys were used to locate fluid entries in a wellbore (Schlumberger et al. 1937). The subsequent years saw more development in the techniques and methodologies with injection of cool fluid to locate permeable zones (Millikan 1941), inclusion of flow rate and pressure measurements to the temperature surveys (Dale 1949; Riordan 1951), and finally density and capacitance measurements to resolve complex multiphase flow behavior issues (Wade et al. 1965). Since then, production logging has evolved significantly to how it is known at present and more evolving approaches and techniques are still being added today. Though PL service companies now boast of a whole suite of tools that can aid in logging interpretation, one measurement that has always remained at the forefront of production logging is temperature logging. This is primarily because of its reliability; no matter what the wellbore flow conditions, temperature can be measured accurately.

A temperature log is probably the simplest, most accurate, and most widely applicable production log. Temperature logging has been used for a variety of purposes in the past that included location of gas entries, detection of casing leaks and fluid

movement behind casing, location of lost circulation zones, and evaluation of cement placement (Schlumberger et al. 1937; Millikan 1941; Halbouty 1939; Goins and Dawson 1953; Kunz and Tixier 1955). However the most common use over the years has been qualitative identification of injection or production zones. There have been different methods in literature attempting to quantify the fluid inflow or outflow as well. Ramey (1962) developed the pioneer equations that related wellbore fluid temperature to several formation and completion parameters for the case of flow in tubing or casing. Witterholt and Tixier (1972) extended the applicability of Ramey's work for quantitative temperature log interpretation for injection. Similar was done by Curtis and Witterholt (1973) for producing wells. Meanwhile Romero-Juarez (1969) published his own method for quantitative interpretation. Hill (1990) has summarized quite a few of those methods. Since then, there have been other works in the area. More recently, flow rates from temperature measurements have been estimated by Wang et al. (2008), Yoshioka et al. (2009), Izgec et al. (2010), Kabir et al. (2012) and Kabir et al. (2014). In most cases except the last, these works have used steady-state models that do not factor in time dependence and therefore neglect the transient response of the reservoir. This part of the thesis proposes to use the described model as a means for continuous production surveillance. Permanent downhole sensors can be used to relay temperature of the flowing fluid which can then be used with a calibrated transient model to predict rate from different zones, hence eliminating or reducing the need for expensive production logging surveillance runs during the course of a well's lifetime.

Flow for Optimization During Plunger Lift

Towards the end of a well's production, fluid and heat flow become more interesting especially with artificial lift methods involved. With depletion of gas reservoirs, the removal of produced water from the wellbores becomes less efficient. This inefficiency gives rise to water accumulation in the wellbore, a phenomenon known as liquid loading. The consequent increase in bottomhole flowing pressure significantly reduces gas production. A recent study of Riza et al. (2016) explored various mechanisms of liquid loading. One of the many methods used to combat this issue involves a plunger. Plunger lift is a method that uses the energy of the gas/liquid well in a more efficient way by allowing a free piston to travel up and down the tubing in a cycle.

Plunger lift is a great option for low productivity, high gas/liquid ratio (GLR) wells. Its major advantages include zero input energy, relatively small investment, reasonable operating costs, and efficient removal of paraffin and scale depositions. Perhaps the main disadvantages may stem from the requirement for continuous monitoring, complexity of the lift process itself, and a lack of understanding of optimizing and troubleshooting the lift method.

Several authors have addressed the modeling of plunger-lift installations. Some of these models have been accepted due to their simplicity, others require a greater deal of time and data for designing and analyzing plunger-lift system performance. One of the earliest seminal works was that of Foss and Gaul (1965), in which they presented a force-balance analysis on plunger lift. They presented their design criterion in the form

of charts that use values of parameters, including an average plunger velocity, based on their experience from operations at a particular field. Attempts have been made to improve on the Foss and Gaul study by changing values of liquid load size, plunger average velocity, flow line pressure, effect of pipe diameter, etc. (Hacksma 1972, Abercrombie 1980).

Lea (1982) developed a model expressing plunger velocity in terms of its acceleration, thus allowing plunger velocity to vary with depth. Improvement on Lea's model was attempted by many investigators (Rosina 1983, Marcano and Chacin 1994, Baruzzi and Alhanati 1995, Maggard et al. 2000, to name a few), generally by accounting for liquid fallback through field data or laboratory work. Gasbarri and Wiggins (2001) further advanced Lea's work by considering the plunger downstroke.

Recent advances in plunger lift system include development of 'smart plungers' that can record pressure and temperature data. This real-time measurement, in turn, helps optimizing the plunger lift performance. Chava et al. (2008, 2010) introduced significant improvement through the use of 'smart plunger' and developed a model for them. Tang and Liang (2008) also improved on dynamic modeling of plunger-lift system by combining it with field test data and not limiting to constant tubing pressure. More recently, simpler models for optimizing plunger lift performance in field operations have gained traction. For instance, Luo and Kelkar (2014) provided such a model that enables determining target casing pressure, leading to sustained production. Their model accounts for casing and tubing pressures before and after a plunger cycle, and the volumes of the tubing and tubing/casing annulus.

The modeling in this work offers a simple flow model for plunger lift based on energy balance by developing an expression for the minimum casing pressure needed for sustained production. To achieve this objective, the wellbore model is connected to a numerical reservoir model. This wellbore/reservoir connectivity allows determining the shut-in time needed to achieve the desired casing pressure for prolonging the production cycle. Equally important, besides understanding the current production and shut-in cycles in a given well, this forward model allows probing the suitability of a given well for plunger lift application.

CHAPTER III

MODEL DEVELOPMENT[1,2,3]

Flow problems such as those mentioned in the previous chapters can be broadly classified into either momentum transport or thermal transport. Though both kinds of transport problems may assume various forms, this thesis only discusses channel flow and more specifically pipe flow since that is the most significant form of momentum transport occurring inside wellbores. Similarly thermal transport can occur through various means but this work only accounts for the major components of thermal transport occurring inside the wellbore: the molecular energy transport and the convective energy transport.

For momentum transport in wellbores the main objective is to get a relationship between the volumetric flow rate and the pressure drop and elevation change. This relationship is addressed when modeling for short-term fluid flow models for reservoir evaluation and for flow optimization during plunger lift. Thermal transport in wellbores, on the other hand, involve accounting for heat conduction in fluids moving through the wellbore, heat conduction between the different tubulars and cement and finally

---

[1] Part of this chapter is reprinted with permission from "Simplified Modeling of Plunger-lift assisted production in gas wells" by G.M. Hashmi, A.R. Hasan, and C.S. Kabir, 2018. *J. Nat. Gas Sci. & Eng.*, **52**, 454-460, © 2018 by Elsevier B.V.

[2] Part of this chapter is reprinted with permission from "Design and Interpretation of Transient Tests at Well's Inception" by G.M. Hashmi, C.S. Kabir, and A.R. Hasan, 2016. *J. Pet. Sci. & Eng.*, **145**, 573-584, © 2016 by Elsevier B.V.

[3] Part of this chapter is reprinted with permission from "Estimating Reliable Gas Rate with Transient-Temperature Modeling for Interpreting Early-Time Cleanup Data During Transient Testing" by G.M. Hashmi, C.S. Kabir, and A.R. Hasan, 2015. *J. Pet. Sci. & Eng.*, **133**, 285-295, © 2015 by Elsevier B.V.

conduction between the well system and the rock formation. The convective part of the transport is due to the bulk motion of the fluid and is dependent on the density of the fluid. These methods of energy transfer are accounted for in the thermal modeling to inversely predict rate.

Each of the modeling techniques is separately discussed below for the sake of clarity.

Short-term Fluid Flow Models for Reservoir Evaluation

The study explores the feasibility of conducting short-term tests at a well's inception to evaluate reservoir parameters that can aid in long-term testing, if needed. Our first objective was to develop a design tool for such tests. The design tool allows for the generation of pressure and flow data for a given set of reservoir and wellbore parameters. Similar to conventional tests, both pressure and flow rates are required for test interpretation. Most published studies are intended for test analysis and are not conducive for design calculations or forward simulations. In contrast to previous studies, this one presents a simple model based on a mechanistic approach to design these short-term tests. Although simple, the model comprehensively accounts for the pressure drop in both the wellbore and reservoir.

Wellbore/reservoir coupling is implicit in our modeling approach. The wellbore model includes the gravitational, frictional, and accelerational effects to allow estimation of rate from pressure data. The accelerational effects are often insignificant for liquids. However, frictional effects are very significant due to high initial flow rates. Most

existing models for short-term tests neglect frictional effects. The reservoir model assumes infinite-acting radial flow, which bodes well considering the short duration of the test. Convolution of rate and pressure constitutes the main part of analysis, although short-term pressure analysis, considering just the total accumulated fluid prior to shut-in (Soliman 1986), is also used for comparison.

The slug model is ideal for underpressured reservoirs in which the fluid will not reach the surface without supplementary techniques, such as artificial lift. At the inception of such a well, the well is perforated and the tester valve opened. The consequent liquid influx inside the wellbore continues until the static head equalizes the reservoir pressure. Such a test can be designed easily with the use of static and other pressure-drop components in the wellbore and the flow equation in the reservoir. The model accounts for all fluids inside the wellbore, calculating the bottomhole pressure at each timestep. The bottomhole pressure is then matched with the flow equation, thereby calculating rate given the reservoir parameters. Appendix A provides the details of the model and computational algorithm. The reservoir flow equation used includes the rate superposition effects with the infinite-acting radial flow model. Any reservoir model can be substituted for the problem; however, given the short duration of the test, our approach appears prudent.

Our computational algorithm relies on the premise that the bottomhole pressure (p_{wf}) calculated using heights of various fluids in the wellbore at any timestep j, must equal p_{wf} calculated from the reservoir equation. This equality allows us to calculate flow rate q_j during that timestep. This step is feasible because p_{wf} computed from the reservoir

equation depends on a unique value of reservoir influx. This rate q_j, assumed constant over the small timestep, allows us to compute the volume of reservoir fluid. These entities allow us to compute p_{wf} at the next timestep $j+1$ at the sandface, and the procedure is repeated for the entire test duration. Appendix A presents the computational approach and the working equations.

We note that variation of liquid properties with well depth is minimal; therefore, liquid sections in the wellbore were discretized into no smaller than 250 ft cell in all examples. In contrast, the gas chamber at the top was divided into 100 ft cells. Computation starts with a known fluid level in the wellbore or with a known bottomhole pressure at the start of the test. Thereafter, pressure components for each timestep are calculated using the different pressure components in the wellbore. Next, the bottomhole pressure is calculated using the design parameters of the reservoir, such as permeability, porosity, and compressibility, and the reservoir flow equation. Equating the two sources of pressure yields the desired flow rate. This computation is repeated at each timestep resulting in the desired time-dependent pressure and rate profiles.

Figures 3.1a and 3.1b present the schematics for a slug and a closed-chamber test, respectively. With the rise in the fluid level in Figure 3.1a, the bottomhole pressure increases. This pressure rise, in turn, reduces the drawdown with time and brings about a consequent decline in flow rate. Eventually, the higher density fluid in the wellbore kills the relatively underpressured reservoir, leading to flow cessation. In Figure 3.1b, the top cell contains gas or air, followed by the wellbore liquid, and the incoming reservoir fluid.

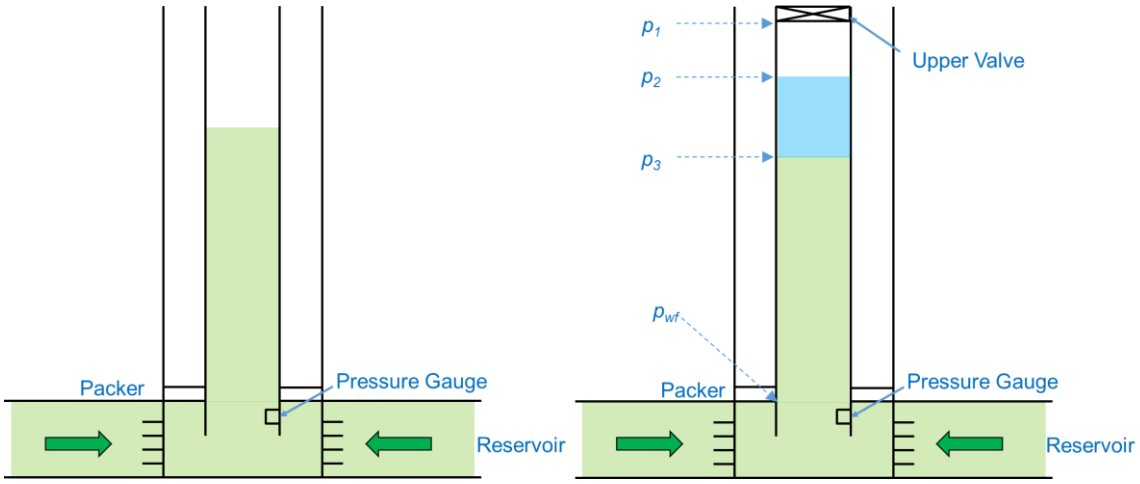

(a) **(b)**

Figure 3. 1 – Schematic for slug (a) and closed-chamber (b) test. (Hashmi et al. 2016)

Figures 3.2a and 3.2b illustrate the typical responses for slug and closed-chamber tests. As in Figures 3.1a and 3.1b, with rise in the fluid level the bottomhole pressure increases, which reduces the drawdown with time and results in a declining flow rate. In the case of a slug test, the higher density fluid in the wellbore kills the underpressured system, whereas in the case of CCT, the chamber pressure increases dramatically along with the rise in static fluid pressure, thereby generating a spike in the bottomhole pressure.

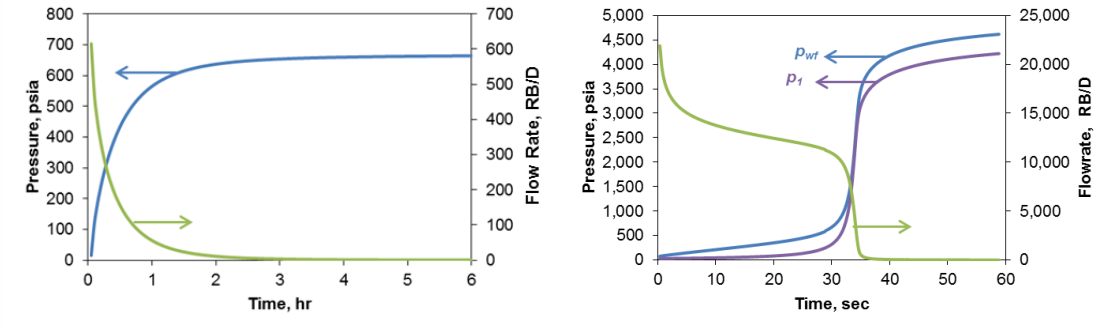

(a) **(b)**

Figure 3. 2 - Typical pressure/rate responses for slug (a) and closed-chamber (b) tests.
(Hashmi et al. 2016)

Our closed-chamber model is very similar to the slug model. However, in this model, the well is shut-in either at surface or at a specific depth in the wellbore, hence the term 'closed-chamber.' Figure 3.1b illustrates the physical mechanism for a CCT where fluid enters the wellbore after perforation, thereby increasing the bottomhole pressure. However, in this case the well being shut-in at the head (or some other appropriate location), the gas between the rising fluid column and the valve becomes trapped. Consequently, this chamber of gas is compressed with the increase in fluid level, causing a dramatic increase in pressure and a corresponding decline in flow rate.

This closed system allows handling of reservoirs with diverse geopressure gradients. Intrinsically, the closed-chamber system demands a different treatment for wellbore pressure computation. For instance, gas compression in the chamber largely influences the static pressure component in the wellbore, which, in turn, increases the chamber and bottomhole pressures. Appendix A provides details of these calculations.

Computation proceeds as it would in a slug test. However, in a CCT, the pressure stabilization takes place after the chamber pressure has stabilized. Just as in the slug test model, this CCT model also allows for forward design calculations to assess various design variables, such as the chamber length and static backpressure at the start of test. Test design calculations are critical to CCT because significant gas compression in the chamber can compress the test duration to seconds in high-conductive formations. This ability to design any test by forward modeling is one of the strengths of this simple yet accurate model.

Heat and Fluid Flow to Inversely Predict Rate

This part of the thesis develops thermal transport equations in the wellbore to inversely predict rate. The study was made with regards to several different applications, the most important of which were pursued and are highlighted. The first application involves predicting rate from measured temperature data at multiple depths to be used during transient testing. The study interprets cleanup data in a gas well using rates that are estimated from distributed-temperature measurements. This strategy requires robust fluid temperature models that estimate rates during drawdown periods. During production, fluid temperature at various depths in the wellbore can be estimated using the fluid rate. When the distributed temperatures are available, the opportunity arises to solve the inverse problem for estimating rates. As discussed earlier, the technique for estimating rate with steady-state models has been used for the stable flow condition. That methodology is applicable only when the fluid and heat flow attain stability. In this

study, we show the innovative use of temperature transients for estimating rates under variable-flow conditions. In addition, we investigate the improvement caused by incorporating depth-dependent temperature superposition in both the steady state and the transient models. In the following sections, we offer the operating equations. Appendix B details the model derivation and definition of various terms.

All flowing fluid-temperature models assume that heat exchange between the formation and the fluids remain constant throughout the entire production period. In general, however, fluid temperature tends to approach the surrounding formation temperature, thereby decreasing heat transfer rate with time. To account for this changing heat flow, the superposition principle is used. We emphasize that this model is intended for superposition of heat flow for a given rate. Therefore, for the models given below, we employ superposition of heat flow to account for temperature transients for a given gas rate. For subsequent changes in gas rate, the final temperature of the previous rate is used as the boundary condition.

Transient-Temperature Model

When production is initiated or when the production rate is changed, thermal transients set in that take a much longer time to stabilize than its pressure counterpart. Generally speaking, the flow rate becomes stable soon after its initiation or change from one rate to another. However, temperature changes for the corresponding period take a much longer time to attain stability. Assuming that mass and momentum transients of wellbore fluids die rapidly, we derive an expression for the transient-fluid temperature

that is detailed in Appendix C. We account for the effect of variable heat flux at any discrete time by adding ξ that represents the superposition term, as shown in Appendix B. Using the ξ term, we derived the following expression for transient flowing fluid temperature:

$$T_f = T_{ei} + \frac{(1 - e^{-at})\left(1 - e^{(z-L)L_R}\right)}{L_R}(\psi + \xi) + (T_{fi} - T_{ei})e^{-at} \tag{3.1}$$

where

$$L_R = \frac{2\pi}{c_p w}\left[\frac{r_t U_t k_e}{k_e + (r_t U_t T_D)}\right] \tag{3.2}$$

and

$$\xi = -T_D\left(t_D - t_{D,n-1}\right)\frac{L_{Rn}Q_{n-1}}{2\pi k_e} + \frac{L_{Rn}}{2\pi k_e}\sum\nolimits_{n-1} \tag{3.3}$$

In Eq. 3.1, the system constant *a* represents thermal storage for both the fluid and tubulars, as defined in Appendix C. The approach adopted here is a major improvement over that reported earlier by Kabir et al. (2014). We discretized the wellbore into sections and calculated the pressure traverse along with the temperature profile.

Computation starts with a known pressure and temperature at the bottomhole. Thereafter, Eq. 3.1 allows calculation of pressure and temperature at the next depth segment, and this computation continues until the desired depth is reached for a given time-step. We calculate the pressure using the methodology explained in Hasan et al. (2010) and Hasan and Kabir (2002). Next, we divided the flow period into time

segments and compute similar temperature and pressure profiles at each time-step, thereby ensuring that the previous history is accounted for as given in Eq. 3.1. Appendix B details the computational approach as outlined here.

We then compare the final calculated temperature with those measured at different depth intervals. As expected, the solution gets increasingly robust with the increase in fidelity of temperature response that occurs at shallower depths. The overall match provides the flow rates by honoring the discrete temperature data at the end of each flow period. We also show the results for a case wherein only one shallow interval is considered to explore the option of rate estimation when data from discrete stable rate intervals are available. Exploring this option has considerable merit in that in most instances the distributed-temperature profile is exception rather than the norm.

Estimating Flow Rate from MTS Data

As Eq. 3.1 shows, the fluid temperature T_f depends on L_R, which, in turn, depends on the mass rate w as shown in Eq. 3.2. This dependence of rate on fluid temperature, however, is nonlinear and requires an optimization approach to calculate the best value for w for a given T_f. Recently, Kabir et al. (2014, 2012) have described methods for best possible rate estimation for a given fluid temperature.

In this study, transient fluid temperature data over more than 100 hours are available for multiple flow rates at various well depths. We use an iterative procedure that consists of guessing a rate, followed by calculating the fluid temperature throughout the wellbore for a given time. The errors in calculated fluid temperatures compared to

the MTS values at various stations constituted a part of the objective function in the optimization scheme. Minimizing the objective function in a spreadsheet yielded the optimum rate. Various thermal properties used in these computations remain unchanged for all rates and wells. Thermal modeling of the entire wellbore allowed accounting for variation in well configuration and attendant changes in heat-transfer coefficient.

Computations showed that dual rate solution, although rare, is possible for a given temperature; a phenomenon we termed temperature inversion. We have noted this phenomenon before and have explained it in detail (Kabir et al. 2014; Ismadi et al. 2012). When temperature inversion occurs, we use fluid pressure in conjunction with temperature to obtain the appropriate rate.

The second application uses similar transport equations to determine production inflow from temperature logging. The models account for the conductive heat loss to the formation as the fluid travels up the wellbore, as well as the convective energy transport in and out of the control volume. The approach includes similar analytical wellbore fluid transient-temperature model as presented previously and shown in Eq. 3.4 through Eq.3. 8.

$$T_f = T_{ei} + \left(T_{fi} - T_{ei}\right)e^{-at} + \frac{(1 - e^{-at})}{L_R}(1 - e^{(z-L)L_R})(\psi) \tag{3.4}$$

Where

$$a = \frac{wc_p L_R}{mc_p(1 + C_T)} \tag{3.5}$$

$$L_R = \frac{2\pi}{c_p w}\left[\frac{r_t U_t k_e}{k_e + (r_t U_t T_D)}\right] \tag{3.6}$$

$$\psi = g_g sin\theta + \Phi + \frac{g\ sin\theta}{g_c J c_p} \tag{3.7}$$

$$\Phi = C_j \frac{\mathrm{d}p}{\mathrm{d}z} - \frac{v\frac{\mathrm{d}v}{\mathrm{d}z}}{g_c\ J\ c_p} \tag{3.8}$$

The procedures undertaken during conventional production logging, such as varying choke settings and different flow and shut-in conditions, often introduce transients into the fluid and thermal transport. Steady-state models for such estimations, therefore, can lead to serious errors. They can often only be used when the fluid and heat flow attain stability, which may require hours after a rate change occurs. Consequently, this study uses the mentioned transient model to estimate rates under variable flow conditions during production logging.

Figure 3.3 summarizes the methodology followed. Unlike logging with a spinner in which the spinner revolutions are measured and then later transformed to flow rate from a certain producing zone, this technique begins with the answer. Similar to the previous application, a flow rate is assumed for each of the producing zones and used to

calculate the fluid temperature profile that should exist in the well, based on the flow rate and the time duration of flow. The model considers the wellbore and completion characteristics and the fluid and formation properties. All properties may or may not be known with certainty, and that is where the spinner helps to calibrate the model. After the model has been calibrated, it can then be used to estimate fluid temperature and to compare that fluid temperature against the measured temperature profile. The difference between the two can be reduced by applying an inversion technique and changing the flow rate. Following the same procedure for different producing zones in the same well should provide a generalized flow rate from each of the zones.

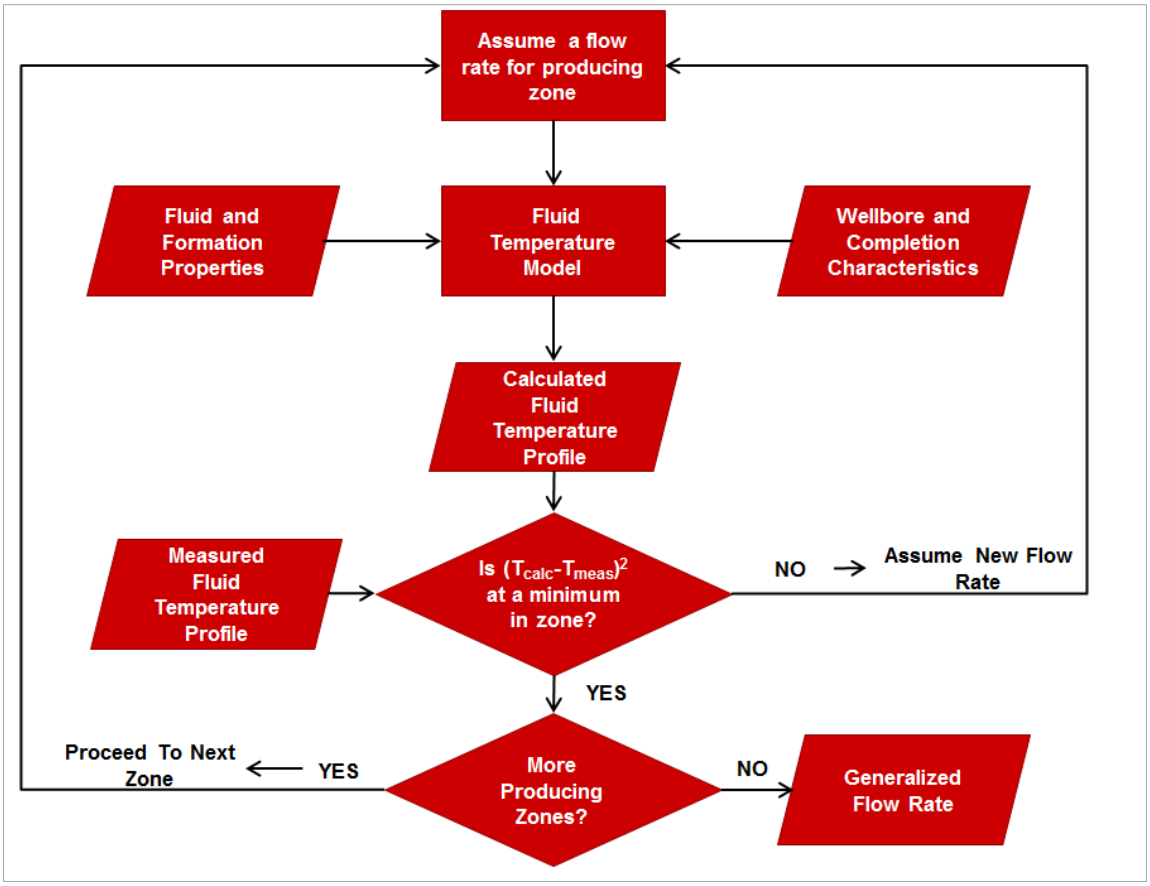

Figure 3. 3 - Summary of the rate estimate workflow from temperature logging.

Flow for Optimization During Plunger Lift

Lastly, this section of the thesis revisits the flow modeling inside the wellbore with different initial, operating and boundary conditions. When a gas well begins to load up, its production starts to decline and ultimately the well dies. One way to avoid a well getting ultimately 'killed' by liquid loading is to shut the well in (stopping production), and let the pressure at the well bottom build up. Then open the well at an appropriate time (when the bottom pressure has built up "enough") so that there is enough energy for

the well to produce again for quite some time. This process of shutting in the well to build up the pressure and then flowing the well can be aided by a plunger. Plunger lift uses the built-up energy of a temporarily shut-in well to move much of the accumulated liquid up from the well bottom to the surface.

To efficiently run this cyclic process of shutting in and restarting production, the well should not be shut-in for too long; yet, must be shut-in for long enough for the pressure to build up to a certain level that allows continuous production for quite some time. The objective of this part of the study study is to develop a model that enables estimation of pressure buildup in the well after shut-in, which allows subsequent sustained production.

Assumptions:

1. Efficient production requires a gas well to operate in the annular 2-phase regime. During annular 2-phase flow, especially at the low pressures of brown fields, liquid volume fraction in the wellbore is likely to be less than 5%. For estimating wellbore gas mass, we assume that most of the tubing and annular spaces are filled with gas.
2. The production ceases upon closing the tubinghead valve, thereby allowing afterflow to occur from the reservoir to accumulate in the tubing/casing annulus.
3. After pressure buildup and when the plunger is released, the pressurized annular gas lifts the plunger along with the liquid and the gas on top of it.

4. The pressure-volume (pV) work done by the pressurized annular gas must also account for energy needed to lift the liquid and gas on top of the plunger, and the friction during plunger movement.
5. After the plunger reaches the top, the pressure at the tubinghead will be the known line pressure that needs to be maintained for quite some time (for sustainable production) before the next cycle begins. Therefore, for calculating pV at the end of upward plunger movement, the line pressure will be used along with the well volume.
6. The pressures at the top and bottom of the tubing and casing are related by the exponential expression for the standing-gas column, $p_{bh} = p_{wh}e^{(gMD)/(RZTg_c)}$ where M is the gas molecular weight and D is the vertical distance between wellhead and bottomhole. In other words, the wellbore liquid is accounted for while estimating liquid holdup.

The plunger should be released from the bottom seat only after the annular pressure has increased high enough so that the tubinghead pressure reaches above the line pressure upon expansion of fluids, and the arrival of the plunger and liquid to the wellhead. We analyze the process by examining the energy available just before the plunger starts ascending and compare that to the final state of the process when the plunger has moved all the way up. We use the pressures at the tubinghead (p_t) and casinghead (p_c) to represent the pressure in the entire tubing and casing, respectively.

Energy available in the annular gas just before the plunger is released is the pressure-volume (pV) work that equals p_cV_c (ft-lbf), where V_c is the total volume of the

gas in the tubing/casing annulus. This energy must be at least equal to the final pV work that is given by $(pV)_{\text{total}} = (p_t V_c + p_t V_t)$. Besides, energy must be spent to move the plunger, and water and gas on top of it to the wellhead (potential energy), and overcoming friction in doing so. The gain in potential energy of the plunger-fluid system is proportional to the total mass of plunger (m_p) plus fluid on top of the plunger (m_L+m_g). Therefore, energy balance is written as

$$p_c V_c = p_t(V_c + V_t) + \left(m_p + m_L + m_g\right)\left(\frac{g}{g_c}\right)D + F \tag{3.9}$$

The frictional loss of energy depends on the mass of the fluid plunger system, in addition to the well depth. For simplicity we assume that the frictional loss F is small compared to the other terms and is included in the gas static-head term as a small fraction C. Therefore, Eq. 3.9 can be rewritten as

$$p_c V_c = p_t(V_c + V_t) + \left(m_p + m_L + (1 + C)m_g\right)\left(\frac{g}{g_c}\right)D \tag{3.10}$$

Before the tubinghead valve is opened to allow the plunger to move up, the casing pressure must rise to a value given by the following expression:

$$p_c = \frac{p_t(V_c + V_t) + \left(m_p + m_L + (1 + C)m_g\right)\left(\frac{g}{g_c}\right)D}{V_c} \tag{3.11}$$

CHAPTER IV

MODEL APPLICATION AND VALIDATION[4,5,6]

The last chapter talked about the details and methodology that was adopted in the development of the mentioned models. Here we present some of the applications of the developed models and some field cases where the models were applied. The data was mostly obtained from literature. In the case of thermal modeling and rate inversion, data was supplied by Hess Corporation from their deepwater asset in Western Australia.

This chapter demonstrates the applicability of the proposed models in the field of transient well testing, production logging and artificial lift. Similar to the previous chapters, each category of the models is discussed separately with examples.

Short-term Fluid Flow Models for Reservoir Evaluation

Pressure and rate data from both slug tests and closed-chamber tests can be analyzed the same way. We adopted the convolution approach proposed by Meunier et al. (1985). All analyses showed that the input parameters of permeability and skin can be reproduced.

---

[4] Part of this chapter is reprinted with permission from "Simplified Modeling of Plunger-lift assisted production in gas wells" by G.M. Hashmi, A.R. Hasan, and C.S. Kabir, 2018. *J. Nat. Gas Sci. & Eng.*, **52**, 454-460, © 2018 by Elsevier B.V.

[5] Part of this chapter is reprinted with permission from "Design and Interpretation of Transient Tests at Well's Inception" by G.M. Hashmi, C.S. Kabir, and A.R. Hasan, 2016. *J. Pet. Sci. & Eng.*, **145**, 573-584, © 2016 by Elsevier B.V.

[6] Part of this chapter is reprinted with permission from "Estimating Reliable Gas Rate with Transient-Temperature Modeling for Interpreting Early-Time Cleanup Data During Transient Testing" by G.M. Hashmi, C.S. Kabir, and A.R. Hasan, 2015. *J. Pet. Sci. & Eng.*, **133**, 285-295, © 2015 by Elsevier B.V.

Case 1: Closed-chamber testing

The test design methodology is also able to replicate a closed-chamber test reported by Simmons (1990). As discussed earlier, reservoir fluid intrudes into the wellbore when the valve opens downhole. The bottomhole pressure increases, and so does the pressure of the gas chamber, which is the volume of gas between the closed upper valve and the rising liquid level. **Figure 4.1** demonstrates that sharp increases in the chamber and the consequent bottomhole pressures result in a precipitous decline in the flow rate. Because Simmons neglected frictional pressure loss, we used our model without accounting for friction to replicate Simmons' results.

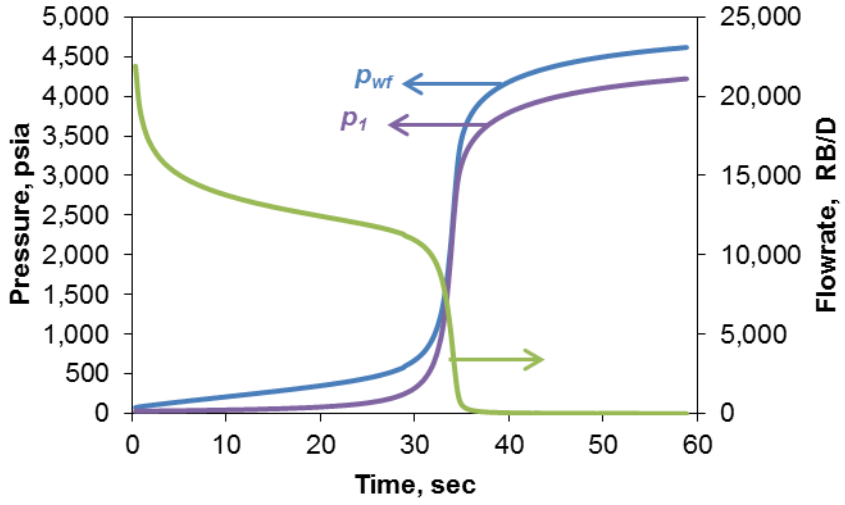

Figure 4. 1 - Pressure and rate response for the test reported by Simmons (1990) using the suggested model.
(Hashmi et al. 2016)

In most cases, frictional effects are very significant due to very high initial flow rates, induced by a large pressure differential in the wellbore. In some cases, acceleration may also play an important role. In the study by Simmons (1990), the accelerational and frictional effects were ignored. The design tool introduced in this study allows us to explore the effects of pressure-drop components and determine their impact quantitatively. **Figure 4.2** illustrates the model's significantly different pressure and rate signatures with and without friction. Many proposed models for short-term tests neglect this effect, which can provide misleading results for permeability. In most test situations, downhole pressure measurement and surface rate metering constitute the norm; therefore, data analysis implicitly accounts for the frictional effects. However, all these factors must be included during the design of such tests. Analyzing both sets of data in Figure 4.2 yielded about 54% higher permeability when friction was not accounted for than when it was.

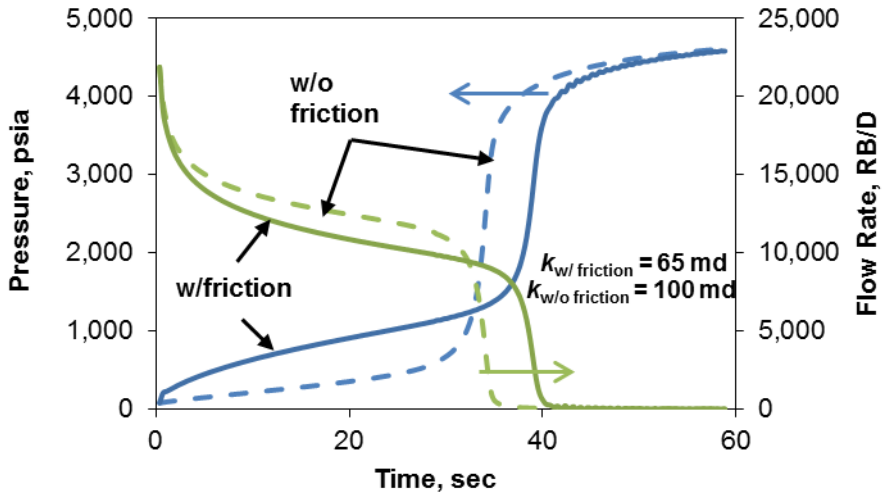

Figure 4. 2 - Pressure and rate responses for a CCT with and without friction; Neglecting friction overestimates permeability. (Hashmi et al. 2016)

When a CCT or a slug test is conducted either individually or in slug/CCT sequence, the signature of the calculated bottomhole pressure will be different, if frictional-pressure loss is accounted for compared to when it is not. When friction is considered, the initial calculated rate will be lower and BHP higher than that in a frictionless system. As the test continues, the calculated cumulative volume with friction will lag much behind that for the idealized frictionless system, thereby causing the liquid column in the wellbore to be much shorter than that for the frictionless case. At some point during the test, the lower static pressure from the shorter liquid column along with lower gas chamber pressure (due to larger volume) will make BHP with friction to be lower than that without. Ultimately, BHP with and without friction will become the same when the flow cessation occurs. Therefore, BHP without friction compared to that with friction, starts at a higher value, becomes equal to, then decreases to a lower value, and

ultimately becomes the same value. The differences between the two calculated BHP values for these tests depend on the flow rate and initial-gas-chamber height and, therefore, demand calculations for the entire time domain.

Case 2: Combined slug and CCT

This example presents a combined slug and CCT test to illustrate its merit and plausible applications in most situations. **Table 1** presents the pertinent reservoir, fluid, and well properties. The open wellhead valve constituted the slug test for the first six minutes, followed by a shut-in to perform the closed-chamber test. The overall test lasted for approximately two hours. The pressure and rate signatures obtained from the design were analyzed using the Meunier et al. (1985) approach to evaluate reservoir parameters.

Figure 4.3a shows the design aspect of the test and **Figure 4.3b** presents the convolution analysis of the combined pressure/rate response. The presence of a substantial amount of fluid in the wellbore before the flow starts keeps the initial chamber pressure low. The availability of the total chamber volume for reservoir fluid influx and the induced reservoir/wellbore pressure differential constitute the two key design variables. Figure 4.3b returns the same input parameters for the simulation, thereby reaffirming the integrity of the combined model.

Table 4. 1 - Input Variables for Example 1.

k	100	md	r_t	0.195	ft
h	30	ft	Depth	14,167	ft
φ	0.2		h_L	4,250	ft
μ	0.7	cp	ε	0.00015	ft
p_i	6676	psi	g_G	0.0081	°F/ft
B	1.33	rb/stb	T_{av}	185	°F
c_t	6.00E-06	psi^{-1}	Oil gravity	35	°API
c_f	1.70E-05	psi^{-1}	Gas gravity	0.65	
c_w	2.58E-06	psi^{-1}	ρ_f	67.32	lb_m/ft^3
r_w	0.42	ft	s	6	

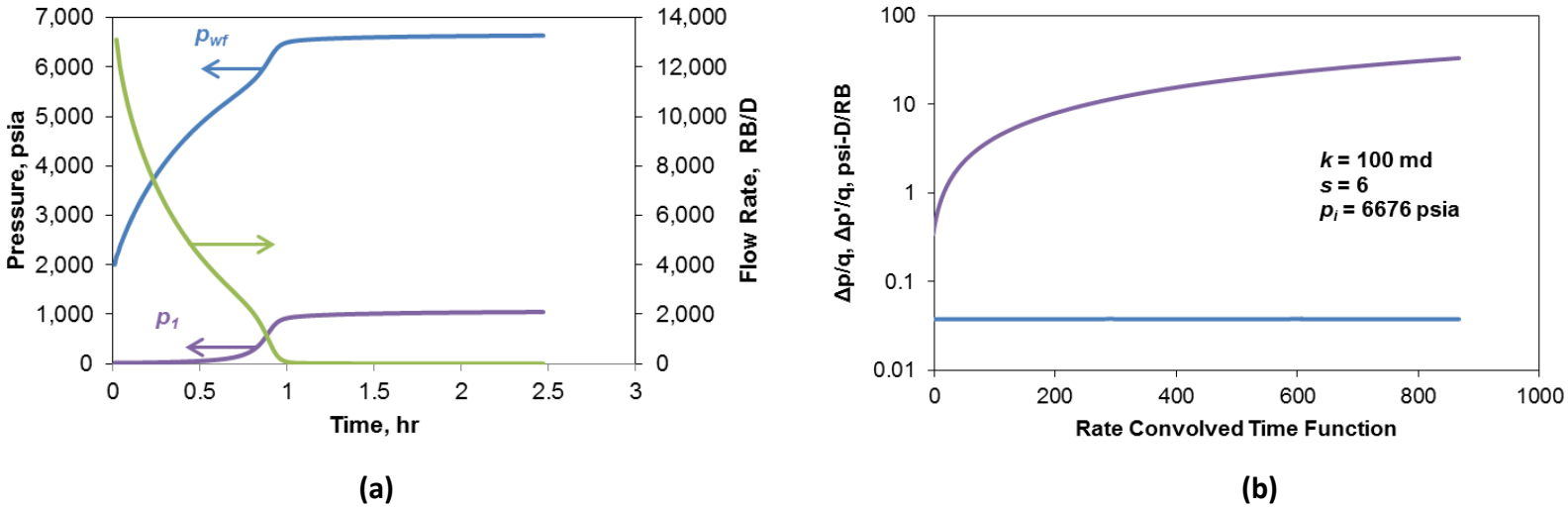

Figure 4. 3 - Pressure and rate responses in combined slug/CCT (a), and its analysis (b), Example 1. (Hashmi et al. 2016)

Case 3: Reverse slug or injection test

Similar to a slug test, fluid injection may be induced into an underpressured formation upon well perforating. In such a system, liquid-filled wellbore fluid triggers higher-pressure differential across the perforations into the reservoir, thereby triggering reverse slug test. The bottomhole pressure and injection rate allow an analysis similar to that discussed in the slug test. **Figure 4.4** presents a synthetic example of a short-term injection test design for an underpressured system and its analysis with the generated response. With the increase in injection volume into the formation, the wellbore liquid level continues to recede, leading to a continual decline in bottomhole pressure or the driving force; consequently, the injection rate declines with increasing backpressure. Flow ceases when the wellbore and the formation pressures are balanced.

Model verification with field examples

Example 1: Slug test

The first case discussed here is taken from Ramey et al. (1975). **Figure 4.5a** shows the test data along with pressures and rates derived from forward simulation, and **Figure 4.5b** illustrates the analysis involving both measured and derived pressures with computed rates. The solids lines represent the simulated response, whereas the symbols reflect measured data. As expected, the noise in pressure data precipitated the scatter in the derivative signature.

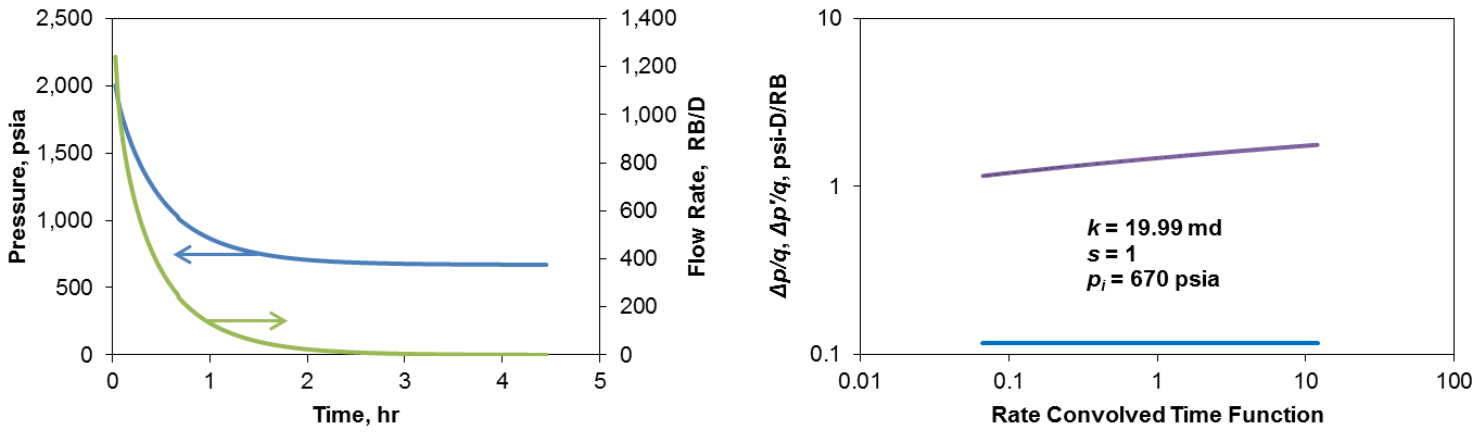

(a) **(b)**

Figure 4. 4 - Pressure and rate responses for a short-term injection test (a), and the convolution analysis (b). (Hashmi et al. 2016)

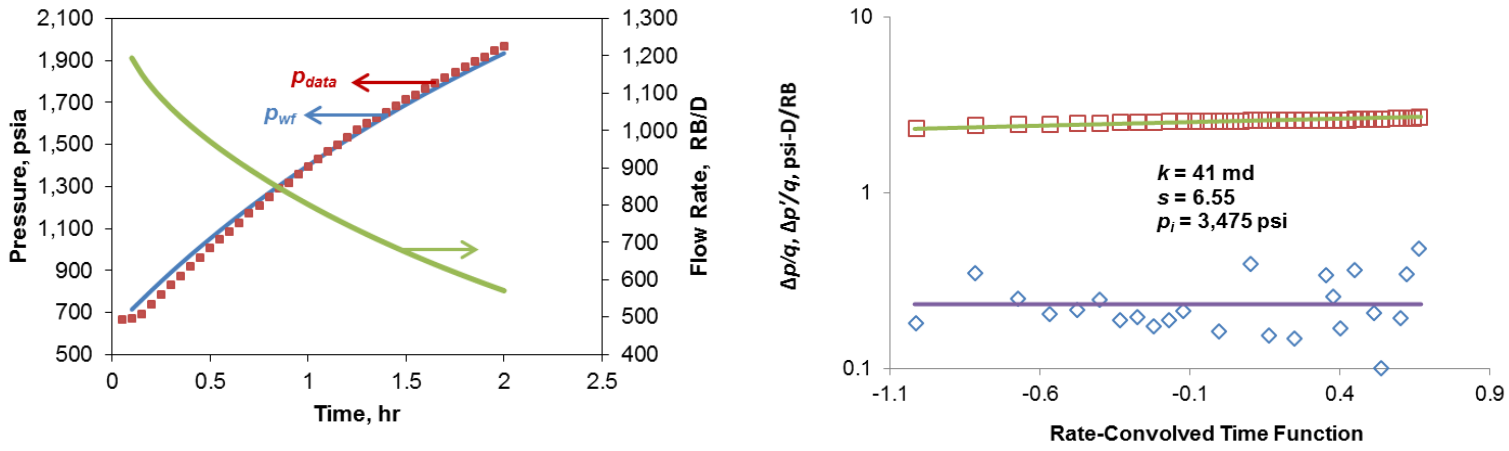

(a) **(b)**

Figure 4. 5 - Pressure and rate responses for the Ramey et al. example (a). Convolution analysis of field data shows some scatter (b).
(Hashmi et al. 2016)

Figure 4.5a shows that pressure increases as the liquid flows into the tubing, thereby increasing the bottomhole pressure and decreasing the drawdown in the reservoir that leads to a decrease in flow rate. The rate-normalized pressure and its derivative (Figure 4.5b) provide the measures for the analysis of such a test whereby permeability, skin, and initial pressure can be determined.

Ramey et al. (1975) introduced this test using a type-curve approach. The approach entails calculating the pressure-difference ratio curves at different times using the different reservoir variables and then matching the curves generated with the actual pressure data. Both the approaches present similar results, which serve to validate the model developed in this study. Rate calculations were not intrinsic to Ramey's analysis; therefore, the design aspect of the test differs from that presented in this work. **Figure 4.6** compares the data from Ramey et al.'s example and the generated response from the proposed model. Similar to Ramey's model, the model proposed in this study gives a good match at larger times.

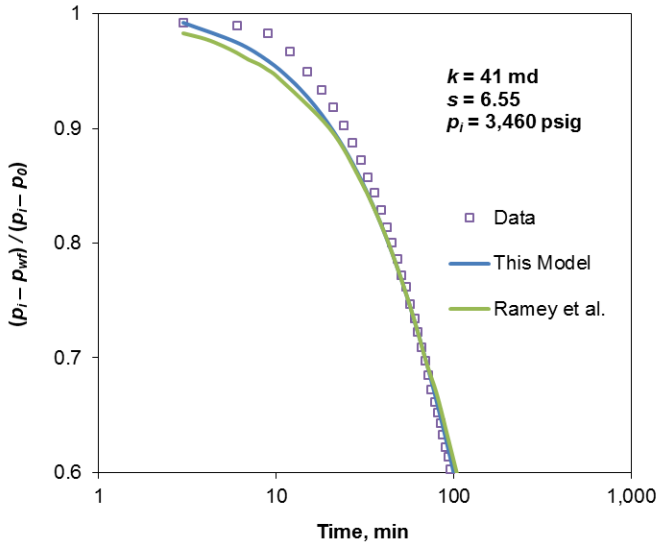

Figure 4. 6 - Semilog type-curve match for Ramey et al.'s example compares the generated and measured pressure responses.
(Hashmi et al. 2016)

Let us generate pressure and rate signatures that are distinctly different by combining the slug test with CCT using forward simulation. The intrinsic idea is to ensure solution uniqueness in these short-duration tests with monotonic trend, if only one is pursued. **Figure 4.7a** presents the simulated response of the combined test, and **Figure 4.7b** shows the solution. As expected, the same results are obtained, as shown earlier in Figures 4.5b and 4.6.

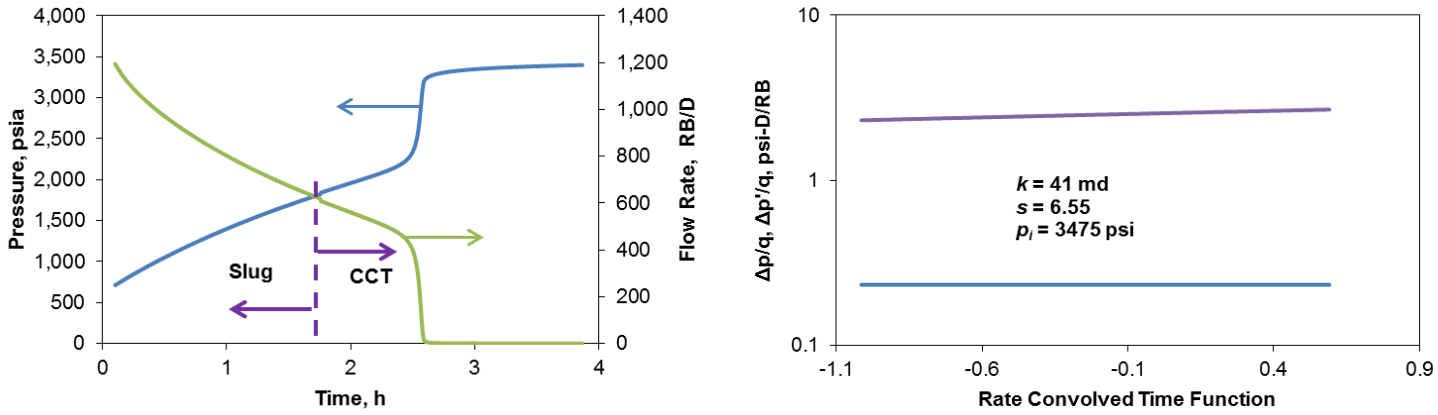

(a) **(b)**

Figure 4. 7 - Pressure and rate response for the combined slug-CCT (a) and analysis (b) for Example 1. (Hashmi et al. 2016)

Example 2: Reverse slug test

This example compares the proposed model with the falling-head test (FHT), an injectivity test illustrated by Sufi and Thompson (1988). The test was conducted on a well in the Athabasca tar-sands deposit in Alberta, Canada. **Table 2** provides the reservoir, fluid, and well properties. The test continued until the pressure stabilized and injection ceased.

Table 4. 2 - Input Variables for Example 2.

k	7	md	r_w	0.4	ft
h	11.8	ft	r_t	0.120	ft
φ	0.35		Depth	754	ft
μ	1.3	cp	ε	0.00015	ft
p_i	130	psi	g_G	0.02	°F/ft
B	1	RB/STB	T_{av}	85	°F
c_t	2.30E-05	psi^{-1}	Oil gravity	1.032	
c_f	1.70E-05	psi^{-1}	skin	0.01	
c_w	2.58E-06	psi^{-1}			

Figures 4.8a and 4.8b provide the design obtained for the test using the proposed model and its analysis using convolution. Flow rate and pressure both decrease

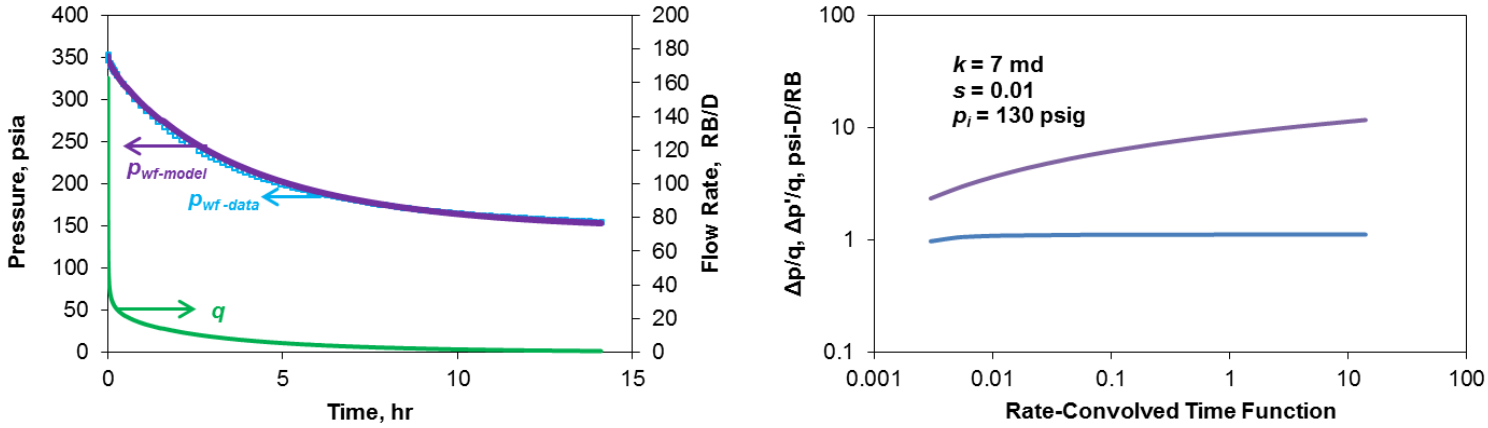

(a) **(b)**

Figure 4. 8 - Pressure and rate responses (a) and analysis (b) for Example 2. The wellbore model reproduces measured pressure well.
(Hashmi et al. 2016)

in this example due to self-injection of fluid in the reservoir that decreases the level of fluid in the wellbore. The test continued for about 14 hours, at which point the flow rate becomes imperceptible. The analysis showed that a permeability of 7 md with a negligible skin was obtained for the example. These results compare favorably with the reported data from the actual test of permeability 5.8 md with a negligible skin (0.04).

The generated pressure response shown in Figure 4.8a compares well with the actual test response that was measured in the field. **Figure 4.9** compares these two responses and shows the type curve match for the test. The overall match quality is a reflection of the fact that the gravity-induced flow triggers minimal friction in the wellbore.

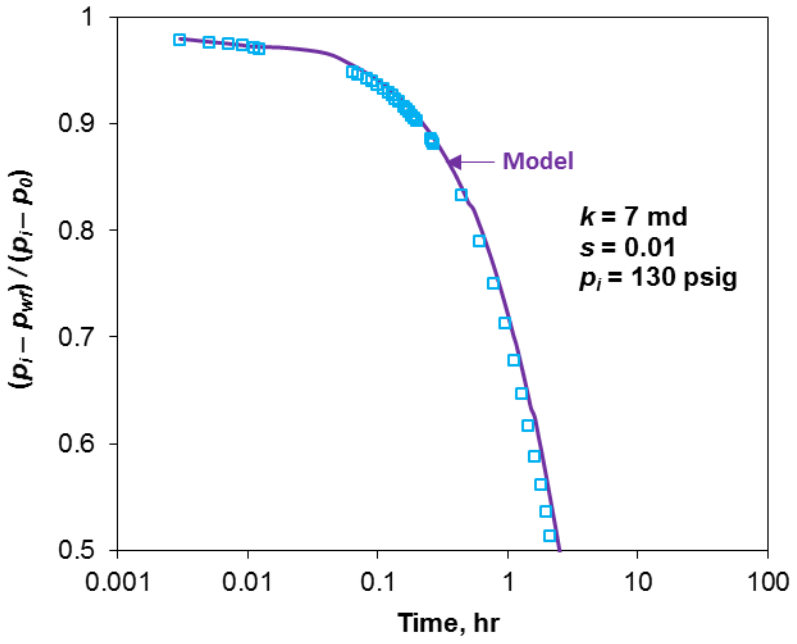

Figure 4. 9 - Semilog type curve match compares with generated and measured pressure responses, Example 2.
(Hashmi et al. 2016)

Besides the heavy-oil setting, FHT is also conducive to any underpressure reservoir that is below the normal hydrostatic-pressure gradient of 0.433 psi/ft. Reservoirs that were deposited with rapid burial followed by tectonic uplift constitute the natural system, and those normal pressure reservoirs that have undergone pressure depletion are amenable to such tests. Examples of naturally occurring underpressured reservoirs include those in the Rocky Mountain basin and some in Nevada. Iraq's Kurdistan region also has reservoirs where the water table occurs above the sea level, thereby causing underpressured hydrocarbon accumulations.

Example 3: Closed-chamber test

Examples 1 and 2 have shown analyses of two forms of slug test. This example allows us to test the model's strength of analysis on yet another case from Alberta, Canada, where closed-chamber testing was conducted. This example was initially presented by Kabir et al. (1991). Although the test involved two-phase flow, fairly accurate analysis was performed with single-phase considerations. This favorable condition resulted from the relatively low-gas rates. Measured pressure was available for both the bottomhole and the top of the enclosed chamber. Using the measured pressure, we calculated the liquid height as a function of time which provided liquid rate. **Figure 4.10a** shows both the pressure profiles and the estimated flowrate. Once pressure and flow rate were estimated, the convolution analysis yielded permeability and initial-reservoir pressure estimates, as shown in **Figure 4.10b**.

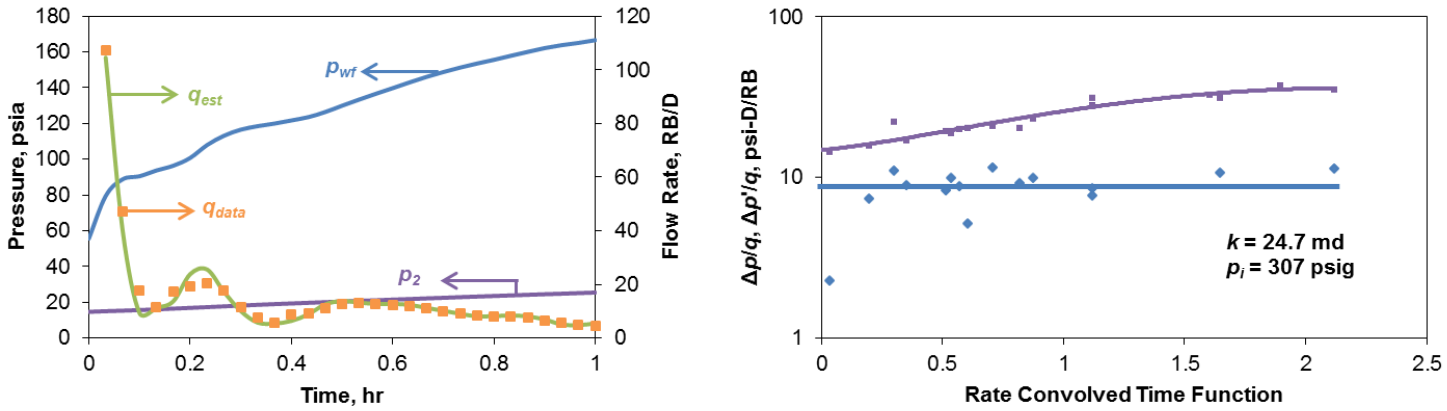

(a) **(b)**

Figure 4. 10 - Pressure and rate profiles for CCT (a) and convolution analysis generates noisy solution of field data (b), Example 3.
(Hashmi et al. 2016)

Example 3 highlights the short-term nature of CCT with meaningful analysis. The test takes about an hour to complete, providing us with important reservoir information. Although the test started with multiphase flow, only single-phase flow was considered during the analysis, culminating in reasonably good match with the reported data.

Example 4: CCT and conventional test

This field example explores the frictional-pressure-drop question with a field example during CCT, a point made earlier with a synthetic case in Figure 4.5. Earlier, Soliman et al. (2004) presented this example while revisiting short-term tests. **Figure 4.11** shows the computational and interpretative results of the short-duration CCT as presented in this study. Inclusion of friction allowed the results to be in better alignment with those obtained from the long-term tests run on this well. **Figure 4.12** illustrates this point when the results are compared with those of previous analyses of CCT and long-term tests**.**

As indicated earlier, the monotonic test response of either the CCT or slug test can be improved by combining these two tests. In this case, let us consider rerunning both tests for the same total time period of 0.3 hr, with 0.15 hr for each test. **Figure 4.13a** captures the two different signatures in this simulated test, and **Figure 4.13b** shows the same solutions as those in Figure 4.11b. This combined test suggests that the afterflow ceased in 0.18 hr, whereas it continued for the total test duration for the CCT alone, as Figure 4.11a shows.

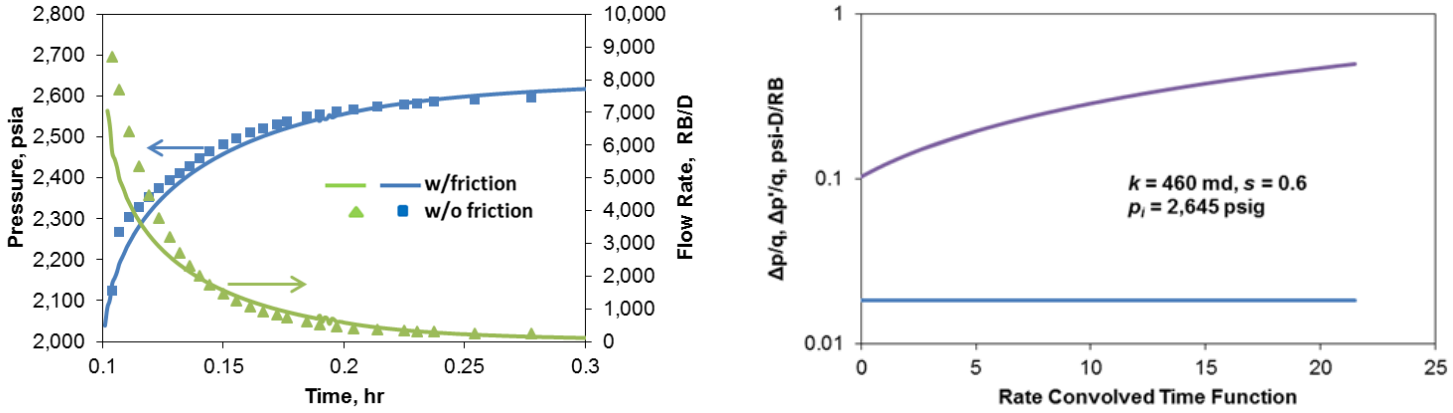

(a) **(b)**

Figure 4. 11 Frictional effect dominates early-time pressure and rate responses (a), and the resultant analysis produces smooth signatures (b), Example 4.
(Hashmi et al. 2016)

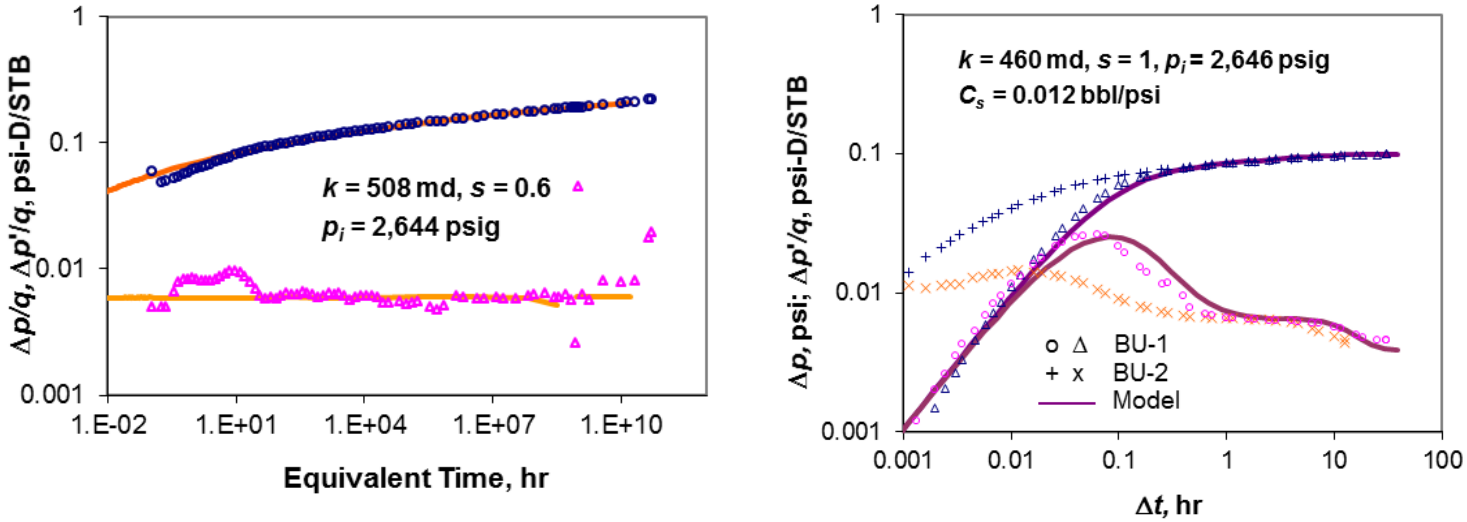

(a) **(b)**

Figure 4. 12 - Convolution analysis of CCT (a), and long-term analysis of two buildup tests (b) for Example 4 (Reprinted from Soliman et al. 2004).

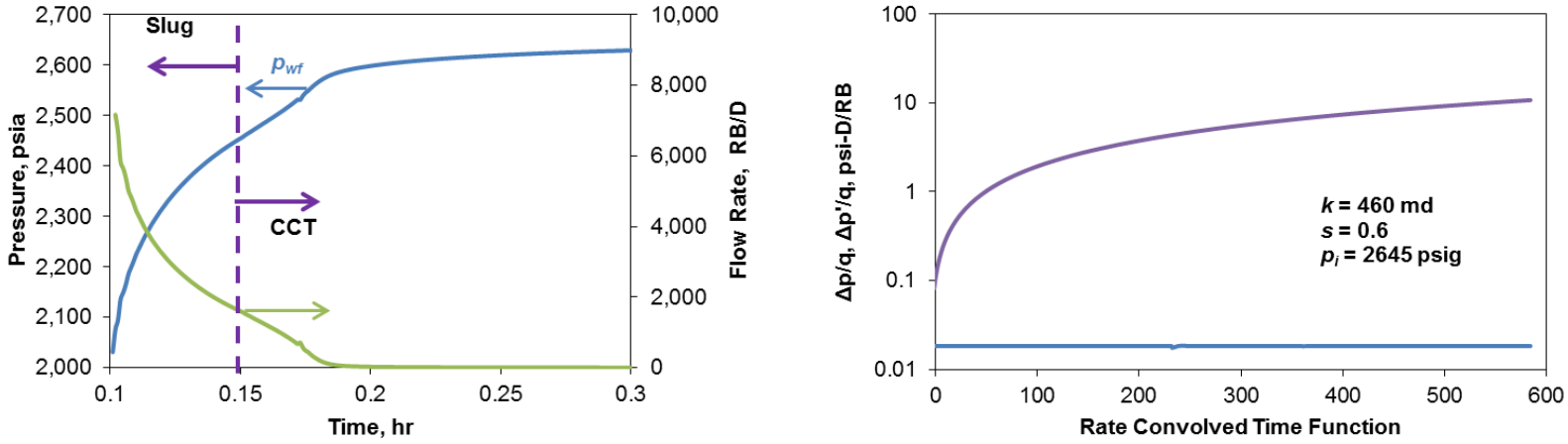

(a) **(b)**

Figure 4. 13 - Pressure and rate response for the combined slug-CCT (a) and analysis (b) for Example 4. (Hashmi et al. 2016)

Heat and Fluid Flow to Inversely Predict Rate

As in the case of the previous model, we validated this one too using multiple sets of data. For the first application, we had MTS and rate data for more than 100 hours from three different wells situated in a formation off the coast of West Australia. Temperature sensors embedded in the acoustic telemetry system at 11 depth locations about 1,000 ft apart in each well provided the distributed-temperature data over the entire test period with rates varying from zero to 60 MMscf/D. **Figure 4.14** shows the discrete nature of temperature sensors that were embedded in the pressure-relay stations during the course of transient testing in this deepwater setting. The rigor of the new analytical model allowed reliable estimation of flow rates during both flow periods, pre- and post-cleanup. This has tremendous potential in the field of transient testing. Because direct rate metering may be obviated in tests involving wireless telemetry, formation permeability may be inferred early on to fine-tune the actual test.

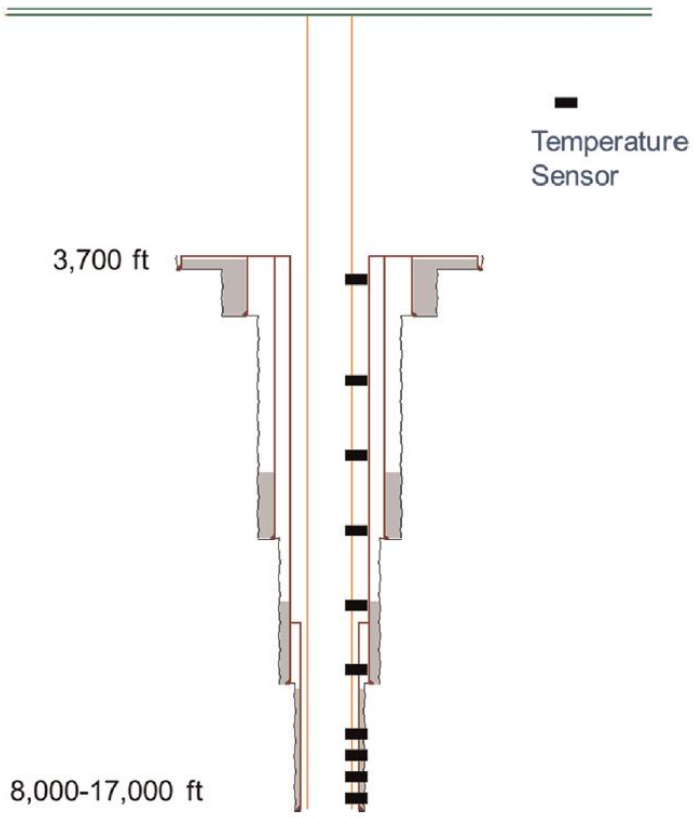

Figure 4. 14 - Schematic of multipoint temperature measurements at relay stations. (Hashmi et al. 2015)

Figure 4.15 shows data from five of those stations for Well 4. As discussed in the subsequent sections, these MTS data sets formed the backbone of this study. As expected, the smallest response occurs near the well bottom, whereas the largest excursion (between fluid and formation temperature) is noted near the mudline.

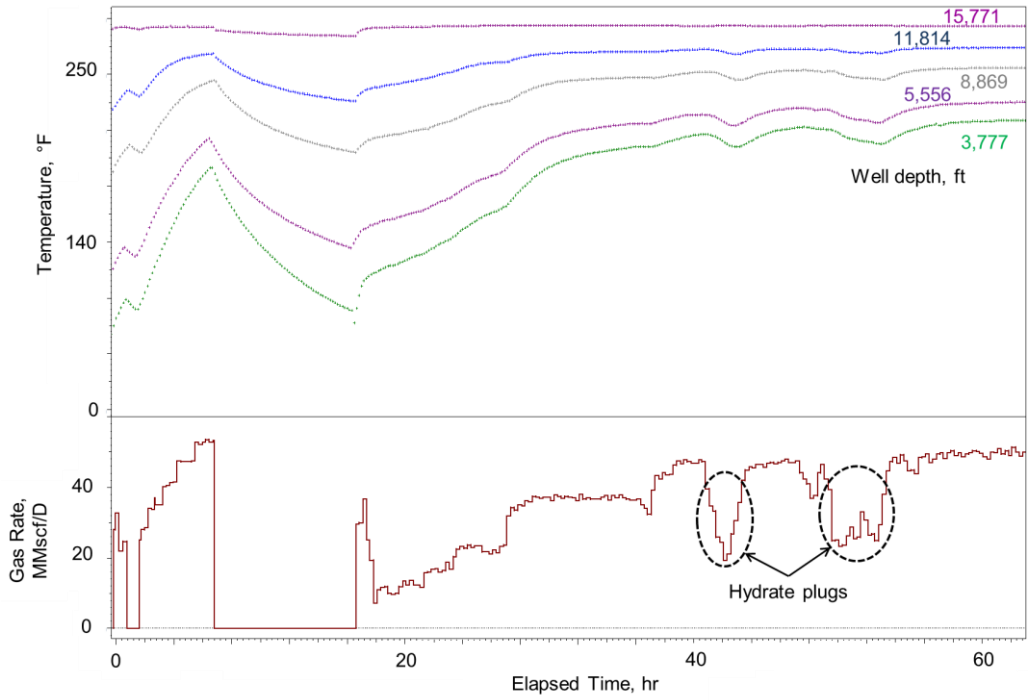

Figure 4. 15 - Depth-dependent measurements of transient temperature in Well 4. (Hashmi et al. 2015)

Figure 4.15 illustrates interesting phenomena that characterize the transient fluid-temperature behavior. One such characteristic evident is the distinctly varying temperature profiles near the mudline while a near-flat line represents the profile close to the bottomhole. The explanation of this gradual flattening of the temperature profiles with increasing depth is simple. Fluid entering the wellbore is at (or nearly at) the same temperature as the formation. Therefore, near the bottomhole, there is little or no difference between the fluid temperature T_f and the surrounding formation T_{ei}. Because $T_f - T_{ei}$ is the driving force for heat transfer, not much heat exchange occurs near the well bottom, which explains the relatively unperturbed temperature profile with time at deeper stations. In contrast, near the mudline the formation surrounding the fluid is at a

much lower temperature than the fluid itself. This larger temperature contrast at shallower depths explains the greater heat exchange.

For the same amount of heat exchange, however, temperature change is smaller for greater rates (because $Q \sim mc_p\Delta T$). Therefore, at higher flow rates the fluid temperature will stay higher than for a lower rate because of a smaller temperature difference. This behavior is observed in the temperature profiles at 2 to 6 hours. During this period, rates keep increasing, resulting in increasing fluid temperature with rate and, therefore, with time.

When fluid flow is initiated from a shut-in well (or when a step increase in rate occurs), the fluid temperature increases for some time, even if the rate is kept constant. This point is illustrated in **Figure 4.16,** wherein at each constant-rate segment, the fluid temperature increases by about 15^oF. This phenomenon is easier to understand for a rate increase than for a rate decrease; although, the same explanation applies to both situations. When a rate increase is initiated and held constant for some time, hotter fluid from greater depth moves up and replaces the colder fluid at any given position. As production continues, increasingly hotter fluid from greater depths does the replacement, thereby allowing the fluid temperature to increase with time at any elevation higher than the point of fluid entry. However, after the bottomhole fluid has replaced the fluid at a given location, the temperature change reaches a point of diminishing returns for a given rate. In other words, this location reaches a pseudosteady-state temperature for a given rate. This explanation also points out why a steady-state temperature model becomes

unsuitable for obtaining accurate flow rates from transient-temperature data, even when the rate remains constant over some periods.

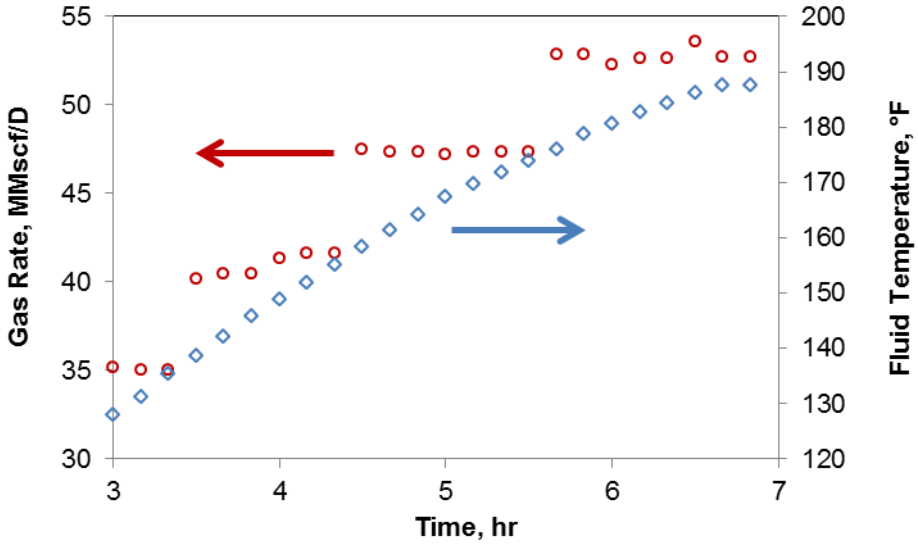

Figure 4. 16 - Gas rate and fluid temperature during the cleaning phase in Well 4. (Hashmi et al. 2015)

Temperature Model Validation

Because accurate rate estimation from MTS data requires rigorous temperature models, we offer both verification and validation of our temperature models in this section. In addition to the data from the three wells mentioned above, we also used temperature estimation from a commercial software package (WELLCAT) to verify our model. The finite-element wellbore simulator uses a detailed description of the wellbore, fluid, and formation to generate transient solution for the flow problem at hand. The simulator estimates temperature profile based on the rate history where temperature at the end of a rate step is used as an initial condition for the next rate step. Although this

simulator is intended for casing design, it solves the heat flow problem of interest in a rigorous fashion.

Figures 4.17 and 4.18 present the history matching effort of the temperature profiles near the mudline for the two wells. The agreement of our model with data provides validation and the commercial simulator verifies the results. As noted earlier, only one set of input parameters was used for history matching temperature data from all depths and rates for both wells in this field.

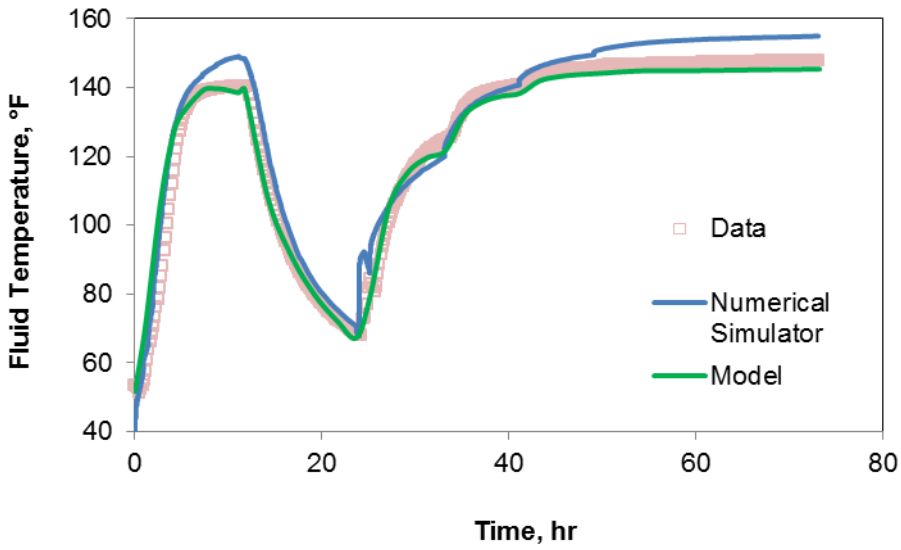

Figure 4. 17 - History matching transient temperature profile, Well 2. (Hashmi et al. 2015)

As shown in **Figure 4.17**, Well 2 depicts a classical temperature profile for a flow-after-flow test, following the cleanup and shut-in periods. The initial period from well startup until about 12 hours corresponds to the cleanup phase wherein the rate is continually increased in a stepwise fashion. After this period of activity, the well is shut

in for about the same period. Following the shut-in, the flow-after-flow test for deliverability, in which the surface rate is increased in each successive step for the same duration, is initiated. This succession of rate profile is accurately captured by the temperature profile. At the start of the test (at approximately 25 hours), the temperature increases due to the hotter fluid rising up the wellbore. The temperature starts to stabilize at around 33 hours when another increase in rate causes the temperature to rise farther. Although the time is the same, this increase in temperature is not the same as with the previous rate. This reduced response is triggered by the decreasing temperature difference between the fluid and the wellbore as mentioned earlier.

The same reasoning applies to Well 4 where the well follows a similar rate schedule. Here, formation of hydrates occurred in the wellbore during the flow period as characterized by the dips in temperature and shown earlier in Figure 4.15. Methanol injection mitigated this problem. However the benefit of using temperature measurements for flow rate estimation becomes more evident here because the fluid temperature captured this anomaly. Figures 4.18 and **4.19a** demonstrate that the model and the commercial simulator both successfully reproduced this signature.

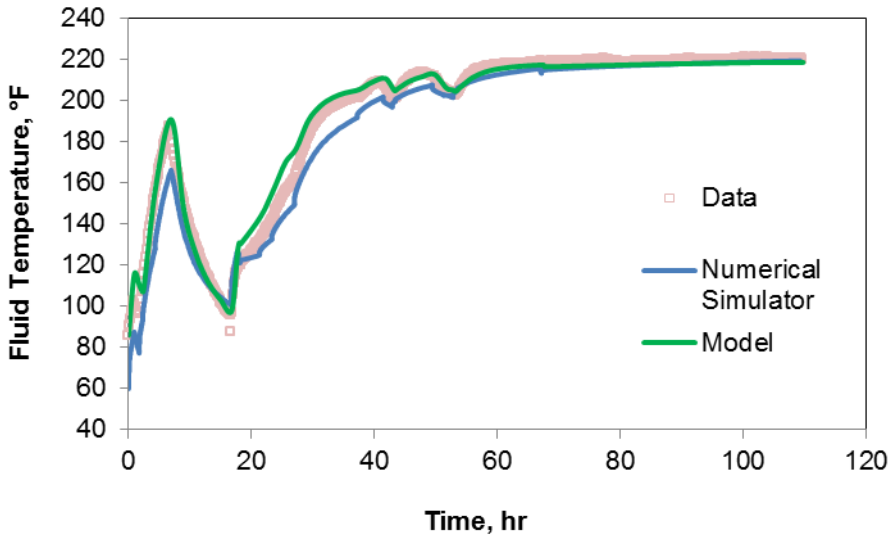

Figure 4. 18 - History matching transient temperatures profile, Well 4. (Hashmi et al. 2015)

Figure 4.19a shows the history match of transient temperature profiles done at various depths. For clarity of presentation, only three depths are shown, but in reality, we have had 10 depths (each 1,000 ft apart) to anchor the model solution. As expected, the fidelity of the temperature response decreases with increasing depth. Yet, the decrease in flow rate is captured at greater depths as well. Such spatial data help in accurate estimation of the fluid flow rates because multiple datasets constrain the problem at hand. This point is illustrated more clearly in **Figure 4.19b,** which shows the rate history match based on the temperature matches in Figure 4.19a.

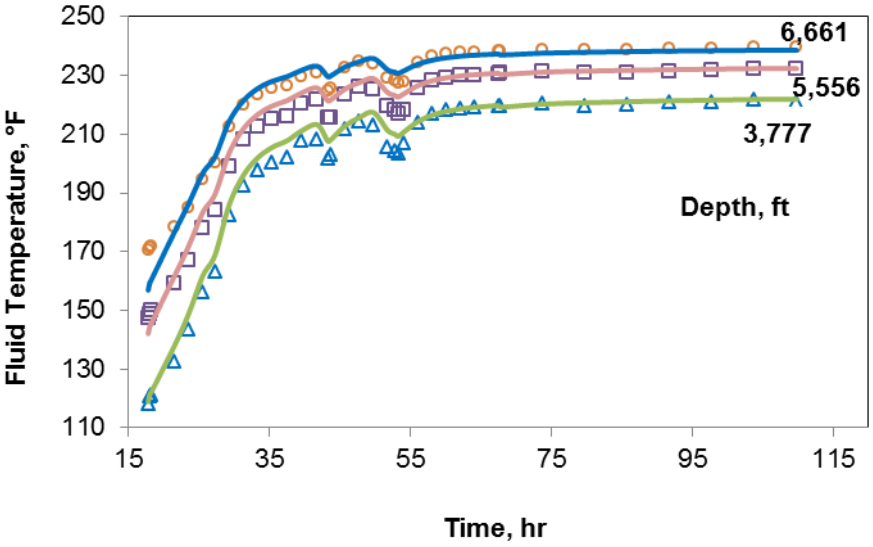

(a)

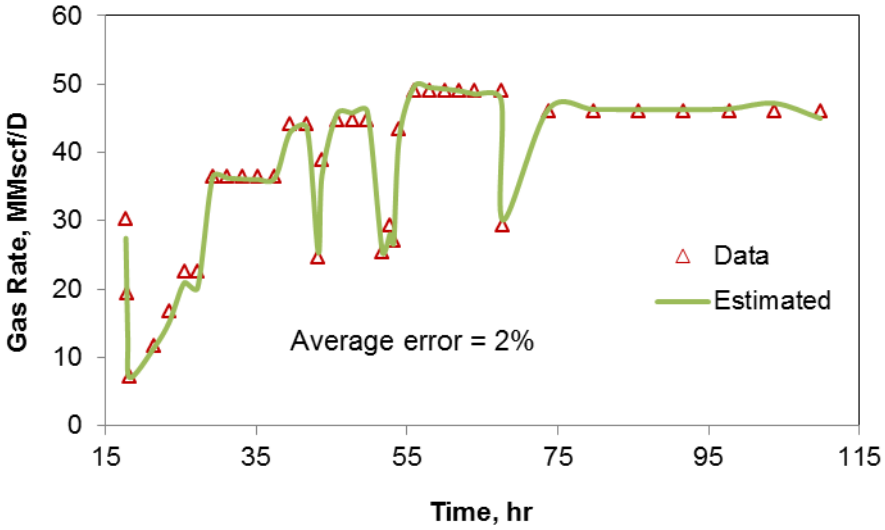

(b)

Figure 4. 19 - History matching transient temperature profiles (a) and rate profile (b) using data at different depths.
(Hashmi et al. 2015)

As shown in Figure 4.19b, the predicted rates closely follow those recorded using the multiphase flow meter. The model's sensitivity enabled us to capture the flow rate restrictions around 42 and 52 hours.

A problem that often creeps up during inverse modeling is the solution nonuniqueness. This aspect is often the case in inverse problems because the problem is often under defined. However, temperature data at multiple depths make up for the lack of under defined parameters. That said, we cannot ignore that more often than not such rich data are lacking in most test settings. Usually the temperature data is limited to the wellhead and bottomhole conditions. Therefore, we employed the same methodology discussed earlier on temperature data from just one depth nearest to the mudline, which is construed as most appropriate for the analysis because of the largest temperature response.

Figure 4.20a offers the results for the history matching of temperature estimates and **Figure 4.20b** presents the rate estimated based on the match shown in Figure 4.20a. As shown, the match quality for the temperature is not much different; however, the rate quality suffers slightly. Here, the non-uniqueness of the inverse problem becomes more evident during our analysis because the problem becomes less constrained. This experience suggests that the model be calibrated and anchored for a known rate to achieve more confidence in the prediction when using data from a single location. This point is further discussed while discussing the next application of thermal modeling.

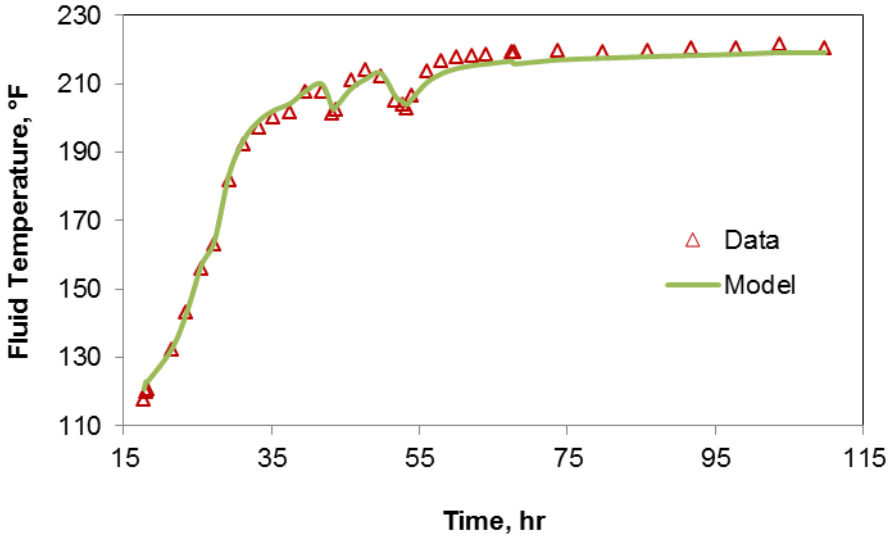

(a)

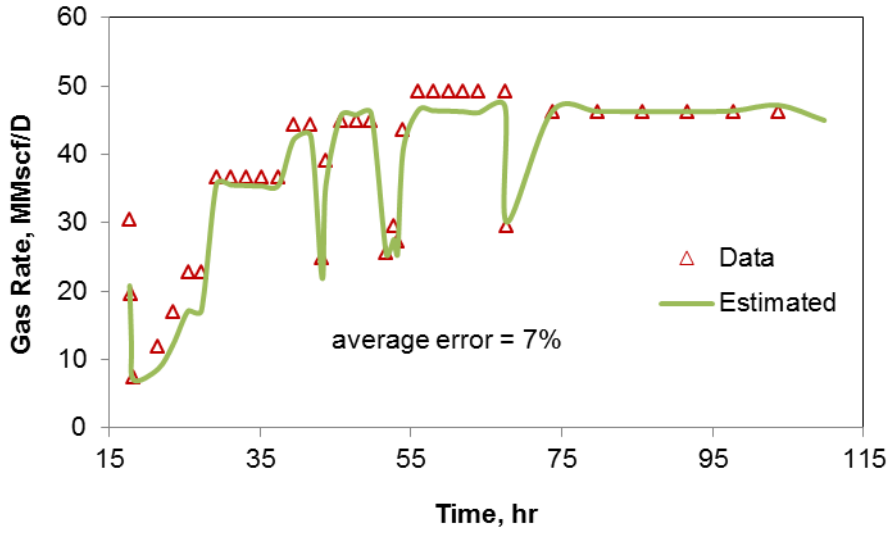

(b)

Figure 4. 20 - History matching transient temperature profile (a) and rate profile (b) using data at the wellhead.
(Hashmi et al. 2015)

Validation of Cleanup Rate Modeling

In most settings, the cleanup period is overlooked from a transient-test interpretation standpoint. This is primarily because rates are seldom metered with a multiphase flowmeter. Obviously, the continuously changing two-phase flow situation presents additional challenges in test interpretation. However, reliable estimations of relevant reservoir parameters may be obtained if rates of the dominant phase are inferred from distributed temperature measurements. These estimated parameters, in turn, allow fine-tuning the subsequent test sequence, thereby potentially saving considerable expense.

This section demonstrates the applicability of the proposed rate-estimation model from the distributed-temperature data by verifying its performance with a field example, Well 4. We validated the usefulness of cleanup data analysis with a simulated example. The simulated example was generated with a commercial numerical model, wherein fluid invasion was mimicked by injecting water into the formation and producing gas thereafter by imposing step-wise increase in drawdown at sandface. The use of statistical design of experiments (DOE) provides clues about the relative importance of input parameters.

Estimating Reliable Rates with Temperature Modeling

Rates are estimated through an overall temperature match at various depths by honoring discrete temperature data at the end of each time period. **Figure 4.21** depicts the temperature data and estimates using the rigorous transient model (Eq. 3.1) for the

early cleanup phase of Well 4. An important observation in Figure 4.21 is the smooth nature of the temperature profile, which may lead one to think that the rise in temperature was because of production period alone. That notion, however, is inaccurate. In fact, the cleanup fluid flow rate changed significantly and irregularly over time. This item is discussed next.

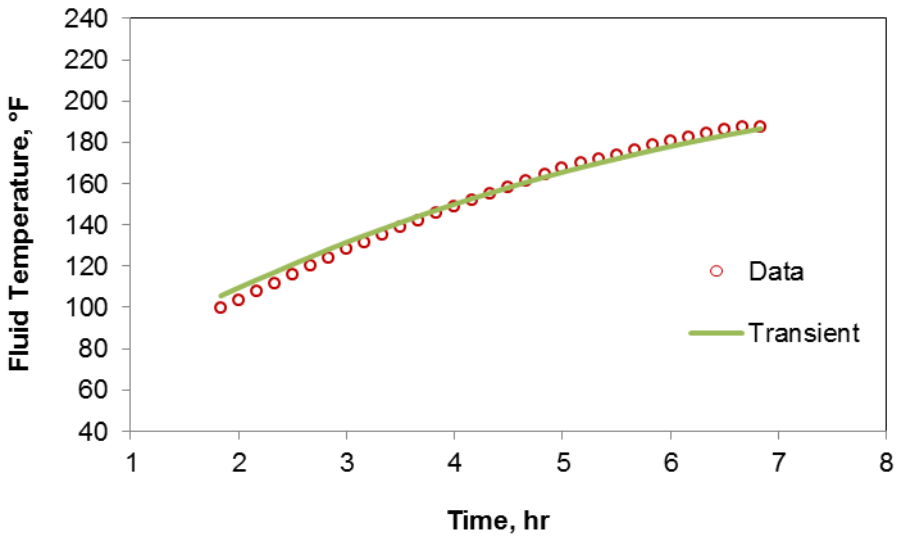

Figure 4. 21 - Temperature history matching using transient and steady-state models for cleanup phase, Well 4.
(Hashmi et al. 2015)

Figure 4.22 provides a comparison between the estimated rates using the described methodology and the measured rates during the early cleanup phase in Well 4. As Figure 4.22 points out, the transient temperature modeling allows for the determination of rate. Despite the steady increase of temperature, Figure 4.22 satisfactorily captures the fluctuations in rate.

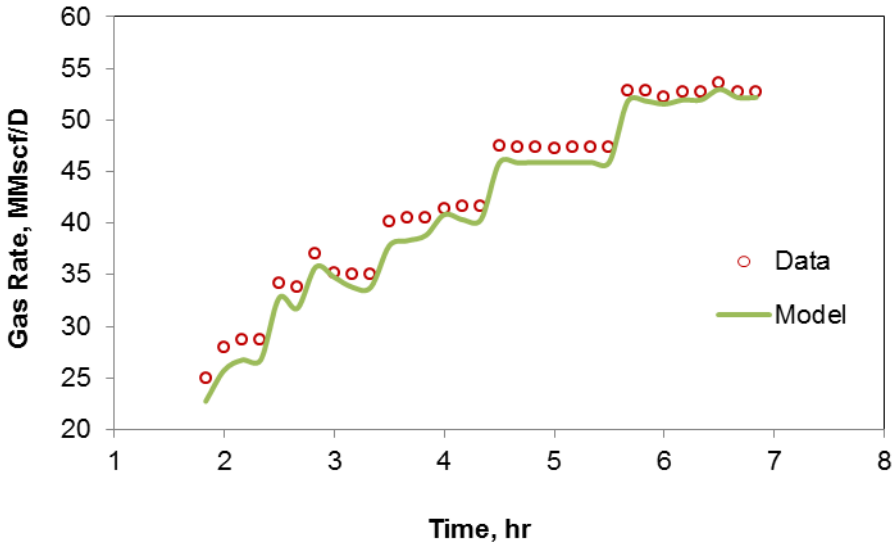

Figure 4. 22 - Comparison of measured and estimated rates during the cleanup phase, Well 4.
(Hashmi et al. 2015)

Figure 4.23 shows the differences in the temperature estimated with and without superposition for one of the rate schedules during the cleanup phase. As the figure shows, the superposition in heat flow does not play a significant part for this flow problem at hand. However, some important items worthy of note confirm the notion of decreasing heat transfer rate with time. As time progresses, the fluid temperature estimated with superposition tends to be slightly higher than without superposition. This observation confirms that the difference in temperature between the wellbore fluid and the formation is decreasing due to the formation being heated up, thereby decreasing the heat transfer rate as highlighted above. Therefore, the fluid temperature with superposition is slightly higher. Another observation is that the effect of superposition declines with increasing depth. This outcome makes intuitive sense in that the difference

between the formation and the fluid temperature declines with increasing depth. The computations for superposition are involved; the example discussed above does not imply that the superposition effects are negligible in all cases.

We investigated conditions under which the effect of temperature superposition can be pronounced in this setting. Because the need for superposition arise due to temperature increase in the near-wellbore area, greater difference between the fluid and formation temperatures may lead to pronounced effect of superposition on fluid temperature. Flow simulations for Well 4 at the same flow rate but with 50% higher geothermal gradient (0.02423 °F/ft) suggested that the estimated fluid temperature at the mudline with superposition is 3.9 °F higher than will be estimated if superposition effects were ignored. This temperature error due to neglecting superposition leads to a 14% lower estimate in gas flow rate. For the same base case, we simulated the effect of formation thermal conductivity on heat retention in the near wellbore zone and its consequent effect on fluid temperature estimated using superposition. A 30% decrease in formation thermal conductivity along with a 50% increase in geothermal gradient led to an increase of 4.25 °F in fluid temperature resulting in a decrease of 15.5% in estimated gas rate.

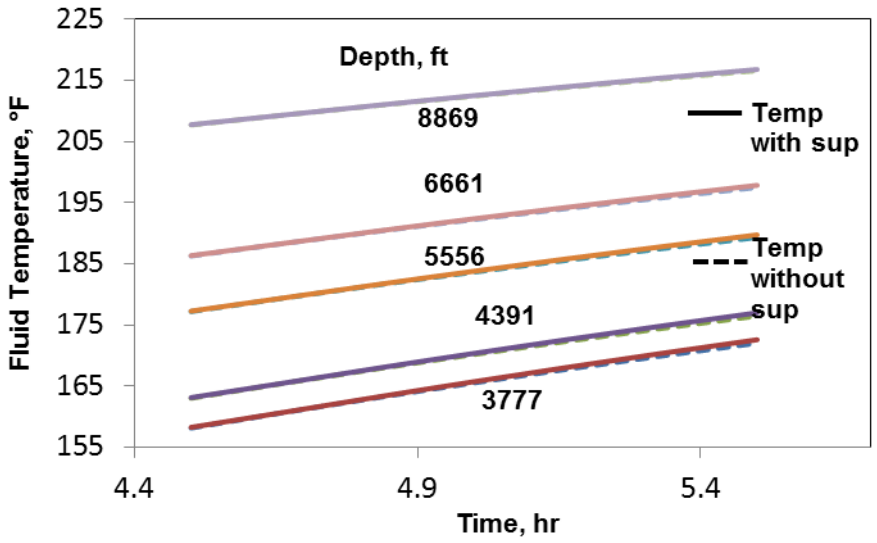

Figure 4. 23 - Temperature estimation at different depths with and without superposition for cleanup phase, Well 4.
(Hashmi et al. 2015)

Cleanup Effect in Pressure-Transient Response

In this section, we use both synthetic and field examples to explore the effect of cleanup in our ability to obtain reservoir permeability. The underlying thought is to obtain a good estimation of permeability from the cleanup period so that the post-cleanup flow and shut-in periods can be fine-tuned. We resort to the statistical DOE to do an objective analysis. To that end, we generate solutions with a numerical simulator by injecting water into the formation to mimic fluid invasion, followed by a rest period and a sequence of flow and shut-in periods, as depicted in the rate profile in **Figures 4.24a** and **4.24b.** Figure 4.24a shows the two buildups: one after the cleanup and the second after the flow-after-flow test. The parameters obtained from the two buildup analyses confirm the hypothesis that both tests yield the same permeability. We

compared the results of two buildups from one of the worst cases considered in this study in terms of depth of invasion. The underlying idea was to underscore the point that permeability estimation during or following the incomplete cleanup period is quite reliable. As **Figure 4.25** suggests only the skin is impacted, not the formation *kh*. Let us study the results of the DOE to learn more about the effect of skin.

Table 4.3 presents the design variables for the full-factorial analysis. **Figure 4.26** presents the summary of these flow-simulation runs on a Pareto chart. In this DOE, skin for both the shut-in periods is the dependent variable, whereas formation conductivity, depth of mud-filtrate invasion, and the initial shut-in time before production constituted the three independent variables. As noted in some of the skin values associated with the second buildup, formation cleanup is not guaranteed in adverse situations when deep filtrate invasion occurs, coupled with inadequate flow periods and/or insufficient drawdown. Figure 4.24b makes this point clearly, in that declining water production continues long after the designated cleanup period, thereby affecting skin for the second buildup.

The positive sign associated with any independent variable on the Pareto chart suggests that an increase of the independent variable will result in an increase of the dependent variable. Although *kh* is by far the dominant variable, the Pareto chart does not imply that the other two variables with absolute *t*-test value below 95% confidence level are not influencing the skin in the second buildup test. Rather, the chart shows that they are statistically insignificant within the 95% confidence interval.

Table 4. 3 - Design Variables for Full Factorial Analysis.

	kh, md-ft	depth of invasion, ft	Initial shut-in time, hr
Low	50	1	0
Medium	1500	2	10
High	4000	3	24

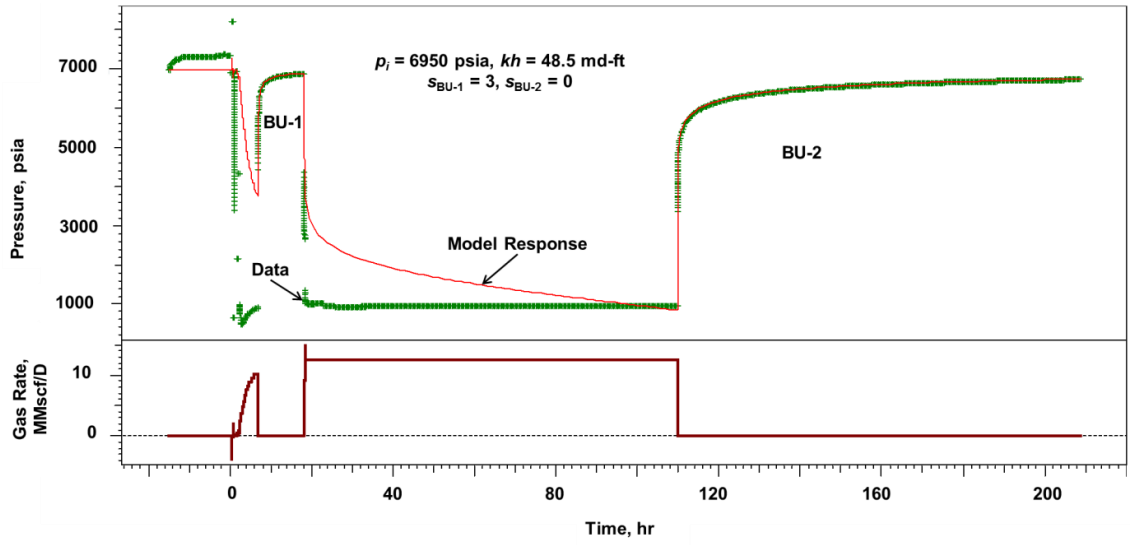

(a)

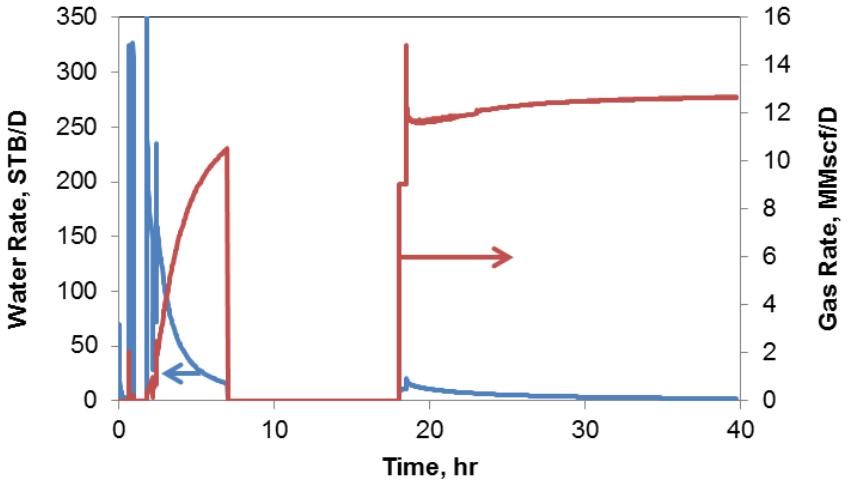

(b)

Figure 4. 24 - Pressure simulation for one of the design cases (a) and rate simulation for the same case (b).
(Hashmi et al. 2015)

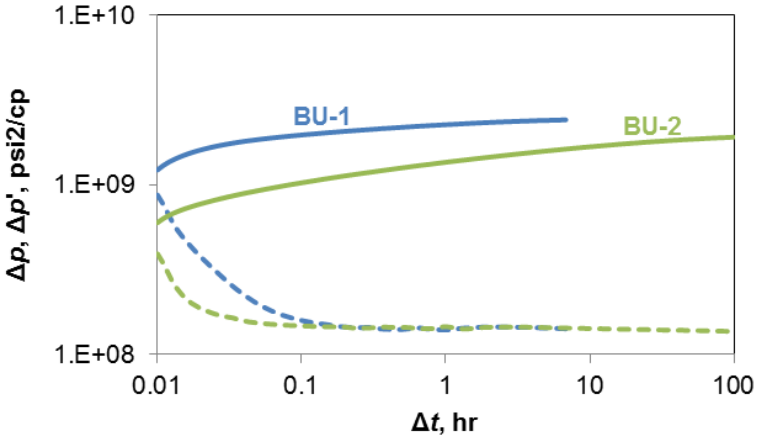

Figure 4. 25 - Buildup charts for the same case as in Fig. 4.24.
(Hashmi et al. 2015)

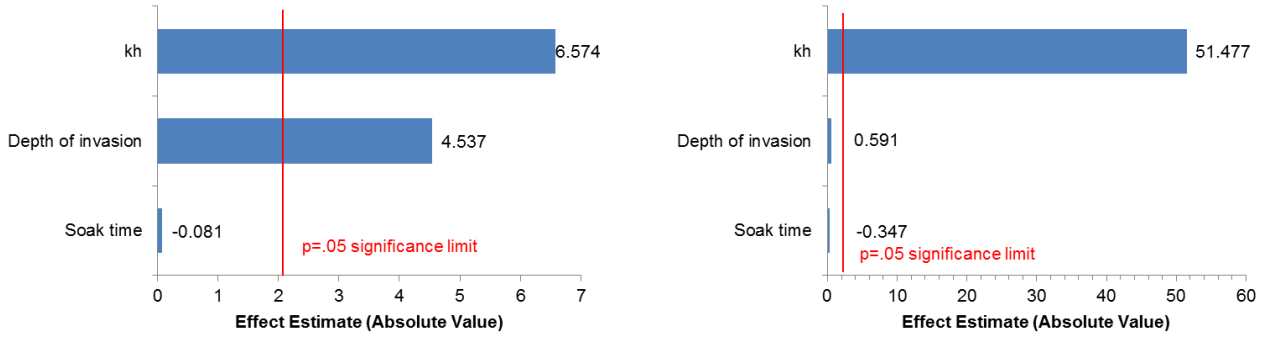

(a) **(b)**

Figure 4. 26 - Pareto charts show the significance of independent variables on skin from (a) BU-1 and (b) BU-2. (Hashmi et al. 2015)

As the results of the DOE with the simulated example show, formation's conductivity or the *kh* product dominates skin. Interestingly, the other significant variable for the pre-cleanup skin is the depth of invasion. However, the significance of filtrate invasion diminishes in the second buildup, reaffirming the contention that the difference in the pre- and post-cleanup response manifests in terms of skin. This point is made by **Figure 4.27**, which shows the results of pre- (BU-1) and post-cleanup (BU-2) shut-in periods for Well 4. As expected, the derivative signatures overlay suggests the same conductivity, but the pressure-difference curves separate indicating the skin effect or incomplete cleanup.

The DOE also provided an opportunity to create a quantitative model for the pre- and post-cleanup skin based on the independent variables used to investigate their effect. While these models are not expected to work outside the range of variables used in this study, they may guide the estimation of relative skin values. The following expressions present the models that can be used to estimate the two skins, respectively:

$$\begin{aligned}\log s_1 = {} & 1.64(\log kh) - 0.037(\log kh)^2 + 10.3(\log r_{inv}) - 2.69(\log kh \log r_{inv}) \\ & - 1.25(\log r_{inv})^2 - 0.01(\log t_{st}) + 0.0008(\log kh)(\log t_{st}) \\ & + 0.011(\log t_{st})(\log r_{inv}) - 0.01(\log t_{st})^2 - 4.59\end{aligned} \tag{4.1}$$

$$\begin{aligned}\log s_2 = {} & 3.36(\log kh) - 0.038(\log kh)^2 - 0.16(\log r_{inv}) + 0.055(\log kh \log r_{inv}) \\ & - 0.18(\log r_{inv})^2 - 0.016(\log t_{st}) - 0.007(\log kh)(\log t_{st}) \\ & - 0.02(\log t_{st})(\log r_{inv}) + 0.009(\log t_{st})^2 - 6.63\end{aligned} \tag{4.2}$$

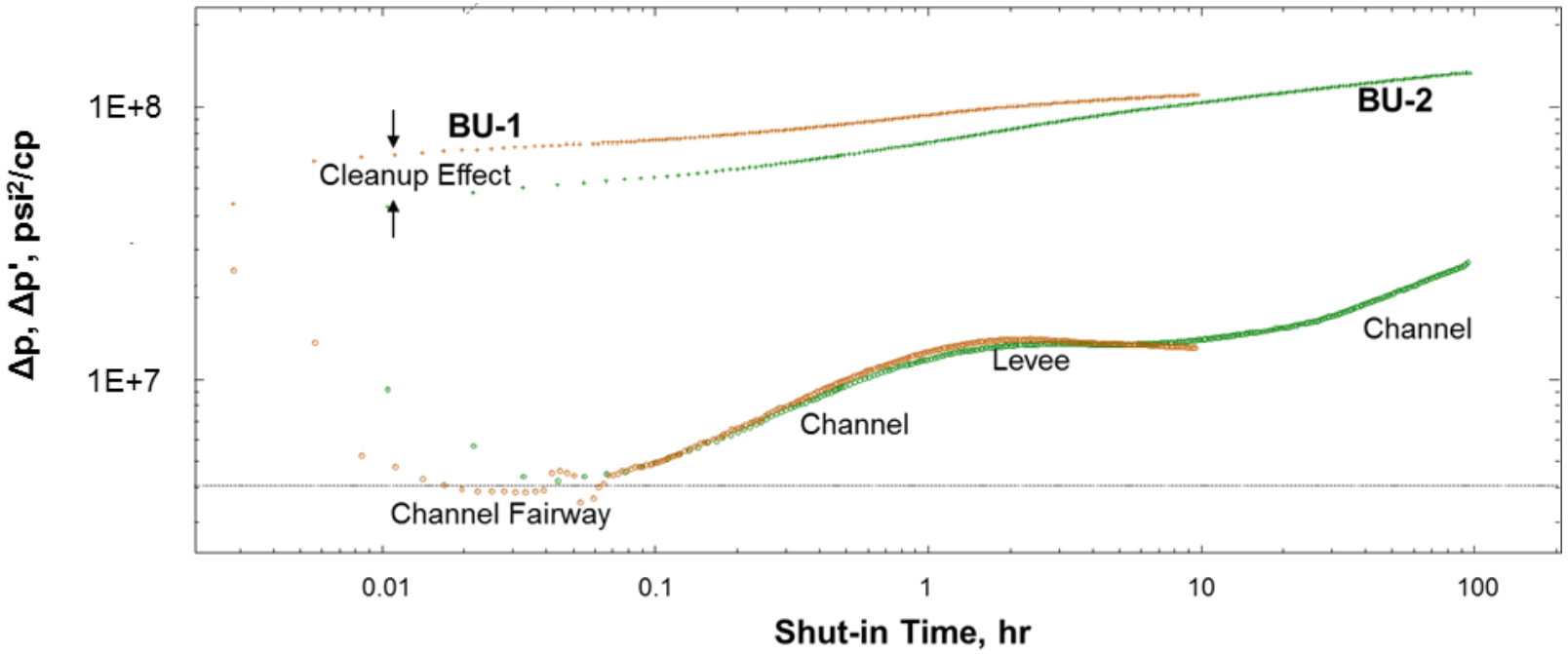

Figure 4. 27 - Incomplete cleanup manifests in terms of skin, Well 4.
(Hashmi et al. 2015)

Validation of Modeling Temperature Logging Data

The second application for rate estimation using thermal modeling was validated with some production logging data. This field example focuses on an oil well in which production logging was run to obtain zonal contributions from each of two sets of perforations. Temperature measurements were part of the suite of production logging tools that were run. The well was run at two different choke settings during the logging run: one with an open choke and another with a choke setting of 60% of total volumetric flow. Complete logs were available for both choke settings, which provided for an interesting set of data that validated the approach and the choice of a transient model. **Figure 4.28** and **Figure 4.29** present the interpreted spinner response from the two different choke settings. The interpretation provides the flow rates from the bottom perforations and the combined flow rate after the top perforations for both of the choke settings.

In both cases, the same input parameters were used to run the model except for the time and rate of fluid flow. Rate was obtained using the same technique of matching the temperature outside of the perforation zones where the flow was not so turbulent. This was done successively on top of each set of perforations so the individual and the combined rates could be determined. The rigor of the analytical model enabled reliable estimation of flow rates from both sections of the wellbore: pre- and post-top perforations. All calculations were performed for each half foot of measured depth interval. Different thermal resistances between the flowing fluid, the completions, and the formation were determined to estimate the overall heat transfer coefficient, U_t.

Physical properties of the fluid were also considered to estimate the effect of pressure drop on the temperature profile.

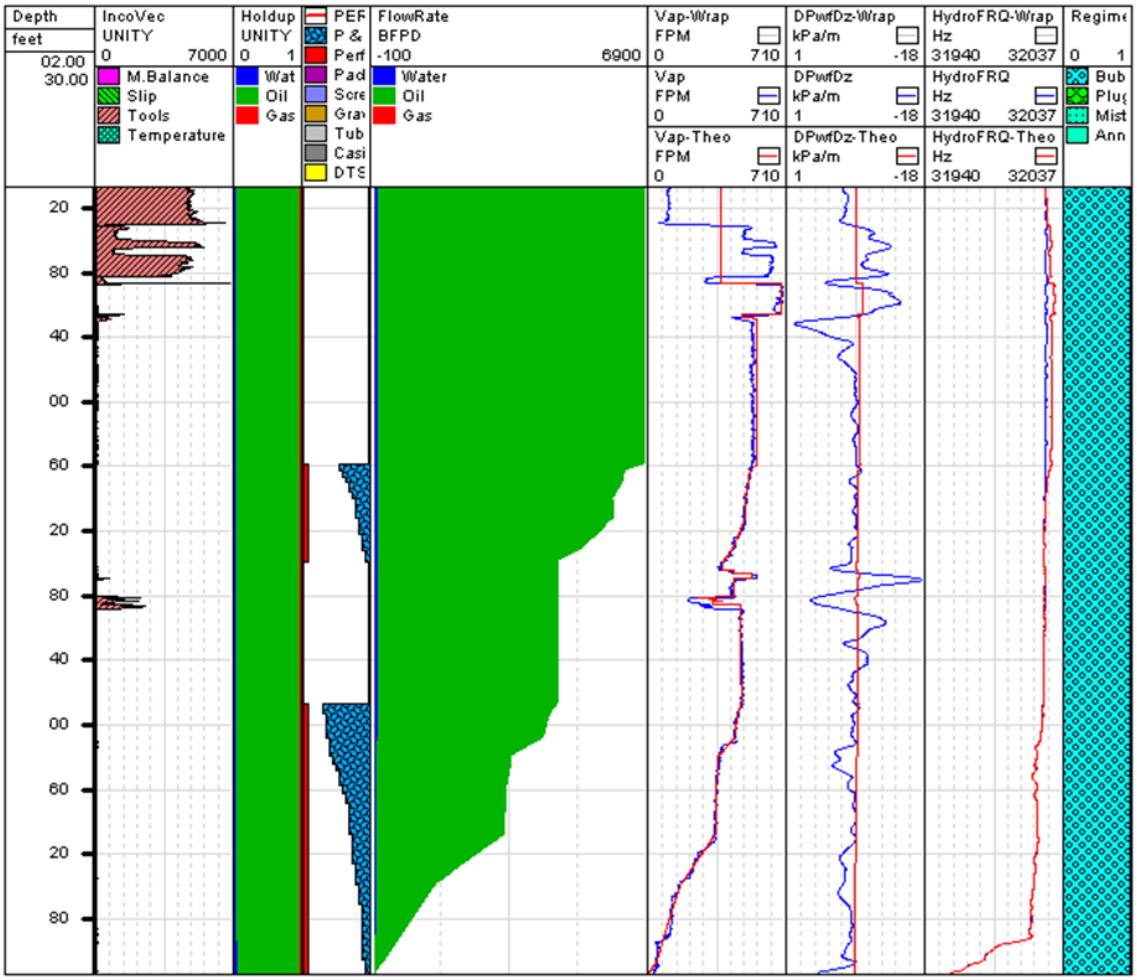

Figure 4. 28 - Flow profile from interpreting spinner data from production logging at 100% flow.

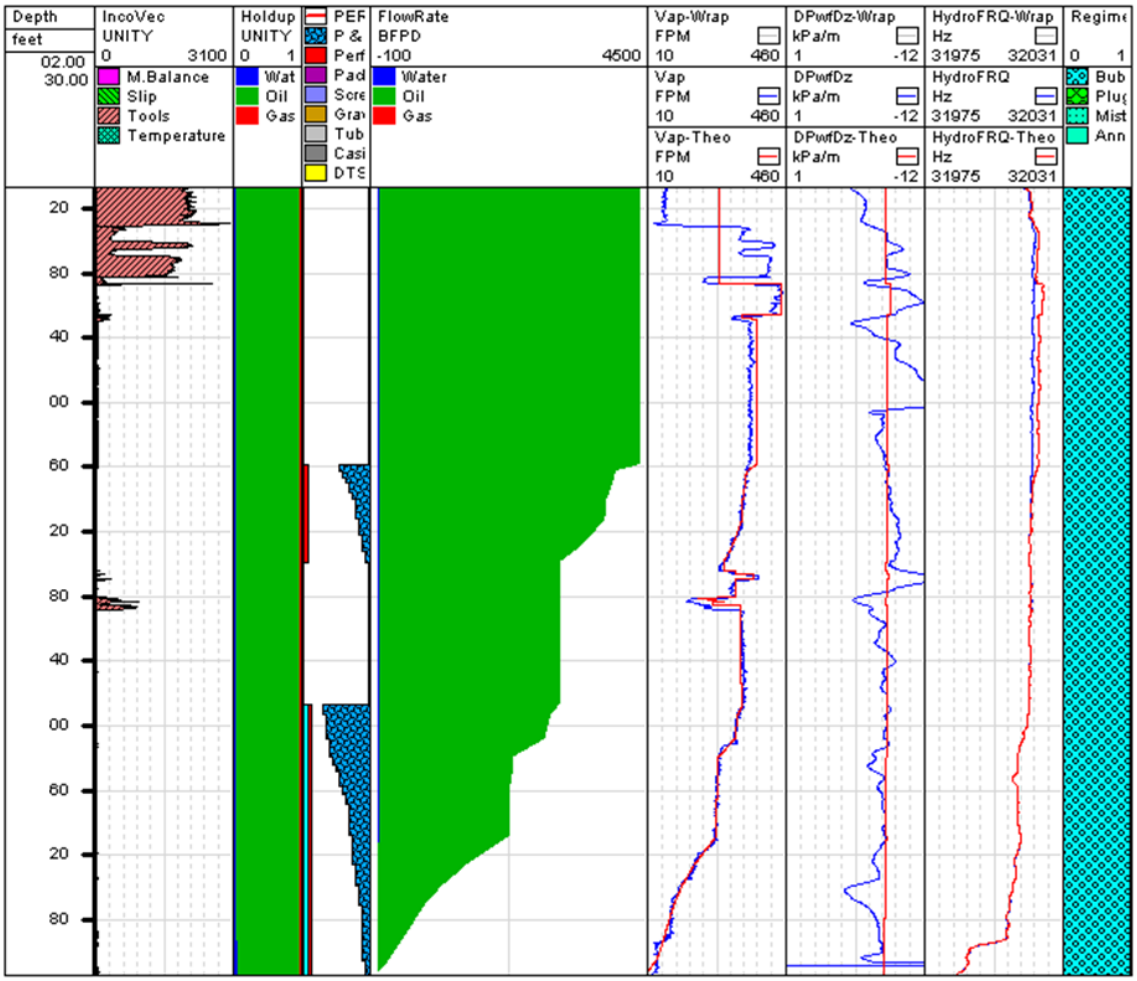

Figure 4. 29 - Flow profile from interpreting spinner data from production logging at 60% flow.

Temperature profile in the wellbore was calculated for both cases of 100% and 60% flow and compared to the measured temperature profiles. **Figure 4.30** and **Figure 4.31** show the different matches that were obtained for both cases. As expected, temperature begins higher at the bottom perforations in both settings. Across the interval between perforations, the fluid undergoes a gradual temperature decrease that is exacerbated by relatively colder fluid entering the wellbore from the top perforations.

This is where the fluid profile observes a dramatic temperature decrease as a result of the mixing of the two streams. The entry from the top perforation is again followed by the gradual temperature decrease through the remainder of the interval. The calculated temperature profile in both cases captures the measured temperature profile satisfactorily in the non-perforated parts of the logged interval; consequently, it provides the flow rates at these respective parts. **Table 4.4** compares the flow rates obtained from the temperature log to the rates obtained from the interpretation of the spinner data and presents the error analysis. It suggests that the rates were obtained with reasonable accuracy when compared with the sophisticated spinner logging.

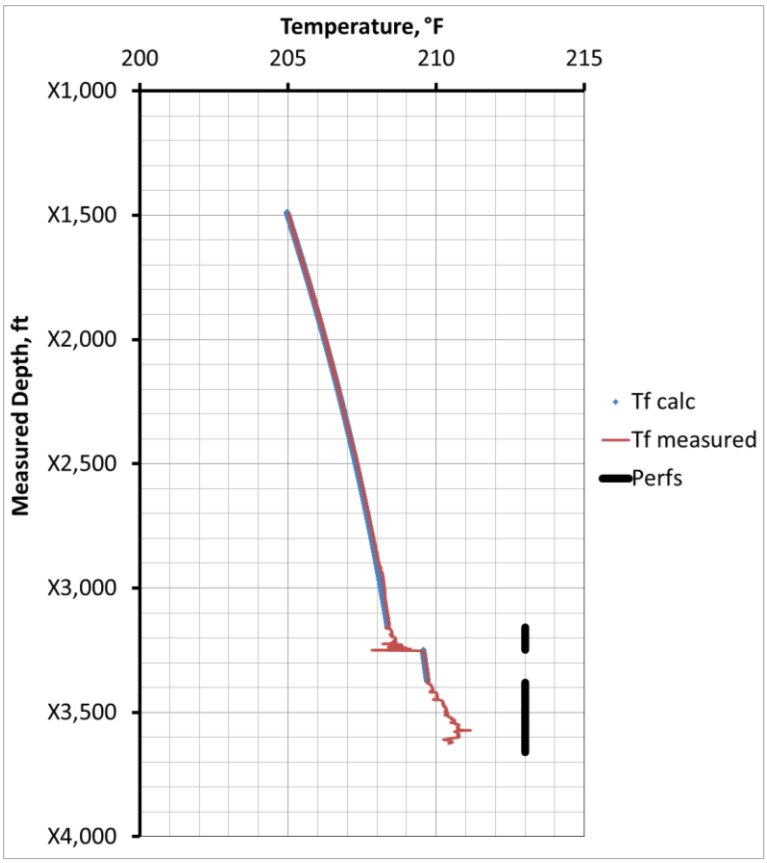

Figure 4. 30 - Match between the measured and calculated temperature profiles at 100% flow.

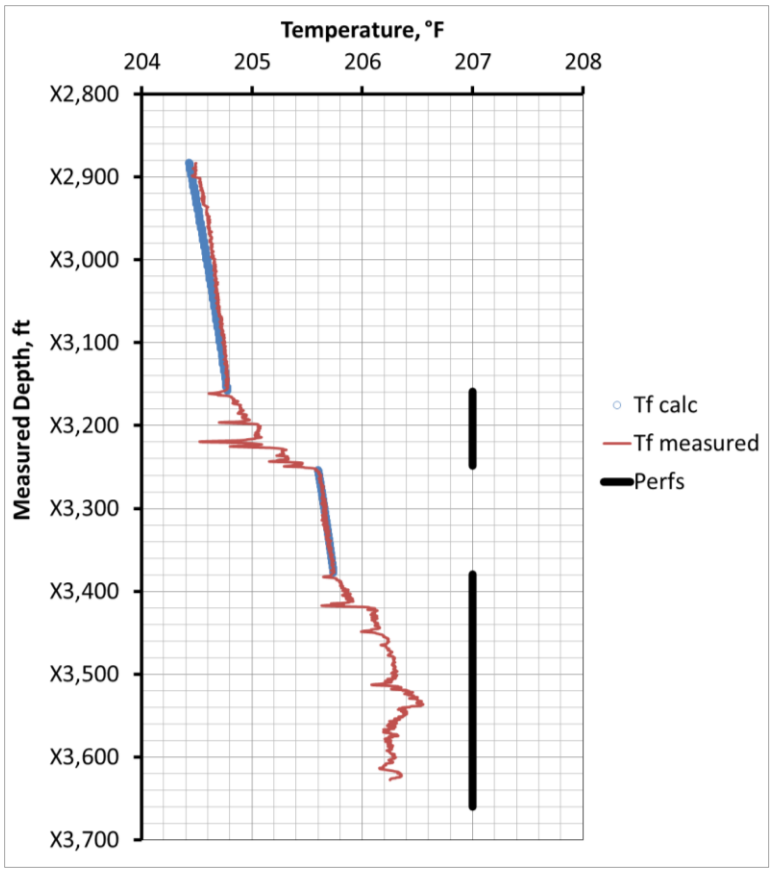

Figure 4. 31 - Match between the measured and calculated temperature profiles at 60% flow.

Table 4. 4 - Comparison between flow rates determined from spinner data and temperature log.

		Determined Rates, STB/D		
		Spinner	Temperature	Error (%)
Open Choke	Bottom perf	4350	4444	2.1
	Total flow	6600	6650	0.8
60% Flow	Bottom perf	2800	2986	6.6
	Total flow	4400	4503	2.3

Flow for Optimization During Plunger Lift

We used the data published by Luo and Kelkar (2014) to validate the proposed modeling approach. They provided data from four wells, two of which sustained continuous production after shut-in, but the other two did not. We first discuss the two wells that could not maintain continuous production after shut-in under field conditions. For Well 1 continuous production would have resulted in if the shut-in had lasted long enough to attain a casing pressure suggested by the proposed model (Eq. 3.11). For Well 2, we show that the reservoir pressure is too low for plunger lift to be a useful lift technique. We then discuss the application of the proposed model to Wells 3 and 4. Thereafter, application of the Hasan et al. (2010) model to examine the existing flow patterns in Well 2 illuminated unfolding events of liquid loading.

Wells 1 and 2

Figure 4.32 presents daily production data along with tubinghead pressures for Well 1 in the Luo-Kelkar study. The decline in gas flow rate, with a consequent rise in tubing pressure, signifies liquid loading. The schedule followed in the field data for the first plunger cycle is given below; subscript 1 represents conditions just prior to shut-in, and subscript 2 represents conditions when the well is opened up again, and the plunger begins its ascent:

$$p_{c1} = 240 \text{ psi} \quad p_{t1} = 178 \text{ psi}$$

$$p_{c2} = 255 \text{ psi} \quad p_{t2} = 185 \text{ psi}$$

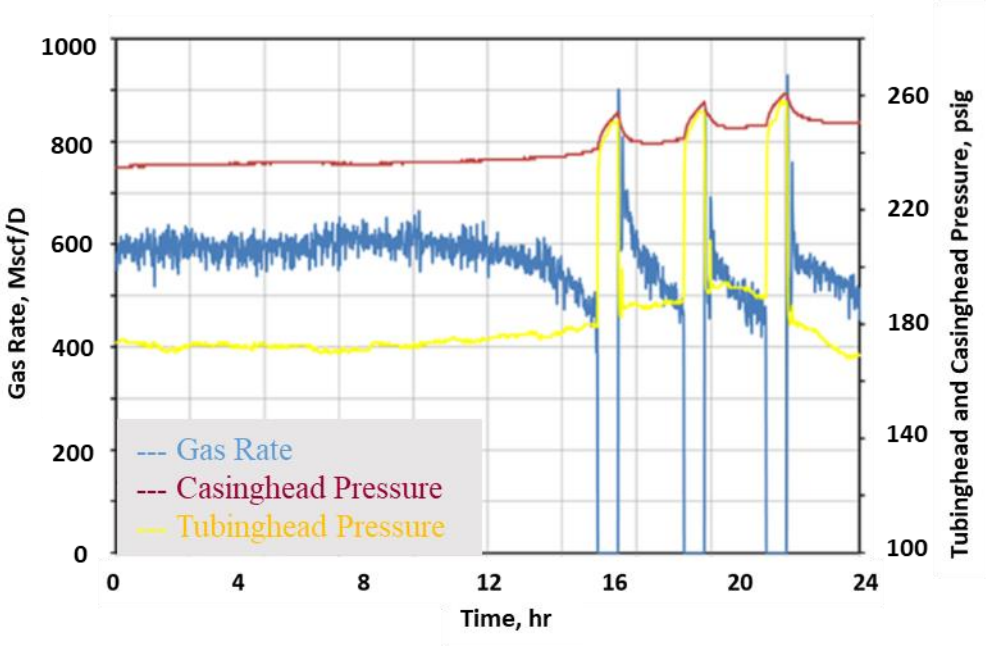

Figure 4. 32 - Production data for Well 1 (Reprinted from Luo and Kelkar, 2014).

This vertical well has a depth of 3,440 ft; other pertinent data and sample calculations are presented in Appendix D. Our model (Eq. 3.11) calculated the required casing pressure for sustained production to be 269 psig, which is higher than the field schedule. Figure 4.32 shows that the field practice of releasing the plunger at 255 psig casinghead pressure did not allow production for more than a couple of hours.

Our contention is that if the plunger is allowed to stay long enough for the casinghead pressure to reach 269 psia, sustainable production can be achieved. To validate that contention, we need the reservoir response to reflect the desired casinghead pressure. However, Luo and Kelkar did not provide any reservoir information. We, therefore, built a reservoir model with a commercial simulator (Rubis 2016), honoring the available production and pressure data. Estimation of reservoir influx provides a

synergy that allows for a holistic approach to modeling the plunger lift system. Appendix E presents some of the pertinent information of the reservoir model. **Figure 4.33** shows daily production data along with tubinghead pressures for Well 1 in the Luo-Kelkar study in addition to showing the match that we were able to obtain using the numerical reservoir modeling. The match allowed reasonable prediction of the future production which could then be compared to the simulations made using the proposed model as shown later in this chapter.

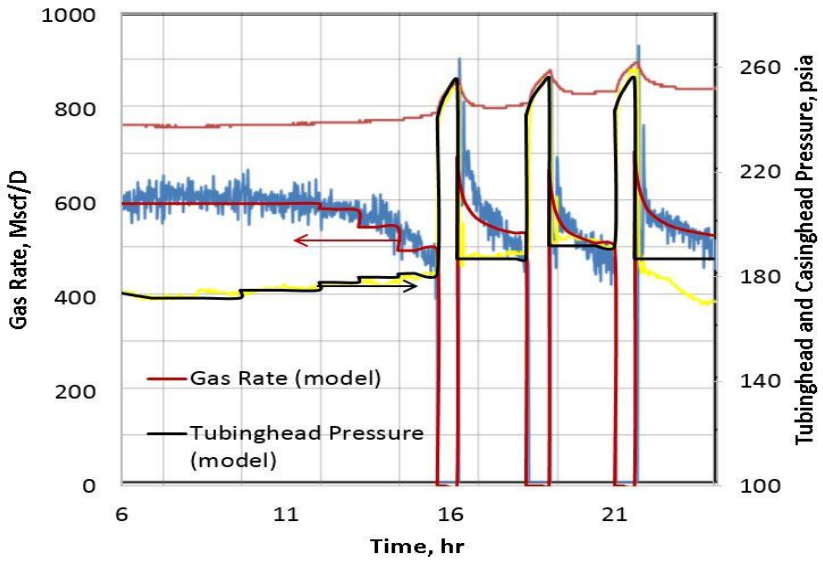

Figure 4. 33 - History matching production performance in Well 1. (Hashmi et al. 2018)

We applied Eq. 3.11 to the other three cases presented by Luo and Kelkar (2014). **Figure 4.34** shows data from Well 2 that exhibits a similar pattern of liquid loading as in Well 1. Here again, the gas rates kept declining and did not maintain a sustained

production after the plunger cycle as intended. The pressure schedule followed for the first plunger cycle is given below:

$$p_{c1} = 221 \text{ psi} \quad p_{t1} = 161 \text{ psi}$$

$$p_{c2} = 235 \text{ psi} \quad p_{t2} = 162 \text{ psi}$$

Our model predicted a required casing pressure of 266 psia, about 31 psi higher than that in the field. The resulting disruption of production, in this case, supports our model's prediction that higher casing pressure can sustain production in this instance as well as in Well 1.

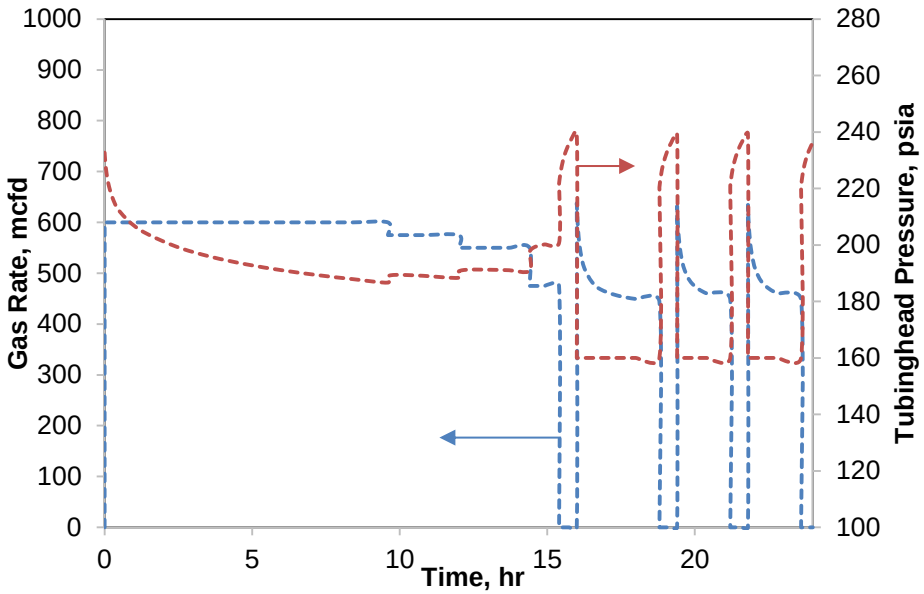

Figure 4. 34 - Production data for Well 2. (Hashmi et al. 2018)

As in the case for Well 1, we built a reservoir model honoring the rate and pressure data for this well. This modeling approach allowed changing the casinghead pressure, leading to more sustainable production periods for these two wells. Let us discuss the benefits of the modeling approach proposed in this study.

Figure 4.35 shows the results of simulations for Well 2 using a required casinghead pressure of 266 psig instead of the actual value of 235 psia used in the field. Appendix E briefly discusses the history matching effort of field data pursued in this study. The simulated results show sustainable production for the entire 39 hours. In contrast, the blue dots in Figure 4.35 indicate the expected interrupted production, if the field schedule of plunger release occurred at a casinghead pressure of 235 psia. The solid magenta line showing the attainable cumulative production amounts to 30% higher than what the current field practice would result.

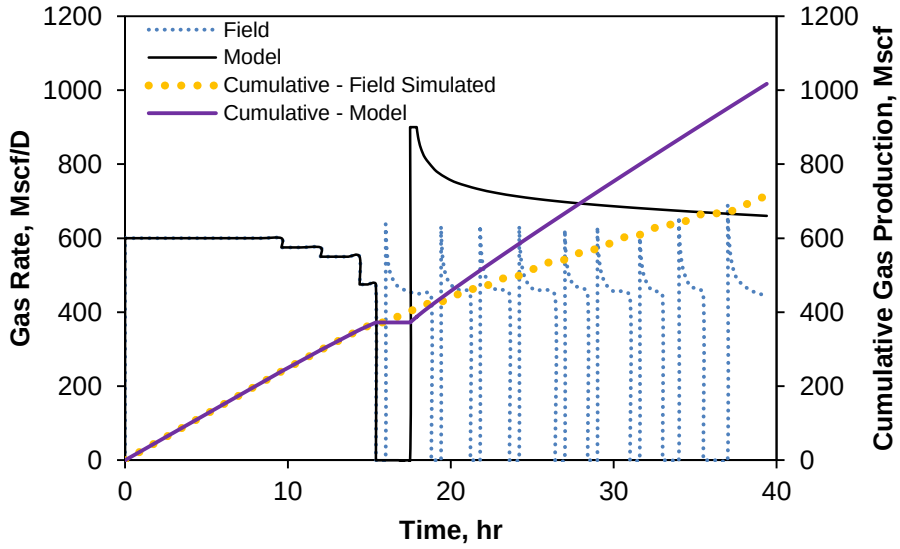

Figure 4. 35 - Simulated rate history and cumulative production for Well 2.

Figure 4.36 shows similar simulation results for Well 1 as Figure 4.35; cumulative production is higher when the proposed schedule is followed. Unlike Well 2, in this case, the field production rate after the third plunger cycle was far greater because the line pressure was reduced by about 15 psi, as shown earlier in Figure 4.32. This lowering of tubinghead pressure has the same effect as raising the casinghead pressure for the same tubinghead pressure. Sustainable production was attained for Case 1 in the field due to lowering of tubinghead pressure.

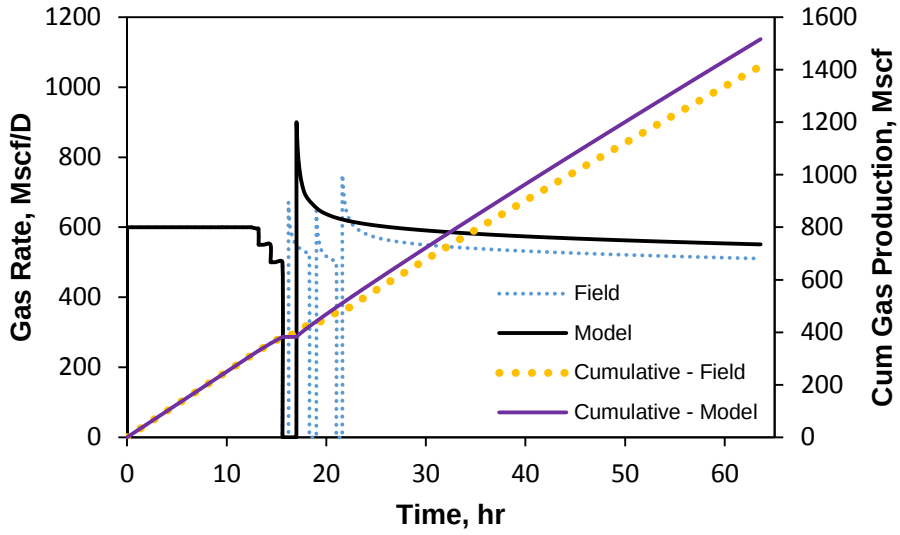

Figure 4. 36 - Simulated rate history and cumulative production for Well 1. (Hashmi et al. 2018)

We think that the required casinghead pressure given by Eq. 3.11 is also the optimum value. In other words, our contention is that cumulative production over a period should be greater using the casinghead pressure given by Eq. 3.11, than using

either a higher or a lower casinghead pressure. We used Well 1 of the Luo-Kelkar study to make this point. We tested the model with a 5% higher and a 5% lower casinghead pressure than was estimated with Eq. 3.11. As expected, both simulations yielded a lower cumulative production than that calculated by following the schedule suggested by Eq. 3.11. These results are shown in **Figure 4.37** and **Figure 4.38**, where we compare the effects of aiming for higher (Figure 4.37) or lower (Figure 4.38) target casinghead pressures.

Figure 4.37 shows that a higher target casinghead pressure requires the plunger to sit at the bottom longer than in the optimum case above. However, this longer shut in does not create much of a change in the final gas flow rate; the cumulative production for a higher casing pressure case ends up being lower than the optimum suggested by Eq. 3.11.

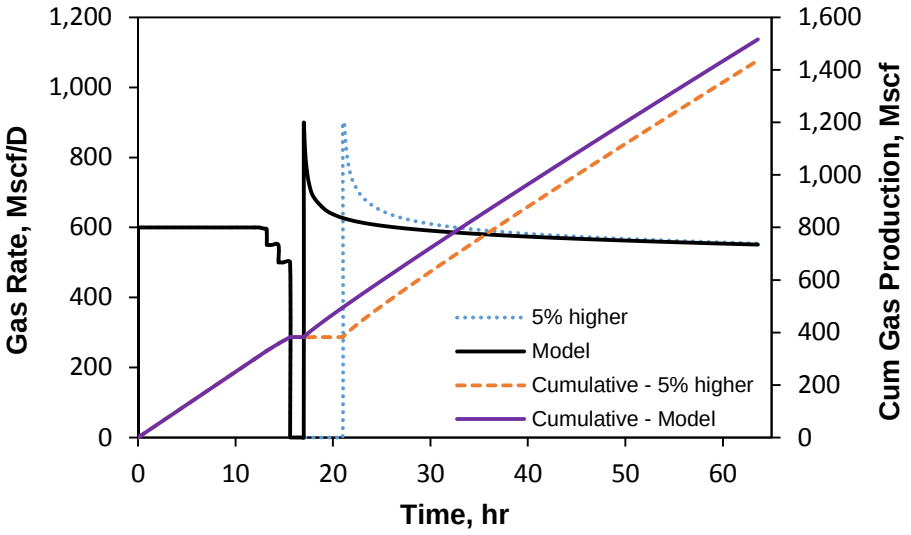

Figure 4. 37 - Comparison of production between optimum and above optimum casing pressure, Well 1.
(Hashmi et al. 2018)

Figure 4.38 represents similar data for a lower than optimum casing pressure. In contrast to the higher casing pressure case shown in Figure 4.37, this one requires shorter shut-in time than is optimum. However, in this case, the pressure does not build up enough to sustain a sufficient rate to maximize production; the cumulative production offered by the casing pressure calculated with Eq. 3.11 ends up being slightly higher. Overall, the results of Figures 4.37 and 4.38 validate that the target casing pressure calculated by the proposed model is, in fact, optimum in a given situation.

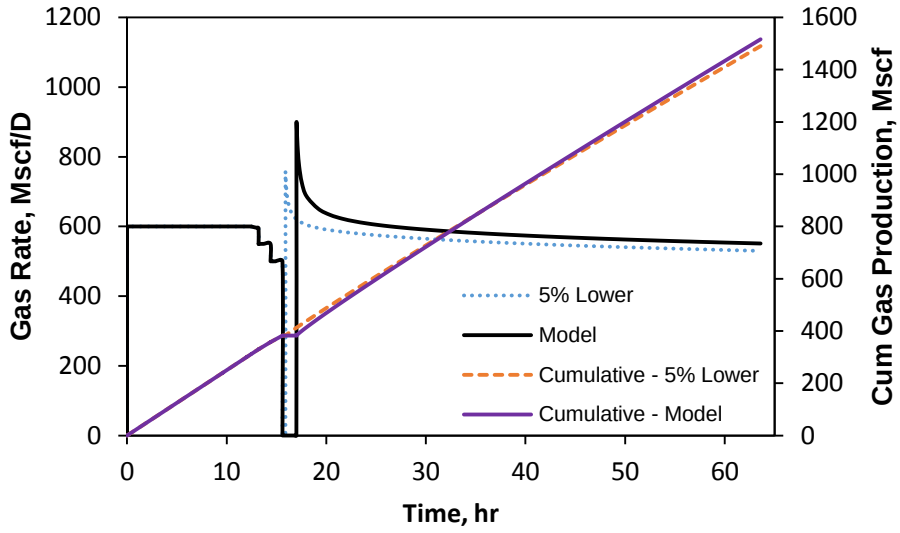

Figure 4. 38 - Comparison of production between optimum and suboptimal casing pressure, Well 1.
(Hashmi et al. 2018)

Wells 3 and 4

Unlike Wells 1 and 2, Wells 3 and 4 of the Luo-Kelkar study perform very differently. **Figures 4.39 and 4.40** show daily production performance data for these two cases, wherein sustained production over prolonged periods is indicated. As shown, the plunger release occurred after attaining a casing pressure of 300 psi for Well 3 and 390 psi for Well 4. In contrast, the proposed model estimated the required casinghead pressures to be 202 and 201 psi for Wells 3 and 4, respectively. Therefore, these two examples support our model's estimation of minimum casinghead pressure requirement for prolonged production cycles.

We note, however, that for both these cases, the model-estimated required casinghead pressures are much lower than what was used in the field. This observation

implies that these two cases may not have required plunger lift (with well shut-in) at all because of the high casinghead pressures. The fact that the steady production rate does not appear to increase after the lift cycle provides another proof of this argument.

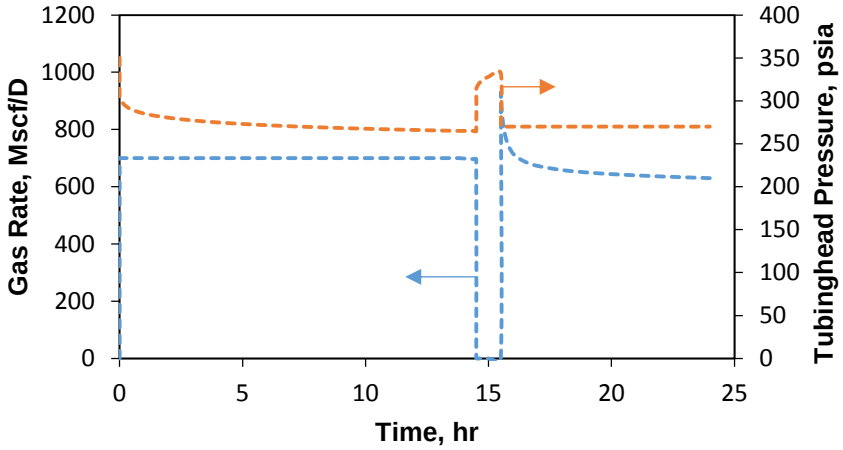

Figure 4. 39 - Production data for Well 3.
(Hashmi et al. 2018)

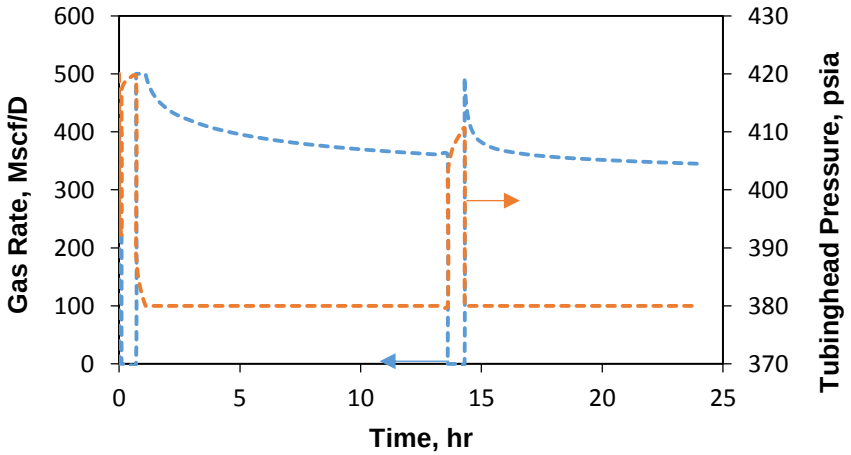

Figure 4. 40 - Production data for Well 4.
(Hashmi et al. 2018)

The significantly higher available casinghead pressure than estimated minimum requirement by our model led us to examine if liquid loading became an issue for these two cases. As Riza et al. (2016), among others, noted, the transition from annular two-phase flow at the well bottom indicates the initiation of liquid loading. We applied the criterion proposed by Riza et al. to Well 3 data to learn if annular two-phase flow occurred at the well bottom. As the sample calculation in Appendix D shows, there are strong indications that annular two-phase flow prevailed at the bottom of Well 3, implying that the well was free of any liquid-loading issues. In the case of Well 4, the evidence of annular two-phase flow throughout the wellbore is inconclusive. Estimation of superficial gas velocity is essential to flow regime determination. In this case, required crucial input data for superficial gas velocity computation, especially formation and fluid temperatures, were unavailable. However, the daily production rate evident in Figure 4.40 strongly implies a lack of imminent liquid-loading issues for this well.

An important aspect of the proposed model is that, although simple, it accounts for all the significant energy elements involved, including the potential energy needed to move the mass of water (m_L) on top of the plunger to the wellhead. This important element of the energy equation is not included in the existing models, including the model proposed by Luo and Kelkar. As the reservoir becomes depleted, more water is likely to be produced, increasing m_L, and hence, the minimum required casing pressure as indicated by Eq. 3.11. An example of this changing optimal casing pressure requirement is given in Appendix A. Note that an operator can estimate water mass, m_L, from water produced per cycle. In the absence of such data, estimated water production

rate from the reservoir model, combined with a wellbore flow model, can be used to estimate m_L.

CHAPTER V

DISCUSSION

This thesis presents different models for fluid flow and heat transfer in the wellbore. As discussed in the last chapter, these models have been verified and validated with simulated and field data. So far the needs for these models have been discussed briefly with their development. This chapter focuses the discussion around the practical implications of these modeling techniques and their applications in the industry.

The motivation for the short duration tests study stemmed from the fact that critical information about a well's productivity or injectivity question arises during a project's field development phase, particularly in high-cost environments, such as in deepwater setting of Gulf of Mexico. Although value of such testing is often questioned, perhaps the problem should be framed in such a way that drilling of an additional well can be explored in the context of a project's economic outcome. This issue may potentially arise due to less than expected outcome in terms of productivity or injectivity index. Short-term tests can provide invaluable insights into a reservoir's overall deliverability potential during exploration, appraisal, and development phase of a project.

Motivated by business drivers, this study presents a unified model for slug, closed-chamber, and injection tests based on the basic similarities of the underlying physical processes. Historically, these tests have often been treated individually. However, the simple mathematical model presented in this work provides an opportunity

to design and analyze test data for any or all of these tests with one single spreadsheet program. This design tool provides a forward model that is simple yet accurate and comprehensive in its formulation. Many simpler models of the past neglected some details, such as the wellbore pressure-loss components and may be unsuitable in high flow-rate situations. Figure 4.2 shows that neglecting wellbore friction can result in over 50% higher estimation of permeability. We also note that, despite various degrees of rigor in the formulation of the reservoir model, not considering frictional pressure-drop may trigger the early-time mismatch in type-curve matching. These type curves have appeared over three decades in the literature, starting with Ramey et al. (1975) and the latest reported by Rahman et al. (2007). We recognize that interpretation methods (Peres et al. 1993) also exist involving both convolution and deconvolution, but with a constant wellbore-storage coefficient. While such analysis may be feasible for a low-velocity flow situation in a slug test, it may be unsuitable for general applications in diverse flow situations.

Detailed studies also exist wherein the coupled reservoir/wellbore flow problem has been pursued numerically; the model by Mfonfu and Grader (1992) is a case-in-point. This model includes all terms of momentum transfer in the wellbore and couples them with a numerical reservoir model that accounts for non-Darcy flow and variable skin to mimic formation cleanup. We note that this study presents a true transient formulation that accounts for velocity transient, dv/dt, which we have neglected. As in this paper, Mfonfu and Grader reproduced the Simmons (1990) example by neglecting frictional pressure loss in the wellbore. However, numerical models in general, and

Mfonfu and Grader model in particular, are burdensome in that they require numerous input data; are often very time consuming; and are not easy to use. In this context, Salas and Sageev (1987) presented a simpler version of the model, accounting for wellbore friction and compressibility changes in fluids for closed-chamber tests.

Combination of CCT and slug test provides a significant advantage of the model proposed in this thesis. Although Kabir (1997) had shown such a possibility with a field example, the design considerations shown in this study can be applied when a CCT alone is infeasible due to its very short duration. In such a case, slug test can precede a CCT, improving the amount of time it takes to test and obtain interpretable data, particularly in highly conductive formations. Furthermore, the analysis of combined tests boosts confidence in interpretation because the solution must honor two distinct signatures. By definition, storage duration in CCT is short-lived because of increasing fluid compressibility; by contrast, slug tests experience a significant wellbore-storage-distortion period because of constant-storage situation. As indicated earlier, CCT is a preferred test from health, safety, and environment (HSE) standpoint, particularly in harsh environments, such as deepwater. Therefore, simplicity, completeness, and ease of applicability of the proposed model are some of its advantages. The validation of the model using various field data and simulated cases provides confidence in the proposed approach.

Although rate computation involved the radial-flow reservoir model, no barrier exists for the use of any analytical model conducive to the system of interest. As shown, computation of variable rates allowed rate-convolution or superposition analysis for the

flow period. Of course, this rate history may also be used for the conventional superposition analysis for the shut-in period. We also used the generalized short-term test solution because only the recovered volume is needed, not the instantaneous rate. To this end, the Soliman approach (1986) provided the desired results. We found this cross-validation of results quite helpful.

The models presented can be very useful in scenarios where surface production is not desired or where conventional well testing is not economically feasible. A short-term test as described can provide an indication of formation permeability and skin and in cases where the test can be made sufficiently long, of initial reservoir pressure. This information would prove valuable especially where log- or core-derived values may be inadequate.

We did not investigate the model's application in a gas well because these tests are rarely applied to such systems. In principle, however, the CCT can be applied to gas wells and elicit useful information. In such cases, both frictional and accelerational components of pressure drop must be properly accounted for to obtain high quality permeability estimates. As Kabir and Hasan (2006) pointed out, friction and acceleration account for much more of the total pressure drop in a gas well than in an oil well. Domination of the accelerational component at shallow depths was clearly illustrated for one example.

The next study presented a new transient-temperature model for computing flow rates from MTS data. The multiphase flowmeter and surface separator verified these rates for both wells. A commercial, numerical wellbore simulator lends further credence

to the analytical solution presented here. Although the solution becomes robust when multiple discrete temperature data sets become available at various depths, the use of single data set at the wellhead is also feasible for estimating rates as outlined in the previous chapter. We note that transient temperature data when used with a steady- state model can potentially lead to errors in estimated rates, although it may be a good approximation in some cases. Stated differently, the rigor of rate-induced superposition solutions for both pressure- and temperature-transient flow problems is the preferred approach. Let us explore this point further.

This study accounts for the effect of formation heating in the form of a variable ξ to account for the depth-dependent superposition effect. For the field conditions studied, ξ did not turn out to be greatly significant. However, simulations run with higher geothermal gradients and lower formation thermal conductivity show noticeable effects of superposition on estimated fluid temperatures, as discussed in Chapter IV. We note that the oft-used formation thermal conductivity of 0.92 Btu/h-ft-°F is considerably lower than 3.59 Btu/h-ft-°F, encountered in the Gulf of Mexico salt domes. To contain severe heat loss, vacuum-insulated tubing is used whose thermal conductivity is 0.92 Btu/h-ft-°F. Therefore, we surmise that parameter ξ will play a more significant role in different circumstances. To begin with, the importance of ξ can be gauged by comparing it with the value of ψ in the model. If ξ is insignificant compared to the value of ψ, it might not cause a significant effect. Conversely, if ξ is significant in comparison to ψ, ignoring it may lead to inaccuracy of the estimated rates. This situation may arise in cases where the resistance between the wellbore and the formation is higher than usual,

such as in presence of vacuum-insulated tubing. Another example of reduced heat loss arises at late times when the formation has had a chance to heat up after a considerable production period.

Interpretation of transient-pressure data using generated rates for both pre- and post-cleanup periods suggested that formation permeability is unaffected by the two-phase flow effects. Stated differently, only the skin is different in the two analyses. The use of statistical DOE provided the initial clue. For instance, a combination of independent variables, such as the permeability-thickness product, soak period, and radius of mud-filtrate invasion collectively suggested that permeability was reproduced without any error. The convergence of the derivative plateaus supports this notion, but the difference in the corresponding pressure curves is a reflection of skin. Both synthetic field examples lend credence to this point.

The soak period in conventional gas reservoirs as studied here did not turn out to be important because capillarity played a minor role. For the same reason this factor will pose fewer problems in an oil reservoir. However, in tight-gas reservoirs when the water saturation exceeds 40 to 50%, the gas production can suffer significantly, as pointed out by Shanley et al. (2004). The problem compounds when the shale gas reservoirs are considered. For instance, the study of Bertoncello et al. (2014) explored the causes of water blockage by incorporating laboratory-derived relative-permeability and capillary-pressure curves into numerical flow simulations while matching well performance. One of the lessons learned is that the flowback should occur as early as possible, followed by a well shut-in period.

This other application of this thermal study presents an approach for computing zonal flow rates from temperature profiles measured using production logging. Field validation was performed using data from a well that was operated at both open choke and 60% flow conditions. The temperature modeling led to a reliable match between the measured and estimated temperatures using the same parameters for both cases. This result provided support for the applicability and utility of the model. Across the perforated interval, temperature fluctuations are observed as a result of flow turbulence that quickly disappear after the fluid leaves the interval and travels up the production tubing. The temperature between and above perforations is modeled and simulated to match the measured temperature, thereby estimating flow rates above and below perforations.

A relatively good match against the spinner interpretation provides additional credence to the workflow presented in Chapter III. The temperature estimate requires knowledge of the different heat transfer parameters previously mentioned. Most of these parameters can be obtained from other sources, such as the offset wells or from information about the field contained in the literature. After a successful calibration has been achieved and the model compares well to spinner interpretation, the process can be automated to provide continuous production surveillance. The technique can provide zonal contributions in real time and can help to optimize production performance, water control and management, and predict and mitigate flow assurance problems.

Furthermore, the methodology can be extended to identify flow behind casing, provide quantitative leaks determination, and determine completion integrity.

The proposed approach, however, includes some limitations. The model assumes a vertical or near-vertical system; the same model cannot be used for horizontal or highly deviated wells. In addition, the model may not be applicable in certain cases, e.g., the relationship between temperature and rate that forms the backbone of this approach may falter at higher rates in gas wells. This limitation was shown by Kabir et al. (2014) in which gas well temperatures are simulated at higher rates. The loss of fidelity attributable to Joule-Thomson cooling at higher rates may reduce the quality of the rate solution. Although translating the temperature measurements to fluid rate each time may pose a challenge, it should be noted that a model is only an attempt to mimic the physical system. The intent is not to replace production logging completely, but to provide another tool to supplement the interpretations provided by the spinner and to possibly reduce the number of required PL runs over the lifespan of the well. For this purpose, the model and the workflow perform fairly well.

This work shows the application of rate estimation during production logging in a single-phase well. The model can also be combined with other sensors, such as dielectric and fluid density sensors, or a gas holdup tool to predict individual holdups and multiphase rates. The combinability greatly enhances the utility of the workflow and provides for a better-suited production monitoring system. Weiland et al. (2008) and Khan et al. (2017) demonstrate that multiple production logging runs can be used over a

long time period to monitor field performance. With the technique presented in this thesis, more continuous monitoring can be achieved, with fewer PL runs.

Lastly, this work presents a wellbore model to assess the desired casinghead pressure for optimal performance of plunger lift operations. Conservation of mass and energy in the wellbore and numerical two-phase flow modeling in the reservoir formed the cornerstone of the proposed approach. Continued operation with liquid loading leads to increased operational expense. Therefore, an understanding of liquid loading should be relevant to any operator of gas wells. Application of a simple expression, such as the one shown in Appendix D, helps determine if actual production rate is below the critical rate for liquid loading. This finding should influence an engineer's decision on the timing of implementation of any artificial lift, such as plunger lift.

The simplicity of the model presented in Chapter III allows for the broad applicability across different regions. Compared to some of the previous relevant studies of Foss and Gaul (1965) and Lea (1982), the proposed approach provides a way to obtain required casinghead pressure. This parameter is more in step with operators' well surveillance and management practices. Although we used a numerical reservoir model to elicit transient IPR to replicate the field responses, one can explore the same with analytical or semianalytical methods.

Given that the brownfields constitute the industry's backbone, optimization of artificial lift methods becomes a necessity. In light of paucity in drilling during downturns in industry, some operators experience a great need for artificial lift for a lot of the wells. Given the low-cost operation, plunger lift is an attractive option and our

approach to optimize the plunger lift cycle for cumulative production makes this lift option to operate more efficiently.

CHAPTER VI

CONCLUSION

This thesis presents different flow models in the wellbore for three different categories of applications. The work has been presented as such to highlight the different modeling techniques separately in order to provide more clarity.

In the first case, a coupled wellbore/reservoir model is formulated to facilitate test design and analysis of both closed-chamber and slug tests. Whereas the wellbore model incorporates all three components of pressure-drop, the reservoir model involves radial flow in a fully penetrating homogeneous reservoir. Computation of rate is implicit in all test settings and convolution of this rate with pressure leads to unambiguous results. A possible design of combining the two tests is also suggested for high mobility reservoirs. The combination of slug/CCT provides two distinct signatures because of the fluid compressibility effect in the wellbore. This combined test, where feasible, can ensure high quality solutions. Reverse-slug tests are also discussed where under-pressured reservoirs lend themselves to slug tests by way of fluid injection. The same design and analysis techniques apply as in fluid production. Multiple field examples are used to validate both forward modeling and data analysis. In this context, the short-term test analysis approach corroborated the results generated with the pressure/rate convolution approach.

The next category of modeling presents a transient temperature model for computing rates with multipoint-temperature (MPT) measurements. The analytical

solution includes a novel depth-dependent-temperature superposition that accounts for the effect of variable heat flux. This analytical solution was validated with field data from two wells and verified by a commercial simulator. Although the new temperature superposition solution did not produce a large difference when compared with the solution excluding superposition for the specific problems studied, this general solution is expected to work for diverse flow problems. The rate estimation algorithm is robust when the MPT data is available. Nonetheless, anchoring one of the transient flow periods with measured rates allows estimation of the same for other transient periods with good engineering accuracy. The modeling technique was applied to two different fields of application that attests to the applicability and utility of the model.

The first application stems from the field of transient testing where distributed temperature measurements allowed for estimation of downhole rates for entire duration of the tests. Analysis of transient data during the pre- and post-cleanup periods suggested that the formation permeability can be estimated without any issues, and that the difference in the buildup response is because of skin. Both field and synthetic tests supported the value of interpreting the pre-cleanup data. Estimating the formation permeability up front allows fine-tuning of the subsequent test periods commensurate with objectives.

The second application involves the use of temperature surveys during production logging to estimate flow rates in oil wells. Transient temperature was captured at various well depths and matched with simulated temperature to determine flow rates from each zone. Robust rate solutions were obtained by honoring the

temperature data at each half-foot interval in this computational algorithm. The interpretation using spinner data lends credence to the computed rates using temperature. The workflow is more rigorous after it has been calibrated so that it can provide continuous surveillance thereafter. Drawdown over extended time periods may alter the system physically, at which time a new calibration may be needed. Nonetheless, anchoring on even the original calibration can provide reasonable estimates of flow rates or zonal contributions. The combination with other logs provides an opportunity to reduce estimation uncertainty when more than one phase is involved. Dielectric or fluid density sensors can provide for another constraining variable to lead to a more unique solution in determining multiphase rates from temperature measurements.

Lastly the study offers a model for one of the artificial lift techniques, i.e. plunger lift. An analytical plunger lift model, based on energy balance, is developed and validated with data from two wells. This wellbore model may be used as a stand-alone tool to optimize the plunger cycle. The model is relatively simple to use and allows operators to determine field parameters without having to provide numerous inputs. Operators could benefit from keeping water production data because it would allow optimizing casing pressure that could change with water production. Reservoir flow models, built by honoring pressure and rate data, further allowed exploring improved lift performance by increasing the casing pressure and the attendant benefit in terms of cumulative gas production. Two other field examples suggested that installation of plunger lift was premature in that sustained production occurs due to presence of annular flow at the well bottom.

All the models developed in this work pertain to fluid or heat flow in the wellbore. As mentioned at the start of this thesis, advancements in technology and data management have given rise to newer ways of characterizing reservoirs and producing wells more effectively. Understanding of flow models such as the ones presented in this thesis will help to elucidate and solve many of the flow problems that are encountered in industry. By accounting for different boundary conditions and initial conditions for the momentum and heat transfer equations, this study aims to provide solutions for a few of those problems.

REFERENCES

Abercrombie, B. 1980. Plunger Lift. In *Technology of Artificial Lift Methods*, Ed. Brown, K.E., Vol. 2b, p. 483, PennWell Pub. Co.

Alexander L.G. 1977. Theory and Practice of the Closed-Chamber Drillstem Test Method. *J Can Pet Technol* **29** (12): 1539–1544. http://dx.doi.org/10.2118/6024-PA.

Alpak, F.O., Elshahawi, H., Hashem, M, and Mullins, O.C. 2008. Compositional Modeling of Oil-Based-Mud-Filtrate Cleanup During Wireline Formation Tester Sampling. *SPE Res Eval & Eng* **11** (2): 219-232. http://dx.doi.org/10.2118/100393-PA.

Bahonar, M., Azaiez, J., and Chen, Z. 2011a. Transient Nonisothermal Fully Coupled Wellbore/Reservoir Model for Gas Well Testing, Part 1: Model Development. *J. Can Pet Techol* **50** (9/10): 37–50. http://dx.doi.org/10.2118/149617-PA.

Bahonar, M., Azaiez, J., and Chen, Z. 2011b. Transient Nonisothermal Fully Coupled Wellbore/Reservoir Model for Gas Well Testing, Part 2: Applications. *J. Can Pet Techol* **50** (9/10): 52–70. http://dx.doi.org/10.2118/149618-PA.

Baruzzi, J. O. A. and Alhanati, F. J. S. 1995. Optimum plunger lift operation. Presented at the SPE Production Operations Symposium, 2-4 April, Oklahoma City, Oklahoma, USA. SPE-29455-MS. http://dx.doi.org/10.2118/29455-MS.

Bertolini, C., Tripaldi, G., Manassero, E. et al. 2009. A Cost Effective and User Friendly Approach for mini-DSTs Design. Paper SPE 122886 presented at the EUROPEC/EAGE Conference and Exhibition, 8–11 June, Amsterdam, The Netherlands. https://dx.doi.org/10.2118/122886-MS

Bertoncello, A., Wallace, J, Blyton, C., et al. 2014. Imbibition and Water Blockage in Unconventional Reservoirs: Well Management Implications During Flowback and Early Production. *SPE Res Eval & Eng* **17** (4): 497-506. http://dx.doi.org/10.2118/167698-PA.

Chava, G., Falcone, G., and Teodoriu, C. 2010. Plunger-lift modeling toward efficient liquid unloading in gas wells. *SPE Projects, Fac. & Const.* **5** (1), 38−45. http://dx.doi.org/10.2118/124515-PA.

Chava, G.K., Falcone, G., and Teodoriu, C. 2008. Development of a new plunger-lift model using smart plunger data. Paper SPE-115934-MS presented at the SPE Annual Technical Conference and Exhibition, 21-24 September, Denver, Colorado, USA. http://dx.doi.org/10.2118/115934-MS.

Clarkson, C.R., Behmanesh, H., and Chorney, L. 2013. Production-Data and Pressure-Transient Analysis of Horseshoe Canyon Coalbed-Methane Wells, Part II: Accounting for Dynamic Skin. *J Can Pet Tech* **52** (1): 41-53. http://dx.doi.org/10.2118/148994-PA.

Coelho, A.C.D., de Camargo, C., Kato, E.T., et al., 2005. Utilizing Mini-DST for Formation Evaluation. Paper SPE 94963 presented at SPE Latin American and

Caribbian Petroleum Engineering Conference, Rio de Janeiro, Brazil, 20–23 June. https://dx.doi.org/10.2118/94963-MS

Curtis, M.R. and Witterholt, E.J. 1973. Use of the Temperature Log for Determining Flow Rates in Producing Wells. Presented at the 1973 SPE Annual Meeting, Las Vegas, Nevada, USA, September 30-October 3. https://dx.doi.org/10.2118/4637-MS.

Dale, C.R. 1949. Bottom Hole Flow Surveys for Determination of Fluid and Gas Movements in Wells. *J Pet Technol* **1** (08): 205-10. SPE-949205-G. http://dx.doi.org/10.2118/949205-G.

Daungkaew, S., Harfoushian, J.H., Cheong., A.O., et al. 2007. Mini-DST Applications for Shell Deepwater Malaysia, Paper SPE 109279 presented at the SPE Asia-Pacific Oil and Gas Conference and Exhibition, Jakarta, Indonesia, 30 October–1 November. https://dx.doi.org/10.2118/109279-MS

Dranchuk, P.M. and Abou-Kassem, J.H. 1975. Calculation of z-Factors for Natural Gases Using Equations of State. *J Can Pet Technol* **14** (3): 34–36. http://dx.doi.org/10.2118/75-03-03.

Duru, O.O. and Horne, R.N. 2010. Modeling Reservoir Temperature Transients and Reservoir-Parameter Constrained to the Model. *SPE Res Eval & Eng* **13** (6): 873–883. http://dx.doi.org/10.2118/115791-PA.

Fan, L., Lee, W.J., and Spivey, J.P. 2000. Semianalytical Model for Thermal Effect on Gas Well Pressure-Buildup Tests. *SPE Res Eval & Eng* **3** (6): 480–491. http://dx.doi.org/10.2118/68020-PA.

Ferris, J.G. and Knowles, D.B. 1954. The Slug Test for Estimating Transmissibility. USGS Ground Water Note **26**, 1–7.

Foss, D. L. and Gaul, R. B. 1965. Plunger-lift performance criteria with operating experience-Ventura Avenue field. Drill & Prod Practice, New York, New York. API.

Frimann-Dahl, C., Irvine-Fortescue, J., Rokke, E., et al., 1998. Formation Tester vs. DST–The Cost Effective Use of Transient Analysis to Get Reservoir Parameters. Paper SPE 48962 presented at the SPE Annual Technical Conference and Exhibition, New Orleans, Louisiana, 27–30 September. https://dx.doi.org/10.2118/48962-MS

Gasbarri, S. and Wiggins, M. L. 2001. A dynamic plunger lift model for gas wells. *SPE Prod. & Fac.* **16** (2), 89−96. http://dx.doi.org/10.2118/72057-PA.

Goins, W.C. Jr. and Dawson, D.D. Jr. 1953. Temperature Surveys to Locate Zone of Lost Circulation. *Oil & Gas J* **52** (7): 170-71.

Gok, I.M., Onur, M., Hegeman, P.S., et al. 2006. Effect of an Invaded Zone on Pressure Transient Data from Multiprobe and Packer-Probe Wireline Formation Testers. *SPE Res Eval & Eng.* **9** (1): 39–49. http://dx.doi.org/10.2118/84093-PA.

Goode, P.A. and Thambynayagam, R.K.M. 1996. Influence of an Invaded Zone on a Multiprobe Formation Tester. *SPE Form Eval* **11** (1): 31–40. http://dx.doi.org/10.2118/23030-PA.

Grader, A.S. and Ramey, H.J., Jr. 1988. Slug-Test Analysis in Double-Porosity Reservoirs. *SPE Form Eval* **3** (2): 329–339. http://dx.doi.org/10.2118/15479-PA.

Hacksma, J.D., 1972. Users guide to predict plunger lift performance. Proc, Southwestern Petroleum Short Course, Lubbock, Texas.

Halbouty, M.T. 1939. Temperature Effects on Oil Well Drilling. *Oil Weekly* **96** (02): 10-16.

Harmawan, I., Kabir, C.S., Habib, S.M. et al. 2012. Integrating Mini-DST-Derived Permeability With Other Sources: A Case Study. *SPE Res Eval & Eng* **15** (3): 361–369. http://dx.doi.org/10.2118/145764-PA.

Hasan, A.R. and Kabir, C.S. 2002. *Fluid Flow and Heat Transfer in Wellbores*. Richardson, Texas: Textbook Series, SPE.

Hasan, A.R., Kabir, C.S., Lin, D., 2005. Analytic wellbore temperature model for transient gas-well testing. *SPEREE* **8** (3), 240–247. https://dx.doi.org/10.2118/84288-PA.

Hasan, A.R., Kabir, C.S., and Sayarpour, M. 2010: Simplified Two-Phase Flow Modeling in Wellbores. *J Pet Sci & Eng* **72** (3-4): 42−49. http://dx.doi.org/10.1016/j.petrol.2010.02.007.

Hashmi, G. M., Hasan, A. R., and Kabir, C. S. 2018. Simplified modeling of plunger-lift assisted production in gas wells. *J. Nat. Gas Sci. & Eng.* **52**: 454–460. https://doi.org/10.1016/j.jngse.2018.02.009.

Hashmi, G.M., Kabir, C.S., and Hasan, A.R. 2015. Estimating Reliable Gas Rate with Transient-Temperature Modeling for Interpreting Early-Time Cleanup Data During Transient Testing. *J. Pet. Sci. & Eng.* **133**: 285–295. https://doi.org/10.1016/j.petrol.2015.06.001.

Hashmi, G. M., Kabir, C. S., and Hasan, A. R. 2016. Design and Interpretation of Transient Tests at Well's Inception. *J. Pet. Sci. & Eng.* **145**: 573–584. https://doi.org/10.1016/j.petrol.2016.06.035.

Hegeman, P. and Abbaszadeh, M. 1988. An Analytical Simulator for Drillstem Test Interpretation. *SPE Form Eval* **3** (4): 725–732. http://dx.doi.org/10.2118/16380-PA.

Hill, A.D. 1990. *Production Logging: Theoretical and Interpretive Elements*. SPE Monograph Series, vol. 14., Richardson, Texas, USA: Society of Petroleum Engineers.

Ismadi, D., Kabir, C.S., and Hasan, A.R. 2012. The Use of Combined Static and Dynamic-Material-Balance Methods With Real-Time Surveillance Data in Volumetric Gas Reservoirs. *SPE Res Eval & Eng* **15** (3): 351–360. http://dx.doi.org/10.2118/145798-PA.

Izgec, B., Hasan, A.R., Lin, D. et al. 2010. Flow-Rate Estimation from Wellhead-Pressure and Temperature Data. *SPE Prod & Oper* **25** (1): 240-47. SPE-115790-PA. http://dx.doi.org/10.2118/115790-PA.

Izgec, B., Kabir, C.S., Zhu, D., and Hasan, A.R. 2007. Transient Fluid and Heat Heat Flow Modeling in Coupled Wellbore/Reservoir Systems. *SPE Res Eval & Eng* **10** (3): 294–301. http://dx.doi.org/10.2118/102070-PA.

Kabir, C.S. 1997. Seeking Synergy Between Drawdown and Buildup Analyses. *SPE Form Eval* **12** (2): 125–131. http://dx.doi.org/10.2118/30551-PA.

Kabir, C.S. and Hasan, A.R. 2006. Simplified Wellbore Flow Modeling in Gas-Condensate Systems. *SPE Prod Opns.* **21** (1): 89–97. http://dx.doi.org/10.2118/89754-PA.

Kabir, C.S., Badry, R.A., and Hasan, A.R. 1991. Two-Phase Gas/Liquid Flow Rate Estimation During Closed-Chamber Testing. *J Can Pet Techol* **2** (30): 102. http://dx.doi.org/10.2118/91-02-08.

Kabir, C.S., Hasan, A.R., Jordan, D.L., and Wang, X. 1996. A Wellbore/Reservoir Simulator for Testing Gas Wells in High-Temperature Reservoirs. *SPE Form Eval* **11** (2): 128–134. http://dx.doi.org/10.2118/28402-PA.

Kabir, C.S., Izgec, B., Hasan, A.R., and Wang, X. 2012. Computing flow profiles and total flow rate with temperature surveys in gas wells. 2012. *J. Natural Gas Sci & Eng* **4** (2012): 1–7. http://dx.doi.org/10.1016/j.jngse.2011.10.004.

Kabir, C.S., Yi, X., Jakymec, M., and Hasan, A.R. 2014. Interpreting Distributed-Temperature Measurements in Deepwater Gas-Well Testing: Estimation of Static and Dynamic Thermal Gradients, and Flow Rates. *SPE Prod & Opns.* **29** (2): 97−104. http://dx.doi.org/10.2118/166333-PA.

Kamal, M.M., et al. 2009. *Transient Well Testing*, SPE monograph, Volume 23, SPE, Richardson, Texas.

Khan, W., Azari, M., Hamza, F. et al. 2017. Case Study: Multirate Multizone Production Logging and Testing Provides Real-Time Reservoir Insight for Stimulation Treatment Optimization in Deepwater GOM. Presented at the 2017 SPE Annual Technical Conference and Exhibition, San Antonio, Texas, USA, 9-11 October. SPE-187407-MS. http://dx.doi.org/10.2118/187407-MS.

Kunz, K.S. and Tixier, M.P. 1955. Temperature Surveys in Gas Producing Wells. *Petroleum Transactions, AIME* **204**: 111-119. SPE-472-G.

Larsen, L. and Kviljo, K. 1990. Variable-Skin and Cleanup Effects in Well-Test Data. *SPE Form Eval* **5** (3): 272–276. http://dx.doi.org/10.2118/15581-PA.

Larsen, L. and Kviljo, K., and Litlehamar, T. 1990. Estimating Skin Decline and Relative Permeabilities From Cleanup Effects on Well-Test Data With Buckley-Leverett Methods. *SPE Form Eval* **5** (4): 360–368. http://dx.doi.org/10.2118/17566-PA.

Lea, J.F. 1982. Dynamic analysis of plunger lift operations. *J. Pet. Technol.* **34** (11), 2617−2629. http://dx.doi.org/10.2118/10253-PA.

Luo, S. and Kelkar, M., 2014. Effective method to predict installation of plunger in a gas well. *J. Energy Res. Technol.* **136** (2): 024501. http://dx.doi.org/10.1115/1.4025799.

Maggard, J.B., Wattenbarger, R.A., and Scott, S.L. 2000. Modeling plunger lift for water removal from tight gas wells. SPE/CERI Gas Technology Symposium, 3-5 April, Calgary, Alberta, Canada. http://dx.doi.org/10.2118/59747-MS.

Marcano, L. and Chacin, J. 1994. Mechanistic design of conventional plunger lift installations. *SPE Advanced Tech Series* **2** (1): 15-24. http://dx.doi.org/10.2118/23682-PA.

Meunier, D.F., Wittmann, M.J., and Stewart, G. 1985. Interpretation of Pressure Buildup Test Using In-Situ Measurement of Afterflow. *J Pet Tehnol* **37** (1): 143–152. http://dx.doi.org/10.2118/11463-PA.

Mfonfu, G. and Grader, A. 1992. An Implicit Numerical Model for the Closed-Chamber Test. *SPE Form Eval* **2** (7): 185–192. http://dx.doi.org/10.2118/19832-PA.

Millikan, C.V. 1941. Temperature Surveys in Oil Wells. *Transactions of the AIME* **142** (01): 15-23. SPE-940015-G. http://dx.doi.org/10.2118/941015-G.

Peres, A.M.M., Onur, M., and Reynolds, A.C. 1993. A New General Pressure Analysis Procedure for Slug Tests. *SPE Form Eval* **8** (4): 292–298. http://dx.doi.org/10.2118/18801-PA.

Petak, K.R., Finley, D.B., and Coble, L.E. 1991. Drill Stem Test and Closed-Chamber Drill Stem Test Simulation. Paper SPE 23115 presented at the Offshore Europe

Conference, Aberdeen, Scotland, UK, 3-6 September. https://dx.doi.org/10.2118/23115-MS.

Rahman, N.M.A., Santo, M.S., and Mattar, L. 2007. A New Approach for Interpreting Pressure Data to Estimate Key Reservoir Parameters From Closed-Chamber Tests. Paper SPE-109860-MS presented at the SPE Annual Technical Conference and Exhibition, 11–14 November, Anaheim, California, USA. http://dx.doi.org/10.2118/109860-MS.

Ramaswami, S.R., Elshahawi, H., and El-Battaway, A. 2012. Integration of Wireline Formation Testing and Well Testing Evaluation–An Example from the Caspian. *SPE Form Eval* **15** (3): 300–313. http://dx.doi.org/10.2118/139837-PA.

Ramey, H.J. Jr. 1962. Wellbore Heat Transmission. *J Pet Technol* **14** (04):425-35. SPE-96-PA. http://dx.doi.org/10.2118/96-PA.

Ramey, J.J., Jr., Agarwal, R.G., and Martin, I. 1975. Analysis of 'Slug Test' or DST Flow Period Data. *J Can Pet Technol* **14** (3): 37–47. http://dx.doi.org/10.2118/75-03-04.

Riordan, M.B. 1951. Surface Indicating Pressure, Temperature and Flow Equipment. *J Pet Technol* **3** (09): 257-262. SPE-951257-G. http://dx.doi.org/10.2118/951257-G.

Riza, M.F., A.R. Hasan, and C.S. Kabir. 2016. A pragmatic approach to understanding liquid loading in gas wells. *SPE Prod. Oper.* **31** (3), 185-196. http://dx.doi.org/10.2118/170583-PA.

Romero-Juarez, A. 1969. A Note on the Theory of Temperature Logging. *SPE J* **9** (04): 375-377. SPE-2464-PA. http://dx.doi.org/10.2118/2464-PA.

Rosina, L. 1983. A study of plunger lift dyanmics. MS Thesis. The University of Tulsa, Tulsa, Oklahoma, USA.

Rubis–Multipurpose Numerical Model. Kappa Engineering. (https://www.kappaeng.com/software/rubis/overview).

Salas, B. and Sageev, A. 1987. Closed Chamber Testing: The Effects of Wellbore Friction and Fluid Compression. Paper SPE-16800-MS presented at the SPE Annual Technical Conference and Exhibition, 27-30 September, Dallas, Texas, USA. http://dx.doi.org/10.2118/16800-MS.

Saldana-C, M.A. and Ramey, H.J., Jr. 1986. Slug Test and Drillstem Test Flow Phenomena Including Wellbore Inertial and Frictional Effects. Paper SPE-15118-MS presented at the SPE California Regional Meeting, 2-4 April, Oakland, California, USA. https://dx.doi.org/10.2118/15118-MS.

Schlumberger, M., Doll, H.G., and Perebinossoff, A. 1937. Temperature Measurements in Oil Wells. *J. Inst. Pet. Technologists* **23** (159): 1-25.

Shanley, K.W., Cluff, R.M., and Robinson, J.W. 2004. Factors Controlling Prolific Gas Production From Low-Permeability Sandstone Reservoirs: Implications for Resource Assessment, Prospect Development, and Risk Analysis. *AAPG Bull.* **88** (8): 38. http://dx.doi.org/10.1306/03250403051.

Shinohara, K. and Ramey, H.J., Jr. 1979. Analysis of Slug Test DST Flow Period With Critical Flow. Paper SPE-7981-MS presented at the SPE California Regional Meeting, 18-20 April, Ventura, California, USA. http://dx.doi.org/10.2118/7981-MS.

Simmons, J.F. 1990. Convolution Analysis of Surge Pressure Data. *J Pet Technol* **42** (1): 74–83. http://dx.doi.org/10.2118/15477-PA.

Simmons, J.F. and Grader, A.S. 1988. Application of Closed-Chamber Theory to Backsurge Completion Testing. *SPE Prod Eng* **3** (4): 527–536; Trans., AIME, 285. http://dx.doi.org/10.2118/14252-PA.

Soliman, M.Y. 1986. Analysis of Buildup Tests With Short Producing Time. *SPE Form Eval* **1** (4): 363–371. https://dx.doi.org/10.2118/11083-PA.

Soliman, M.Y., Azari, M.Y., Ansah, J., Kabir, C.S. 2004. Design, Interpretation, and Assessment of Short-Term Pressure-Transient Tests. Paper SPE-90837-MS presented at the SPE Annual Technical Conference and Exhibition, 26-29 September, Houston, Texas. http://dx.doi.org/10.2118/90837-MS.

Sufi, A.H. and Thompson, R.J. 1988. Injectivity Testing in Underpressured Reservoirs. *J Pet Technol* **40** (1): 105–110. http://dx.doi.org/10.2118/15112-PA.

Tang, Y. and Liang, Z., 2008. A new method of plunger lift dynamic analysis and optimal design for gas well deliquification. Presented at the SPE Annual Technical Conference and Exhibition, 21-24 September, Denver, Colorado, USA. http://dx.doi.org/10.2118/116764-MS.

Tardy, P.M.J., Ramondenc, P., Weng, X. et al. 2012. Inversion of Distributed-Temperature-Sensing Logs to Measure Zonal Coverage During and After Wellbore Treatments With Coiled Tubing. *SPE Prod & Opns.* **27** (1): 78–86. http://dx.doi.org/10.2118/143331-PA.

Theuveny, B.C., Mikhailov, D., Spesivtev, P. et al. 2013. Integrated Approach to Simulation of Near-Wellbore and Wellbore Cleanup. Paper SPE-166509-MS presented at the SPE Annual Technical Conference and Exhibition, 30 September – 2 October, New Orleans, Louisiana, USA. http://dx.doi.org/10.2118/166509-MS.

Wade, R.T., Cantrell, R.C., Poupon, A. et al. 1965. Production Logging–The Key to Optimum Well Performance. *J Pet Technol* **17** (02): 137-44. SPE-944-PA. http://dx.doi.org/10.2118/944-PA.

Wang, Y., Lee, W.J., Thigpen, et al. 2008. Modeling Flow Profile Using Distributed Temperature Sensor (DTS) System. Paper SPE 111790-MS presented at the Intelligent Energy Conference and Exhibition, 25–27 February, Amsterdam, The Netherlands. http://dx.doi.org/10.2118/111790-MS.

Weiland, J., Azari, M., Suparman, F. et al. 2008. Case History Review of the Application of Pressure-Transient Testing and Production Logging in Monitoring the Performance of the Mars Deepwater Gulf of Mexico Field. Presented at the 2008 SPE Annual Technical Conference and Exhibition,

Denver, Colorado, USA, 21-24 September. https://dx.doi.org/10.2118/115591-MS.

WELLCAT Casing Design Software. Landmark. Halliburton, https://www.landmarksoftware.com/Pages/WELLCAT.aspx.

Witterholt, E.J. and Tixier, M.R. 1972. Temperature Logging in Injection Wells. Presented at the 1972 SPE Annual Meeting, San Antonio, Texas, USA, 8-11 October. SPE-4022-MS. http://dx.doi.org/10.2118/4022-MS.

Yoshioka, K., Zhu, D., Hill, A.D. et al. 2009. A New Inversion Method to Interpret Flow Profiles From Distributed Temperature and Pressure Measurements in Horizontal Wells. *SPE Prod & Oper* **24** (4): 510-521. http://dx.doi.org/10.2118/109749-PA.

APPENDIX A

SLUG AND CLOSED-CHAMBER TESTS

This appendix presents the derivations for the slug and closed-chamber test models along with the computational algorithm. Most of the design equations used for both tests are similar. The differences in approach, where they arise, are mentioned. We assume a piston-like displacement of any fluid already present in the wellbore by the reservoir influx in a vertical well. Well deviations, if any, can be easily integrated into these pressure-drop calculations.

Referring to Figure 3.1, the flowing bottomhole pressure p_{wf} can be expressed in terms of pressure at the top of the gas chamber p_1, the static pressure exerted by the gas in the chamber, and the pressure exerted by any existing initial wellbore fluid, and reservoir fluid in the system. While pressure exerted by the chamber (wellbore) gas is purely static, those exerted by the initial wellbore fluid and reservoir fluid must also account for the frictional and accelerational pressure losses experienced by a moving fluid column. Therefore, at any timestep, we can write

$$p_{wf} = p_1 + \Delta p_g + \Delta p_{if} + \Delta p_{rf} \tag{A.1}$$

The difference between gas chamber bottom and top pressures Δp_g is due only to the static head. Therefore, the gas chamber bottom pressure p_2 can be obtained from the

known chamber top pressure p_1 in terms of the chamber height Δz_g, gas specific gravity γ_g, and absolute temperature T by the following expression:

$$p_2 = p_1 \exp\left(\frac{29\gamma_g \Delta z_g}{1545(T+460)Z}\right) \tag{A.2}$$

When the gas-column height is large, Δz_g can be subdivided into a number of sections to estimate gas chamber bottom pressure more accurately through stepwise computations. The Z-factor is calculated with the Dranchuk and Abou-Kassem (1975) correlation. During a slug test, the wellhead is open; therefore, p_1 is taken to be 14.7 psia at all times. For a CCT, the initial value of p_1 must be directly or indirectly available. Note also that as the test progresses, all pressure values, including p_1, evolve with time.

To estimate the pressure exerted by the initial wellbore fluid and reservoir fluid columns, Δp_{if} and Δp_{rf}, we must account for static, frictional, and accelerational heads because the wellbore fluid columns move covering a distance equivalent to the fluid entry from the reservoir into the wellbore during each timestep. The static head for the wellbore initial-fluid column remains constant. Pressure p_3 is computed from the following expression:

$$p_3 = p_2 + \Delta p_{if} = p_2 + \left(\frac{\mathrm{d}p}{\mathrm{d}z}\right)_H \Delta z_{if} + \left[\left(\frac{\mathrm{d}p}{\mathrm{d}z}\right)_F + \left(\frac{\mathrm{d}p}{\mathrm{d}z}\right)_A\right] \Delta z \tag{A.3}$$

In Eq. A-3, $(\mathrm{d}p/\mathrm{d}z)_H(\Delta z_{if})$ is the static-head pressure exerted by the fluid initially in the wellbore. In Eq. A-3, Δz is the height of fluid entering the wellbore, which is calculated from the volume of fluid entering during a particular time-step j, divided by the wellbore

cross-sectional area A; that is, $\Delta z = (\Delta t)\, q_j/A$. Because q decreases with increasing time, Δz declines as a consequence.

The flowing bottomhole pressure p_{wf} can now be calculated by adding the pressure drop contribution of the reservoir fluid to p_3. Note that Δp_{rf} computation requires the static head contribution of the entire reservoir-fluid column Δz_{rf} in addition to the frictional and accelerational components of that column through a distance of Δz, as follows:

$$\Delta p_{rf} = \left(\frac{\mathrm{d}p}{\mathrm{d}z}\right)_H \Delta z_{rf} + \left[\left(\frac{\mathrm{d}p}{\mathrm{d}z}\right)_F + \left(\frac{\mathrm{d}p}{\mathrm{d}z}\right)_A\right]\Delta z \tag{A.4}$$

In Eqs. A.3 and A.4, the hydrostatic pressure gradient in field units (psi/ft) is calculated by

$$\left(\frac{\mathrm{d}p}{\mathrm{d}z}\right)_H = \frac{\rho}{144} \tag{A.5}$$

The frictional pressure gradient uses the following relationship:

$$\left(\frac{\mathrm{d}p}{\mathrm{d}z}\right)_F = \frac{2fv^2\rho}{d(32.2)(144)} \tag{A.6}$$

Lastly, the accelerational pressure gradient or the kinetic pressure drop is calculated using

$$\left(\frac{\mathrm{d}p}{\mathrm{d}z}\right)_A = \bar{v}\rho\left(\frac{v_2 - v_1}{z_2 - z_1}\right)\frac{1}{(32.2)(144)} \tag{A.7}$$

Velocity v in Eq. A.6 and A.7 is calculated from q_j/A, and $\bar{v}$ represents the arithmetic average of velocities at two different depths. Computation is initiated by first calculating p_{wf} using Eqs. A.1 through A.7, then using this bottomhole pressure to calculate q from the following expression:

$$q = \frac{kh(p_{wf} - p_i)}{70.6B\mu E_i\left(-\frac{948\varphi\mu c_t {r_w}^2}{kt}\right)} \tag{A.8}$$

Using a very short time-step in which we assume flow rate remains constant, we calculate the amount of reservoir fluid entering the wellbore during this period. This additional fluid in the wellbore will compress the gas in the chamber at the top, thereby increasing its pressure. This gas-chamber pressure increase can be calculated by noting that during time $j-1$ to time j, the gas-chamber height changes from Δz_{j-1} to Δz_j as follows:

$$p_{1,j} = p_{1,j-1}\frac{\Delta z_{g,j-1}}{Z_{j-1}}\frac{Z_j}{\Delta z_{g,j}} \tag{A.9}$$

The change in gas-chamber pressure will result in a changed p_{wf} and q. Therefore, an iterative procedure is needed for computations of rate and bottomhole pressure. Once convergence is achieved for a given time-step, computation for the next time-step is initiated and the procedure is repeated until the end of the test period. We note that at very early times, the exponential integral function E_i is used rather than its logarithmic approximation in Eq. A.8.

Eq. A.8 can only be used once to calculate the flow rate based on the bottomhole pressure calculated using Eq. A.1. Thereafter, estimation of reservoir influx requires prior rate history. This step is done using Eqs. A.10 through A.12 where p_{wf} is calculated using the superposition principle. This estimated bottomhole pressure is then matched with the bottomhole pressure calculated using Eq. A.1 to provide the flow rate. Because the approach requires knowledge of q_j, the process is iterative.

$$p_{wf} = p_i - q_n m' \left(\sum_{j=1}^{n} \left\{ \left[\frac{q_j - q_{j-1}}{q_n} \right] log\left(t_n - t_{j-1}\right) \right\} + A \right) \tag{A.10}$$

where

$$m' = \frac{162.6\mu}{kh} \tag{A11}$$

and

$$A = log \frac{k}{\varphi \mu c_t {r_w}^2} - 3.23 + 0.869s \tag{A.12}$$

The computational objective is to estimate a flow rate that enables p_{wf} calculated with Eq. A.1 equal to that estimated with Eq. A.10. We achieve this objective by using the Generalized Reduced Gradient (GRG) nonlinear optimization algorithm, available in a spreadsheet, which minimizes the difference between the two values by finding a flow rate that satisfies both the pressure equations. Because Eq. A.10 superposes different flow rates at each timestep, the minimization algorithm provides an efficient way for accurate estimation of flow rates. Based on influx rates and time intervals, cumulative inflow can then be calculated, leading to estimation of increasing height of the reservoir fluid in the wellbore. Simple material balance for the heights of the fluid in the wellbore

and the gas chamber can be worked out based on the applicability of the test, slug or CCT. This approach of pressure and flow rate calculations are based on the physical mechanism of a test, thereby allowing design calculations or forward simulations for a set of input variables.

APPENDIX B

DEPTH DEPENDENT HEAT FLOW

As mentioned earlier, the process of producing hot fluid gradually heats up the near wellbore area, thereby decreasing heat transfer rate with time even when the production rate remains constant. To account for this changing heat flow during steady production, the superposition principle is used. Superposition of heat is modeled after an approach similar to that taken by Meunier et al. (1985) for modeling afterflow. Modeling depth dependent heat flow however, is more complicated than Superposition in fluid flow because heat transfer varies with both time and depth.

Let us consider a new well that produces fluids at a constant rate; that is, at a steady-state for a time t_n. To estimate the fluid temperature at time t_n, we divide the total time into n periods (not necessarily equal) – $(t_1 - 0)$, $(t_2 - t_1)$, $(t_3 - t_2)$, ..., $(t_{n-1} - t_n)$ as shown in **Figure B.1.**

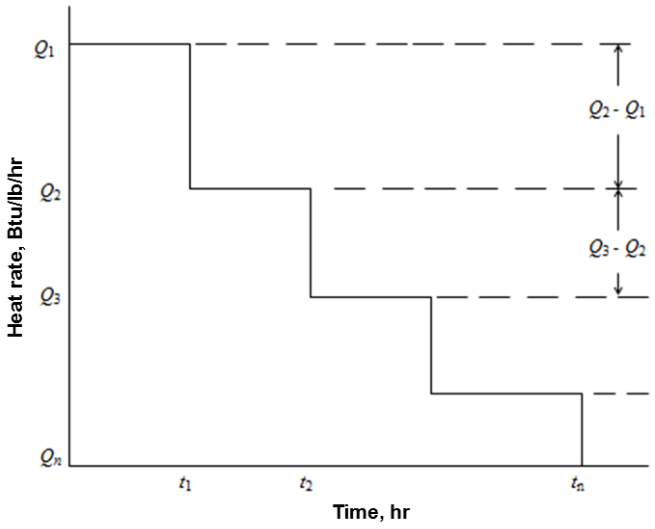

Figure B. 1 - Schematic representation of the superposition principle.

For each time period, the heat exchange between the formation and tubing fluid can be related in terms of the dimensionless temperature $T_{D,}$ and for the first time period can be written as:

$$Q_1 = -\frac{2\pi k_e}{T_D(t_D)}(T_{wb} - T_{ei})_1 \qquad \text{(B.1)}$$

where t_D (dimensionless time = $\alpha t/r_{wb}^2$) is used to calculate dimensionless temperature, T_D, as follows (Hasan and Kabir 2002)

$$T_D = \ln\left[e^{-0.2t_D} + \left(1.5 - 0.3719e^{-t_D}\right)\sqrt{t_D}\right] \qquad \text{(B-2)}$$

Note that in Eq. B.1, temperatures (T_{wb} and T_{ei}) are functions of well depth and that T_D (t_{Dn}) is the value of the dimensionless temperature function for a dimensionless producing time of t_{Dn}. In this particular case, the independent variable is in the parenthesis for the dependent variable. In all other situations, the general expression $y(x)$ implies y is multiplied by x *not* that y is a function of x. When y is a function of x, we simply write y and assume that the reader will understand the variability of y with respect to x (and any other variable, such as t) from the context.

Let us recast Eq. B.1 in the temperature difference form as:

$$T_{ei} - T_{wb,1} = \frac{Q_1 T_D(t_{Dn})}{2\pi k_e} \tag{B.3}$$

The heat flow rate Q_2 during the second timestep, t_2 - t_1, is represented by adding another constant heat source to the well at time > t_1, whose magnitude is equal to Q_2 - Q_1. The wellbore/formation interface temperature at this step, $T_{wb,2}$, is then the sum of these two heat sources, which is given by:

$$T_{ei} - T_{wb,2} = \frac{Q_1 T_D(t_{Dn}) + (Q_2 - Q_1) T_D(t_{D,n} - t_{D1})}{2\pi k_e} \tag{B.4}$$

Similarly, the third period can be represented by three sources of heat and so on. Hence, for the n^{th} period we have

$$T_{ei} - T_{wb,n} = \frac{\sum_n}{2\pi k_e} \tag{B.5}$$

where

$$\sum_n = \sum_{i=1}^{n} (Q_i - Q_{i-1}) T_D(t_{D,n} - t_{D,i-1}) \tag{B.6}$$

and both Q_0 and T_{D0} are zero.

Let us emphasize that $T_D\left(t_{D,n} - t_{D,i-1}\right)$ in Eq. B.6 and similar expressions in other equations represent the value of the dimensionless temperature T_D corresponding to the dimensionless time, $\left(t_{D,n} - t_{D,i-1}\right)$. The flowing wellbore fluid temperature is obtained from an energy balance between the wellbore fluid and the surrounding formation at the time of interest, t_n. The rate of heat transfer from the wellbore fluid to the wellbore/formation interface, in terms of the overall-heat-transfer coefficient for the wellbore, can be written as:

$$Q_n = -2\pi r U\left(T_f - T_{wb}\right)_n \tag{B.7}$$

$$T_{wb,n} = T_{f,n} + \frac{Q_n}{2\pi r U} \tag{B.8}$$

Substituting this expression for $T_{wb,n}$ into Eq. B.4, we get

$$T_{ei} - T_{f,n} = \frac{Q_n}{2\pi r U} + \frac{(Q_n - Q_{n-1}) T_D\left(t_{D,n} - t_{D,n-1}\right)}{2\pi k_e} + \frac{\sum_{n-1}}{2\pi k_e} \tag{B.9}$$

where Σ_{n-1} is defined the same way as Eq. B.6 for n-1 elements. Energy balance on the flowing fluid for a differential depth, dz, gives

$$\frac{\mathrm{d}T_f}{\mathrm{d}z} = \frac{1}{c_p}\left[-\frac{Q_n}{w} - \frac{g\ sin\theta}{g_c J} - \frac{v}{g_c J}\frac{\mathrm{d}v}{\mathrm{d}z}\right] + C_J\frac{\mathrm{d}p}{\mathrm{d}z} \tag{B.10}$$

Substituting Eq. B.9 into Eq. B.10 and rearranging,

$$\frac{\mathrm{d}T_{f,n}}{\mathrm{d}z} = -L_R T_{ei} + L_R\left(T_{f,n}\right) - \frac{g\ sin\theta}{g_c J c_p} + \Phi + \boldsymbol{\xi} \tag{B.11}$$

where

$$\xi = -T_D\left(t_D - t_{D,n-1}\right)\frac{L_{Rn}Q_{n-1}}{2\pi k_e} + \frac{L_{Rn}}{2\pi k_e}\sum\nolimits_{n-1} \tag{B.12}$$

$$\Phi = C_j\frac{\mathrm{d}p}{\mathrm{d}z} - \frac{v\frac{\mathrm{d}v}{\mathrm{d}z}}{g_c\ J\ c_p} \tag{B.13}$$

and

$$L_{Rn} = \frac{2\pi}{c_p w}\left[\frac{r_t U_t k_e}{k_e + \left\{r_t U_t T_D\left(t_{D,n} - t_{D,n-1}\right)\right\}}\right] \tag{B.14}$$

L_{Rn} defined by Eq. B.14 reduces to L_R given by Eq. 3.2 in the main body, when superposition is neglected. We can rewrite Eq. B.11 as

$$\frac{\mathrm{d}T_{f,n}}{\mathrm{d}z} = \frac{\mathrm{d}T_{fws}}{\mathrm{d}z} + \xi \tag{B.15}$$

where T_{fws} is the fluid temperature estimated without superposition. Assuming that ξ is invariant, the linear differential equation, Eq. B.15 is solved as

$$T_f = T_{ei} + \frac{\left(1 - e^{(z-L)L_R}\right)}{L_R}(\psi + \xi) \tag{B.16}$$

where

$$\psi = g_g sin\theta + \Phi + \frac{g\ sin\theta}{g_c J c_p} \tag{B.17}$$

APPENDIX C

TRANSIENT FLUID TEMPERATURE

For this analysis, we assume that fluid flow transients subside quickly and that flow rate, *w*, is independent of well depth. An energy balance indicates that any heat received/lost from the formation would change the fluid temperature with time and depth. In terms of fluid internal energy fluid enthalpy (*H)*, fluid mass rate (*w)*, and fluid mass in the control volume (*m)*, the energy-balance equation can be expressed as:

$$Q = \frac{\mathrm{d}}{\mathrm{d}t}\left[mc_pT_f(1+C_T)\right] - \frac{\mathrm{d}}{\mathrm{d}z}\left[w(H + \frac{1}{2}v^2 - g\ z\ sin\theta)\right] \tag{C.1}$$

The term C_T, represents the heat storage effect of the tubulars and cement sheaths in the wellbore. The heat received from (or lost to) the formation, *Q*, is:

$$Q = -\frac{2\pi k_e}{T_D(t_D)}(T_{wb} - T_{ei}) \tag{C.2}$$

As we discussed in Appendix B, the requirement of constant *Q* may be made by subdividing the time in consideration to discrete temporal steps. Analogous to the derivation of Eq. B.10, we obtained the following differential equation for fluid temperature as a function of time and depth:

$$\frac{\mathrm{d}T_f}{\mathrm{d}z} = \frac{wc_pL_R}{mc_p(1+C_T)}\left(T_{ei} - T_f\right) + \frac{wc_p}{mc_p(1+C_T)}(1 - e^{(z-L)L_R})(\psi + \xi) \tag{C.3}$$

In Eq. C-3, ξ is given by an expression similar to Eq. B.12. Assuming ξ and ψ to be constant, we arrive at the following expression for fluid temperature:

$$T_f = T_{ei} + \left(T_{fi} - T_{ei}\right)e^{-at} + \frac{(1 - e^{-at})}{L_R}(1 - e^{(z-L)L_R})(\psi + \xi) \tag{C.4}$$

$$a = \frac{wc_pL_R}{mc_p(1 + C_T)} \tag{C.5}$$

APPENDIX D

SAMPLE CALCULATIONS FOR PLUNGER LIFT

Well 1: Estimating desired casinghead pressure

The following sample calculation shows how the proposed approach works using Luo and Kelkar (2014) data. The following data were available:

Tubing pressure after plunger travel, p_{t2} = 185 psia

Casing volume V_c = 436 ft^3. Tubing volume V_t = 169 ft^3.

Vertical well depth = 3,443 ft. Liquid column on plunger top = 40 ft.

Gas gravity = 0.62

The following quantities were derived from these field data:

Gas pressure at tubing bottom, p_{tb} = 185 $p_{bh} = 185e^{(gMh)/(RZTg_c)}$ = 198 psia

Gas density for average tubing pressure (~pM/RT) = 0.573 lbm/ft^3

Mass of gas in the tubing (= tubing volume × gas density) = 96.6 lbm

Mass of liquid on top of plunger (= liquid volume × liquid density) = 123 lbm

We can use Eq. 3.11 to calculate the required casing pressure before the plunger release for sustained production:

$$p_c = \frac{p_t(V_c+V_t)+(m_p+m_L+(1+C)m_g)\left(\frac{g}{g_c}\right)h}{V_c} = 269 \text{ psia.}$$

The actual casinghead pressure at the time of plunger release was 255 psia, which is 14 psi lower than that recommended by Eq. 3.11. As a result, the well did not sustain continued production.

Casinghead pressure estimate for higher plunger water column

If water column on top of the plunger is higher at the time of plunger release, the casing pressure needed for sustainable gas production would be greater. In the above example, if water produced per cycle indicate a plunger top water column of 100 ft. (306 lb of water) instead of 40 ft., then the p_c calculated by the previous equation would be 279 psia.

Well 3: Delineating annular flow regime

The following sample calculation is presented for Well 3 with the following data:

Tubing bottomhole pressure, p_{t2} = 129 psia

Bottomhole temperature (assumed) = 120 ^{o}F

Tubing flow cross-sectional area = 0.0491 ft^2

Producing gas rate = 700 Mscf/D

Actual gas velocity, v_{sg} = 21 ft/sec

$$v_{gc} = 3.1\left[\frac{g(\rho_l - \rho_g)\sigma}{\rho_g{}^2}\right]^{0.25}$$

Minimum velocity needed for annular two-phase flow = 19.5 ft/sec

Therefore, annular two-phase flow exists at the well bottom and, therefore, in the entire wellbore.

APPENDIX E

RESERVOIR MODEL FOR PLUNGER LIFT

A 2D radial model was used to history match production from all four wells. This model has 25 logarithmically spaced cells along the horizontal plane and 5 cells in the vertical plane. The following relative permeability curves were used for all wells.

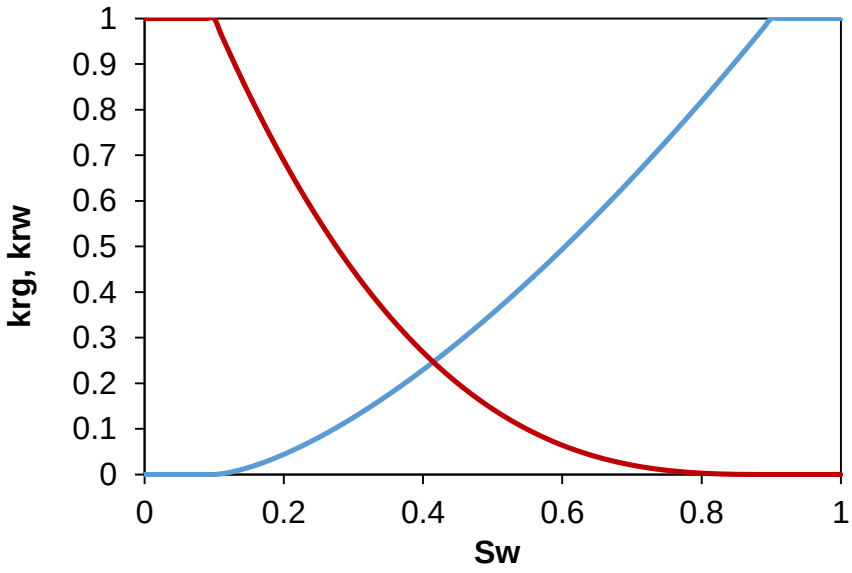

Figure E. 1 - Relative permeability curves for gas and water.

The tubinghead pressures were matched following conversion of the bottomhole pressure to surface condition, with the gas rate as the boundary condition for each well. Given the unavailability of water production data, the model results should be construed

as first approximation of the physical fact. The parameters presented in **Table E.1**were used for all the four wells.

Table E. 1 - Parameters used for history matching all four wells.

	Well 1	**Well 2**	**Well 3**	**Well 4**
k, md	90	95	130	115
ϕ	0.2	0.15	0.3	0.3
h, ft	20	20	20	20
T_{res}, °F	140	140	140	140
γ_g	0.7	0.7	0.7	0.7
p_i, psia	280	265	350	420

This approach yields the pressure and rate history that is matched with the given production history for model calibration. Because there was no other information provided in the Luo-Kelkar study, the calibrated model is then used with the wellbore model to determine the casinghead pressure needed to provide a sustainable flow rate. With the increase in water saturation with time, the relative permeability of each phase changes in accord with **Figure E.1**. Overall, this last model merely attempts to show a coupled wellbore/reservoir modeling approach to diagnose the problem first before offering realistic solutions.